

Linköping Studies in Science and Technology
Dissertations, No. 1590

Modeling and control of actuators and co-surge in turbocharged engines

Andreas Thomasson



Linköpings universitet
INSTITUTE OF TECHNOLOGY

Department of Electrical Engineering
Linköping University
SE-581 83 Linköping, Sweden

Linköping 2014

Linköping studies in science and technology. Dissertations, No. 1590

Modeling and control of actuators and co-surge in turbocharged engines

Andreas Thomasson

ISBN 978-91-7519-355-7

ISSN 0345-7524

© 2014 Andreas Thomasson, unless otherwise noted. All rights reserved.

Andreas Thomasson

andreast@isy.liu.se

www.vehicular.isy.liu.se

Division of Vehicular Systems

Department of Electrical Engineering

Linköping University

SE-581 83 Linköping

Sweden

Paper 1 is reproduced here with permission from IFP Energies nouvelles

Paper 2 is reproduced here with permission from IFAC

Paper 3 is reproduced here with permission from Elsevier

Paper 4 is reproduced here with permission from IFAC

The cover: Photo of an electronic throttle, a pneumatic actuator, and a measurement of mass flows during co-surge, illustrating the main topics of the thesis.

Typeset with L^AT_EX 2_ε

Printed by LiU-Tryck, Linköping, Sweden 2014

Abstract

The torque response of the engine is important for the driving experience of a vehicle. In spark ignited engines, torque is proportional to the air flow into the cylinders. Controlling torque therefore implies controlling air flow. In modern turbocharged engines, the driver commands are interpreted by an electronic control unit that controls the engine through electromechanical and pneumatic actuators. Air flow to the intake manifold is controlled by an electronic throttle, and a wastegate controls the energy to the turbine, affecting boost pressure and air flow. These actuators and their dynamics affect the torque response and a lot of time is put into calibration of controllers for these actuators. By modeling and understanding the actuator behavior this dynamics can be compensated for, leaving a reduced control problem, which can shorten the calibration time.

Electronic throttle servo control is the first problem studied. By constructing a control oriented model for the throttle servo and inverting that model, the resulting controller becomes two static compensators for friction and limp-home nonlinearities, together with a PD-controller. A gain-scheduled I-part is added for robustness to handle model errors. The sensitivity to model errors is studied and a method for tuning the controller is presented. The performance has been evaluated in simulation, in test vehicle, and in a throttle control benchmark.

A model for a pneumatic wastegate actuator and solenoid control valve, used for boost pressure control, is presented. The actuator dynamics is shown to be important for the transient boost pressure response. The model is incorporated in a mean value engine model and shown to give accurate description of the transient response. A tuning method for the feedback (PID) part of a boost controller is proposed, based on step responses in wastegate control signal. Together with static feedforward the controller is shown to achieve the desired boost pressure response. Submodels for an advanced boost control system consisting of several vacuum actuators, solenoid valves, a vacuum tank and a vacuum pump are developed. The submodels and integrated system are evaluated on a two stage series sequential turbo system, and control with system voltage disturbance rejection is demonstrated on an engine in a test cell.

Turbocharged V-type engines often have two parallel turbochargers, each powered by one bank of cylinders. When the two air paths are connected before the throttle an unwanted oscillation can occur. When the compressors operate close to the surge line and a disturbance alters the mass flow balance, the compressors can begin to alternately go into surge, this is called co-surge. Measurements on co-surge in parallel turbocharged engines are presented and analyzed. A mean value engine model, augmented with a Moore-Greitzer compressor model to handle surge, is shown to capture the co-surge behavior. A sensitivity analysis shows which model parameters have the largest influence of the phenomena. The compressor operation in the map during co-surge is studied, and the alternating compressor speeds are shown to have a major impact on the continuing oscillation. Based on the analysis, detection methods and a controller are proposed, these detect co-surge and control the turbo speeds to match during co-surge. The controller is evaluated both in simulation and on a test vehicle in a vehicle dynamometer, showing that co-surge can be detected and the oscillations quelled.

Populärvetenskaplig sammanfattning

Momentsvaret från motorn är viktigt för körkänslan i en bil. För bensinmotorer är momentet proportionellt mot luftmassflödet till cylindrarna, att styra momentet är därför nära kopplat till att styra luftflödet. I moderna motorer översätts förarens gaspådrag till en momentbegäran av motorns styrsystem som sedan skickar styr signaler till flertalet elektromekaniska och pneumatiska ställdon. Ett av dessa är det elektroniskt styrda trottelspjället som reglerar luftflödet till insugsröret. Spjället är kopplat till en elmotor och för att få önskat luftmassflöde krävs därför precision och tillförlitlighet i styrningen av denna. I turboladdade motorer utvinns energi ur avgaserna av en turbin som driver en kompressor med uppgiften att öka laddtrycket och därmed luftmassflödet till motorn på höga laster. Turbon styrs vanligtvis med en wastegate på avgassidan som kan leda avgaser förbi turbinen. Wastegaten är kopplad till ett pneumatiskt ställdon där trycket regleras av en elektroniskt styrd ventil. Dynamiken hos dessa komponenter påverkar motorns respons, och styrsystemet måste kalibreras för att hantera detta vilket kan vara mycket tidskrävande.

I avhandlingen utvecklas reglerorienterade modeller av motorställdon för att underlätta kalibrering av motorns styrsystem. En regulator för motorns elektroniska trottelspjäll föreslås. Regulatorn består av en olinjär statisk framkoppling och linjär återkoppling som fås naturligt genom att modellera och förenkla systemet. Vidare presenteras en metod för att parametersätta regulatorns olika delar. Komponentmodeller till ett system för styrning av avancerade turbokonfigurationer tas fram. Systemet består av pneumatiska styrdon, elektroniskt styrda ventiler, en vakuum tank och en vakuum pump. Modellerna är konstruerade för att vara enkla att identifiera från mätdata och ha en sund fysikalisk tolkning för att kunna hantera varierande omgivningsförhållanden. Flera applikationer diskuteras, bland annat kompensering för varierande batterispänning, vilket testas på en motor med ett serieekvensiellt dubbelturbosystem i en motortestcell.

Ett turbokoncept för V-motorer är att använda två parallella turboaggregat, kopplade till ett gemensamt insugsrör. I denna konfiguration kan det uppstå ett oönskat oscillativt fenomen då kompressorerna jobbar vid hög tryckkvot och lågt massflöde. Om balansen mellan aggregaten störs kan en turbo ta över och producera mer flöde, medans flödet genom den andra turbon reverserar. Den turbo som inte producerar flöde kommer att accelerera och flödet vänder tillbaka. Det aggregatet kommer då producera mer flöde och man får en oscillation i massflöde mellan de två turboaggregaten, detta fenomen kallas co-surge. I avhandlingen presenteras och analyseras mätningar av co-surge och en modell som kan användas för att simulera co-surge utvecklas. Modellen används för att analysera systemet, undersöka vilka faktorer som har störst inverkan på oscillationen och för att utveckla detektions och reglerstrategier. Analysen visar att turboaggregatens varierande varvtal under co-surge är en betydande orsak till oscillationen. Detektionsmetoder och reglerstrategi för att snabbt återhämta systemet från co-surge tas fram. Regulatorn öppnar trotteln för att kompensera för det minskade luftmassflödet och flyttar temporärt kompressorns arbetspunkt, samtidigt som den styr turbovarvtalen mot varandra. Regulatorn utvärderas i testbil på chassidynamometer, och experimenten visar att den snabbt för tillbaka systemet till en stabil arbetspunkt.

Acknowledgment

Five years and seventy five days is a long time, at least from my perspective. During that time there are lots of people that have contributed in one way or another, and when summarized, have made this thesis possible.

First of all I would like to thank my supervisor Lars Eriksson for all guidance and support along the way, without you I would not even have started this journey. I want to thank Lars Nielsen for letting me join Vehicular Systems and all co-workers in the group for providing a fruitful research environment and enjoyable discussions during coffee breaks. Special thanks to Oskar Leufvén both as research partner and for supervising the undergraduate project “RATT”, which turned my interest to automotive control systems to begin with.

Then I would like to thank my friends, especially Henrik Svensson, Marcus Wallenberg, Jonas Sjöqvist and Ulf Winberg. For everything from lunches and bowling, to Sweden Rock and the Netherlands, but mostly for always being good company.

I want to thank my father Sten for always being supportive, I will always look up to you, and my mother Eva for always believing that I could manage everything I wanted.

Finally I would like to express my love for Elisabet who has been by my side for more than nine years, you make me happy.

Andreas Thomasson, 2014

Contents

1	Introduction	3
1.1	Summary and main contributions of the papers included in the thesis	5
1.2	Other publications by the author	6
1.3	Future work	7
1.4	Outline	7
2	Background on boost control and its actuators	9
2.1	The electronic throttle	9
2.2	The pneumatic actuation system	11
2.3	Engine modeling and boost control	13
3	Experimental setups	17
3.1	The engine laboratory	17
3.2	The vehicle propulsion laboratory	18
3.3	Sensor equipment and installation	18
	References	21
	Papers	29
1	Model-Based Throttle Control using Static Compensators and Pole Placement	31
1	Control oriented throttle model	33
2	Controller structure	36
3	Identification and controller tuning	40
4	Simulation results on TC benchmark model	45
5	Experimental results	50

6	The throttle control benchmark	51
	References	53
2	Wastegate Actuator Modeling and Model-Based Boost Pressure Control	55
1	Introduction	57
2	Wastegate actuator modeling	59
3	Boost pressure controller	65
4	Controller tuning and results	69
5	Conclusions	72
	References	73
3	Modeling and validation of a boost pressure actuation system, for a series sequentially turbocharged SI engine	75
1	Introduction	77
2	Experimental setup	79
3	Actuator modeling	81
4	Vacuum tank and pump model	90
5	Model applications	92
6	Summary and conclusions	96
	References	96
A	Nomenclature	99
4	Modeling and Control of Co-Surge in Bi-Turbo Engines	101
1	Introduction	103
2	Co-surge	103
3	Engine model	105
4	Compressor model	106
5	Analysis of surge properties	108
6	Pipe dynamics investigation	109
7	Control	111
8	Conclusions	113
	References	115
A	Nomenclature	116
5	Co-Surge in Bi-Turbo Engines - Measurements, Analysis and Control	117
1	Introduction	119
2	Test setup	120
3	Surge and co-surge	121
4	Control oriented engine model	123
5	Co-surge analysis	131
6	Detection	133
7	Co-surge control	136
8	Conclusions	143
	References	143
A	Nomenclature	145

Introduction

Introduction

The modern Internal Combustion (IC) engine is a result of continuous development during the past century up until today. The combination of increasing performance and reliability, together with low cost and high availability of fuel, has led to the point where the IC engine is, without competition, still the most widely used power source for vehicle propulsion. Even if fossil fuels will be phased out eventually, the introduction of renewable fuels gives good reason to believe that the IC engine will continue to be of major importance for a foreseeable future.

The basic working principles of the IC engine is simple. A mixture of air and fuel is compressed by a piston inside a cylinder and ignited. The mixture burns which increases temperature and pressure inside the cylinder, the piston is pushed down and work is extracted. The burnt gases are then replaced by fresh air fuel mixture and the cycle is repeated. A more in-depth description of basic internal combustion engine operation will not be given in this thesis, and the interested reader is referred to e.g. Heywood (1988); Stone (2012).

A combination of increasingly strict emission legalization and a demand for lower fuel consumption, with equal or improved performance, has pushed the development to more complex engine systems. A part of this development is the movement toward more drive-by-wire systems, and one important step was the introduction of the electronic throttle controlled by the Engine Control Unit (ECU). By removing the direct connection between the gas pedal position and the throttle angle, the torque response of the engine can be shaped by the control system design. It also allows the ECU to more accurately predict the air flow to the engine and controlling the air fuel ratio, improving emissions, fuel economy and driveability (Tudor, 1993; Strieb and Bischof, 1996). Today all modern car engines use electronic throttles, which in addition to the benefits above, allows the control system to coordinate the throttle command with other systems that affects torque.

Another concept that has become common practice is downsizing and turbocharging, where large naturally aspirated engines are replaced by smaller turbocharged ones (Emmenthal et al., 1979; Watson and Janota, 1982). The turbocharger increases the intake pressure which increases the air flow into the cylinders. Since torque is proportional to the amount of fuel burnt in the cylinder, which is limited by the amount of available air, this enables the turbocharged engine to produce more torque and power compared to a naturally aspirated engine of the same size. For a given power requirement the engine can therefore be reduced, improving fuel economy by lowering friction and pumping losses (Guzzella et al., 2000). To gain further benefits from downsizing more advance turbo concepts are being developed (Petitjean et al., 2004). There are systems with both series sequential (Chasse et al., 2008; Galindo et al., 2009c), and parallel sequential turbochargers (Borila, 1986; Galindo et al., 2009a).

The turbo is powered by energy in the exhaust gas, and the power generated can be controlled by letting part of the exhaust gas bypass the turbine through a wastegate. The wastegate is usually operated by a pneumatic actuator, and the pressure in the actuator is controlled by a solenoid valve connected to the ECU. The addition of these systems to the engine increases the flexibility and degrees of freedom for the air charge management, since in addition to the electronic throttle, also the wastegates have a large influence on the air flow to the cylinders. To be able to both minimize fuel consumption and have desired transient response of the engine, control of these actuators needs to be coordinated. This coordination could not be expected to be handled by the driver and a modern engine is therefore a drive-by-wire system, where the driver commands are interpreted by the ECU that controls engine operation through electromechanical and pneumatic actuators.

The behavior of these actuators affect both static and transient engine response, and to get the desired behavior a lot of time is required for calibration. The traditional approach has been to store controller parameters in look-up tables to handle different operating points and surrounding conditions. This approach has a clear downside when the degrees of freedom increase, since the number of parameters increase exponentially with the number of inputs. To reduce this burden, model based approaches are getting more attention. By exchanging maps for model based relationships, the number of parameters can be reduced and the calibration time shortened. This requires models with good accuracy over their operating region, and that are easily identified from measurements. The models should handle varying surrounding conditions and behave in a sensible way outside their nominal region to not cause problems for the control system. This is a strength of physically based models, where the surrounding condition can be explicitly included, thereby reducing the need for additional calibration.

1.1 Summary and main contributions of the papers included in the thesis

This section summarizes the five papers included in the thesis and highlights the main contributions.

Paper 1 (Thomasson and Eriksson, 2011b) contributes with a model based controller for an electronic throttle servo that consists of two static compensators and a modified PID-controller. The paper includes an automatic tuning method for the controller parameters and a sensitivity and robustness investigation with respect to the limp-home and friction nonlinearities. The controller is relatively simple, with a less complex friction model than usually proposed in the literature, and a PID-controller with fewer degrees of freedom. It was also the best performing controller of the participants in the Throttle Control Benchmark, described in Zito et al. (2009).

The main contribution of Paper 2 (Thomasson et al., 2009) is a control oriented model for a pneumatic wastegate actuator and air control solenoid. The wastegate model consists of three submodels; the actuator pressure, the static position, and an additional position dynamics. The dynamics of the actuator turns out to be important for the transient response, in particular the actuator characteristics is responsible for an overshoot in boost pressure for step changes in actuator input. The model is incorporated in a complete Mean Value Engine Model (MVEM), that is used to study the system and develop a tuning method for the boost pressure feedback controller, a gain scheduled PID. Together with a static feedforward, the controller achieves desired transient response in boost pressure.

In Paper 3 (Thomasson et al., 2013b) an actuation system for an advanced turbocharging system is studied. It incorporates a vacuum pump and a vacuum tank, pneumatic actuators and pulse width modulation controlled solenoid valves. The paper contributes with component models that are easily identified from measured data. Their physical interpretation enables them to handle varying surrounding conditions. The models are evaluated on a two stage series sequential turbo system with three actuators having different characteristics. Several applications are presented, including a nonlinear compensator for voltage disturbance rejection.

Paper 4 (Thomasson and Eriksson, 2011a) presents experimental data on co-surge in a bi-turbocharged engine, where the two parallel turbos alternately goes into surge. An engine model able to capture the co-surge phenomena is presented. The model consists of a MVEM augmented with a Moore-Greitzer compressor model to handle surge. A sensitivity study with respect to parameter variations and their effect on the co-surge behavior is performed. It is concluded that the parameters with largest influence on the behavior are the size of the volumes after the compressor, the compressor inertia, and the pressure drop from the zero slope point at the surge line to zero mass flow in the compressor speed lines. The effect of adding momentum conservation to the pipes before and after the compressor is studied but the resulting behavior is quantitatively similar. There is also a first investigation of detection and control of co-surge.

A deeper analysis of co-surge is presented in Paper 5 (Thomasson and Eriksson, 2014). The paper includes more precise co-surge measurements from a test vehicle in a chassis dynamometer, used in both model validation and control evaluation. The driving force behind the co-surge oscillation is studied and the diverging turbo speeds during the surge cycle is shown to be of importance. The paper proposes a detection algorithm suitable for either mass flow, pressure or turbo speed sensors. The paper also contributes with a controller that quells the co-surge oscillation by forcing the turbo speeds together during the surge cycle, thereby ensuring a more balanced recovery point and reducing the risk of continuing oscillation.

1.2 Other publications by the author

This section summarizes research publications that the author has been involved in, but that is not included in the thesis.

- A** Andreas Thomasson, Lars Eriksson, Tobias Lindell, James Peyton Jones, Jill Spelina, and Jesse Frey, *Tuning and experimental evaluation of a likelihood-based engine knock controller*, 2013, 52nd IEEE Conference on Decision and Control, Florence, Italy (Thomasson et al., 2013a)
- B** Andreas Thomasson and Lars Eriksson, *Co-Surge Detection and Control for Bi-Turbo Engines with Experimental Evaluation*, 2013, Advances in Automotive Control, Tokyo, Japan (Thomasson and Eriksson, 2013)
- C** Lars Eriksson, Tobias Lindell, Oskar Leufvén, and Andreas Thomasson, *Scalable Component-Based Modeling for Optimizing Engines with Supercharging, E-Boost and Turbocompound Concepts*, 2012, SAE International Journal of Engines (Eriksson et al., 2012b)
- D** Lars Eriksson, Tobias Lindell, Oskar Leufvén, and Andreas Thomasson, *Scalable Component-Based Modeling for Optimizing Engines with Supercharging, E-Boost and Turbocompound Concepts*, Technical paper 2012-01-0713, 2012, SAE World Congress, Detroit, USA (Eriksson et al., 2012a)
- E** Ivan Criscuolo, Oskar Leufvén, Andreas Thomasson, and Lars Eriksson, *Model-based boost pressure control with system voltage disturbance rejection*, 2011, IFAC World Congress, Milano, Italy (Criscuolo et al., 2011)
- F** Andreas Thomasson and Lars Eriksson, *Model-Based Throttle Control using Static Compensators and IMC based PID-Design*, 2009, IFAC Workshop on Engine and Powertrain Control, Simulation and Modeling, Paris, France (Thomasson and Eriksson, 2009)
- G** Andreas Thomasson, *Wastegate Actuator Modeling and Tuning of a PID Controller for Boost Pressure Control*, 2009, Masters Thesis, LiTH-ISY-EX-09/4232-SE, Linköping University (Thomasson, 2009)

The author's contributions to these journal and conference publications are indicated by the author list, where the first author is the main contributor to a publication. In the knock controller evaluation **A**, the author did the implementation on the engine control system, a large part of the engine tests and the experimental part of the paper. In the co-surge control experimental evaluation in **B**, the author has developed the detection and control algorithms, done the implementation on the test vehicle and run the experiments. This work was preliminary to Paper 5 in the thesis (Thomasson and Eriksson, 2014). For publications **C** and **D** the author was contributing to a literature survey of charging concepts. For publication **E** the author was part of the weekly meetings and discussions about the projects development, problems and possible solutions. For publication **F** the author has done the majority of the work, controller development, implementation on the control system and experimental evaluation. This work was preliminary to Paper 1 in the thesis (Thomasson and Eriksson, 2011b). Publication **G** is the author's Masters Thesis that contains preliminary work to Paper 2 (Thomasson et al., 2009).

1.3 Future work

This section gives a very brief outlook on possible extensions to the work in the thesis that has been thought about, but not received the deserved attention.

The tuning of the throttle controller in Paper 1 uses offline calibration together with a limp-home calibration during start up. An interesting continuation would be to investigate if the process curve can be accurately estimated during normal operation, for example during a driving cycle.

One goal of the actuation system modeling in Paper 3 is the use in boost control. The final puzzle for closing the loop with model based control would be an accurate model for the relation between wastegate position and effective flow area. Given a total mass flow, turbo speed and desired turbine power, the correct wastegate position could then be calculated for accurate feedforward.

The focus in Papers 4-5 has been modeling, detection and recovery from co-surge. A challenging topic would be prediction of when co-surge is about to begin, and to develop a controller to stop the onset of the oscillation.

1.4 Outline

The goal of the three introductory chapters is to introduce the topics covered in the thesis, place the contributions of the thesis in the research field and describe the experimental setups used during the thesis work.

The first two sections of Chapter 2 introduces the electronic throttle and pressure actuators, the topics of Papers 1-3. The systems are described and related research results on modeling, simulation and control are presented. Section 2.3 begins with an introduction to engine modeling with mean value engine models, used frequently during the thesis work. Applications of MVEM in control design are then presented followed by a short introduction to surge modeling and control, with focus on research on vehicle applications. Chapter 3

presents two of the experimental setups used in the thesis with information on sensors, their characteristics and installation. The appended papers then cover the thesis' contributions to electronic throttle control, pneumatic actuator modeling with application to boost control, and co-surge modeling and control.

Background on boost control and its actuators

This chapter gives an introduction to engine modeling, boost control and two of its most important actuators, the electronic throttle that controls air flow into the intake manifold, and the pneumatic actuator that is the most common actuator for the wastegate that controls the energy to the turbine in the turbocharger. The basic structure of the actuators are described and an overview of previously published research and the relation to the thesis is presented.

2.1 The electronic throttle

Benefits of replacing the conventional throttle, mechanically connected to the gas pedal by a wire, with an electronically controlled throttle valve was pointed out already in the early 90s. Improvements in both emissions, fuel economy and driveability were shown (Tudor, 1993; Strieb and Bischof, 1996). Advantages also include easier interaction with other systems such as cruise control, traction slip control and idle speed control (Mausner and Pfalzgraf, 1990; Huber et al., 1991). The electronic throttle is a relatively inexpensive DC servomotor that provides position control of the throttle plate and thus controls the air flow to the intake manifold (Pavković and Deur, 2011). To enable feedback control and provide robustness, the throttle position is measured by two potentiometers for redundancy (Jurgen, 1994). The DC motor is controlled by a Pulse Width Modulated (PWM) signal, the most common approach for DC servo control due to the low power requirement, small size and low cost (Alciatore and Hestand, 2003). An example of an electronic throttle and a sketch of the components of the electronic throttle control are shown in Fig. 2.1. The throttle housing contains the DC-motor, gearbox (omitted in the figure), throttle plate, position sensor and return spring. The controller and chopper are integrated in the ECU.

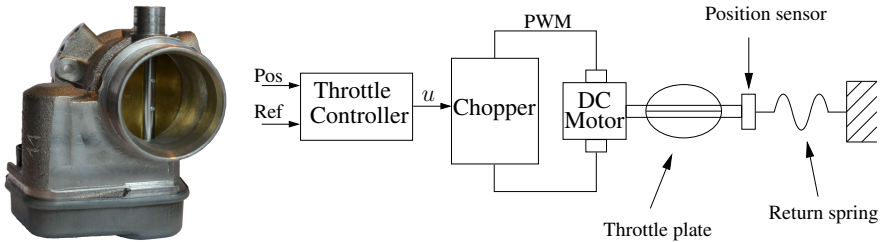


Figure 2.1: *Left:* Example of an electronic throttle body. The housing contains a DC-motor, gearbox, throttle plate, position sensor and return spring.

Right: A sketch of the electronic throttle and position controller.

2.1.1 Throttle modeling and control

The servo control problem for the electronic throttle is complicated by two strong nonlinearities, the torque from the return spring and friction. Since accurate control of this servo is required for precision in the air flow control, modeling, simulation and control of this servo has been an active research topic since the late 90s. The models can usually be divided into three parts, linear terms for the electric motor, a nonlinear model for friction torque, and a nonlinear model for the return spring torque, which is usually piecewise linear. Different models used in the literature then mainly differ in the complexity of these submodels, especially the friction model. For a good overview of the friction models mentioned in this section, see Olsson et al. (1998). In addition, a model for the torque from the air flow on the throttle plate can be included, but is usually omitted or considered an unknown disturbance.

A simulation model of an electronic throttle is presented in Scattolini et al. (1997). Friction effects are modeled by Coulomb friction and stiction effect. Parameter identification are discussed, based on the process static curve and a step response in duty cycle. The Coulomb friction model is also used in Eriksson and Nielsen (2000), but the authors extend it with viscous friction and proposes a control strategy consisting of a PI and friction compensator. An observer is also designed with the main goal of estimating the throttle angular velocity, that is used in the friction compensator. A very similar strategy is used in Al-Assidi et al. (2006) that uses Coulomb friction and an velocity observer to provide friction compensation, together with a PID controller. Also in Özgüner et al. (2001) Coulomb friction and a piecewise linear spring force is used to model the nonlinear effects, but a discrete time sliding-mode controller and observer is designed. A similar model is used in Barić et al. (2005) to implement a neural-network based sliding mode controller, and in Pan et al. (2008) that designs a variable-structure control using backstepping and a sliding-mode observer.

A more advanced friction model is adopted in Canudas de Wit et al. (2001) that uses a dynamic LuGre friction model (Canudas de Wit et al., 1999), and adaptive pulse control to overcome friction for small displacement operation. In Deur et al. (2003b, 2004) it is shown that the LuGre model cannot capture throttle friction dynamics accurately and a hybrid friction model is proposed,

consisting of a Dahl dynamic submodel for the presliding regime and the generalized Striebeck static submodel for the sliding regime. The paper also presents an electronic throttle control strategy based on a PID controller and compensators for friction and limp-home. This controller is also extended with an auto-tuner and a self-tuning strategy in Deur et al. (2003a) and Pavković et al. (2003, 2006). A comprehensive treatment of modeling and control of the electronic throttle together with this controller, auto-tuning and self-tuning strategies and applications is found in Pavković and Deur (2011).

The performance of state estimators for the electronic throttle is studied in Vašák et al. (2003). An Extended Kalman Filter (EKF) and an Unscented Kalman Filter (UKF) are compared, and the UKF is shown to behave better for this application. This filter is used in Vašák et al. (2006, 2007) that applies optimal control theory and full state feedback to the electronic throttle control problem. Full state feedback is also used in Loh et al. (2007), where input-output state feedback linearization together with pole-placement are utilized. Control schemes that use a reference model directly in the controller to adapt model parameters online have also been suggested for the throttle control problem. In Jiang and Kitchen (2010), a PID controller together with model reference adaptive control (see e.g. Åström, 1983) is utilized. An adaptive linear quadratic controller is presented in di Bernardo et al. (2010).

The controller presented in Paper 1 combines previous ideas and adds new contributions. It consists of two nonlinear static feedforward compensators for friction and limp-home effects, and in contrast to Deur et al. (2004) they are active simultaneously. Friction compensation is based on Coulomb friction only as in Eriksson and Nielsen (2000); Al-Assidi et al. (2006), but estimation of the throttle plate angular velocity is avoided by always acting in the direction to reduce the tracking error. This approximately linearizes the system and then PID control is applied. The I-part is gain scheduled with high gain for small errors to ensure fast response and robustness to model errors for small reference changes, which are typically problematic. The controller is relatively simple, easy to tune with the provided tuning method, and has proved satisfactory performance. It was also the best performing controller in the throttle control benchmark at the 2009 IFAC Workshop on Engine and Powertrain Control, Simulation and Modeling (Delarue and Tona, 2011).

2.2 The pneumatic actuation system

Pneumatic actuators are used in modern internal combustion engines to control different systems, many that affect boost pressure such as wastegate (WG) valves, bypass (BP) valves, exhaust gas recirculation (EGR) valves, variable geometry turbine (VGT) position (Moraal et al., 1999; Galindo et al., 2009b). The pressure in these actuators are usually controlled by the ECU through PWM solenoid valves, connected to a vacuum reservoir or boost pressure. An example of a pressure actuator and a sketch of the principal system is shown in Fig. 2.2. The pressure in the actuator will be in the range $[p_1, p_2]$ depending on the duty-cycle of the PWM signal. The pressure in the actuator results in a

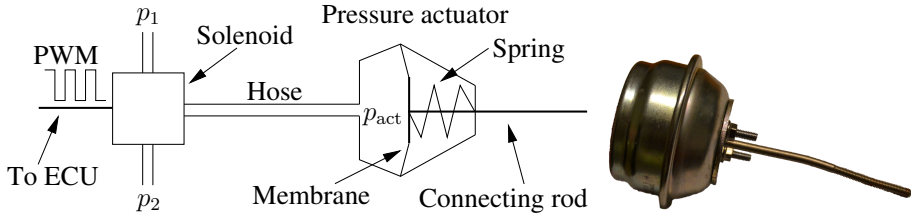


Figure 2.2: *Left:* A sketch of a pressure actuator connected to a solenoid. The pressure in the actuator, p_{act} is controlled in the range $[p_1, p_2]$ by varying the duty-cycle of the PWM signal from the ECU. The pressures p_1 and p_2 can be connected to either a vacuum reservoir, boost pressure or ambient pressure.

Right: An example of a pressure actuator used to control a wastegate.

force on the membrane that transfers to the connecting rod, that is attached to the control target. The system could then include more components such as a vacuum pump, reservoirs, several actuators and valves.

2.2.1 Modeling and control of pneumatic actuators

Models for pneumatic systems with varying levels of detail have been proposed in the literature. In Moraal et al. (1999) modeling and identification of a control valves and pressure actuator for a VGT is presented. Isothermal control volumes with fixed size are used to model the pneumatic part of the actuator and the vacuum reservoir. Mass flows to and from the actuator are modeled with compressible flow equations and effective areas that depend on control signal and actuator pressure. A mass-spring-damper system is used to describe the actuator mechanics but no friction forces are considered. A very similar model for EGR valve control is studied in Kotwicki and Russell (1998), but adiabatic control volumes are used and compared with isothermal ones. The difference is shown to be very small.

A slightly more advanced model is presented in Galindo et al. (2009b) for a vacuum system used for controlling a two-stage turbocharged engine. In this paper the effective area that governs the mass flow through the pressure control valves are dependent on the actual core position inside the solenoid valve instead of directly on the control signal. The core movement is modeled with a mass-spring-damper system, where the magnetic force depends directly on the PWM signal. More detailed models for the magnetic force inside the solenoid valves can be found in Szente and Vad (2001), that specifically studies simulation of the solenoid valve position. The paper by Galindo et al. (2009b) also compares 1D modeling of the pipes with using 0D models. No advantage of using 1D models for this application is found, the two models behave almost identically with lower computational burden for the 0D models. Friction models for pressure actuators are investigated in Mehmood et al. (2010, 2011), where the vacuum system for a VGT actuator is modeled. This is motivated by hysteresis in the relation between actuator pressure and position. The aerodynamic force affecting the actuator from the VGT is also investigated. Friction in pneumatic actuators had

previously been used in pneumatic brake systems in e.g. Acarman et al. (2001). Another interesting result is found in Håkansson and Johansson (2007), where a state space model for a system consisting of a two solenoid valves and a pressure actuator is developed. The model includes electrical, magnetic, mechanical and flow submodels, and has a total of 9 states. PID and fuzzy control is applied, but satisfactory results are not obtained without adding position feedforward. With feedforward, only P-control is required for desired performance.

Position control of pneumatic actuators have otherwise mostly been concerned with pneumatic cylinders where each side of the piston is connected to a separate control valve. In van Varseveld and Bone (1997), a nonlinear transformation between control signal and PWM duty-cycle is suggested to get a more linear velocity response. PID control and position feedforward is then applied. In Wang et al. (1999) acceleration feedback, PID control and a nonlinear compensator is used to track a velocity reference. Approximate feedback linearization is proposed in Xiang and Wikander (2004) to provide accurate position control. The linearization is made on a block-level, requiring only that specific blocks are invertible or approximately invertible. Force control of pneumatic cylinders are considered in Richer and Hurmuzulu (1999), where a nonlinear sliding mode controller is designed. The closely related pressure control problem is studied in Wang et al. (1999), where an LQG self-tuning controller is proposed.

The model presented in Paper 3, in this thesis, uses zero dimensional isothermal control volumes, which is sufficient for good accuracy according to results in Galindo et al. (2009b) and Kotwicki and Russell (1998). An opportunity for model reduction has been identified by observing that the solenoid valve acts as a controller for the pressure difference, shown also in Paper 2, and that the pressure respond approximately as a first order system. In contrast to previous publications, the need to identify the effective area of the valve is removed and the mass flow out of the tank can be calculated based on the pressure change in the actuator. Leakage flow through the valves, which usually is omitted, has also been modeled. Additionally the effect of different supply voltage is investigated and how the control signal can be modified to compensate for this during modeling and control design is shown.

2.3 Engine modeling and boost control

The use of models for simulation and development of engine controls is becoming increasingly important as the complexity of engine systems increase. Mean Value Engine Models (MVEM) offer good accuracy for low computational cost, and can be used to evaluate new control ideas cost effectively before implementation in a vehicle. They are widely used in industry and academia, and are both utilized and developed in Papers 2, 4 and 5 in this thesis.

The development of MVEM started in the 70s but the term was coined in the late 80s and thereafter there has been a significant amount of research. In Hendricks (1989); Hendricks and Vesterholm (1992), mean value engine models are analyzed in both time and frequency domain. The models are shown to have good predicting capability in a large part of the engine operating region.

A model of a spark ignited (SI) engines is presented in Hendricks and Sorenson (1990), and Jensen et al. (1991) develops a model for a small turbocharged diesel engine. The SI engine has three states, engine speed and pressure in the intake and exhaust manifold. The turbocharged engine also has turbo speed as a state. The SI engine is claimed to have an accuracy of $\pm 2\%$ for most variables over the whole operating region. The validity of MVEM during transient operation is the topic of Chevalier et al. (2000) that concludes that the models perform well, but that isothermal control volumes give inaccurate air density during tip-in and tip-out. This is remedied in e.g. Müller et al. (1998); Eriksson et al. (2002b), where temperature states are added together with more components, such as intercooler and air filter. The publications by Moraal and Kolmanovsky (1999) and Sorenson et al. (2005) are concerned with turbocharger modeling suitable for MVEM. Both use relations between the dimensionless parameters for flow, Φ , and energy, Ψ , to model compressor mass flow and efficiency. Another model that directly parameterize compressor speed lines and can handle both the surge and choke region of the compressor is presented in Leufvén and Eriksson (2013).

Along with development of MVEM, engine control based on these models has developed. An observer for the fuel film in the intake is developed in Hendricks et al. (1992) and used to improve air-fuel ratio control. In Eriksson et al. (2002a) it is shown that for fuel optimal operation of turbocharged SI engines, the wastegate should be fully open when no boost is needed, and for boosted operation the throttle should be fully opened and the intake pressure controlled by the wastegate. The use of MVEM in diesel engine control is found for example in Guzzella and Amstutz (1998) and Jankovic et al. (1998). In Eriksson (2007) the focus is on a component based modeling methodology for MVEM and several applications on control is presented. Publications on model based boost control, where the MVEM equations are used for model based feed forward and feedback linearization, include e.g. Müller (2008); Moulin et al. (2008); Moulin and Chauvin (2011). Coordinated throttle and wastegate control for improved transient response is treated in Kranik et al. (2005) and Gorzelic et al. (2012). A thorough treatment of engine modeling and control with MVEM is also found in Eriksson and Nielsen (2014). The actuator models developed in Papers 2-3 easily fit into the MVEM structure where they can be used to improve model accuracy and aid in the control design.

2.3.1 Surge modeling and control

Compressor surge is a well known mass flow instability phenomena that can occur when the pressure ratio over the compressor gets too large compared to the mass flow. Surge can be categorized in at least four different types: mild surge, classical surge, modified surge and deep surge (de Jager, 1995; Willems and de Jager, 1999). Among those only deep surge has reversed flow, and for co-surge studied in Papers 4-5, it is shown that reversed flow occurs.

A well known model to describe compressor surge is the Moore-Greitzer model (Greitzer, 1976, 1981), originally developed for axial flow compressors but shown to work also for centrifugal compressors in Hansen et al. (1981). A larger survey of modeling and control of surge is given in de Jager (1995), and a rich

treatment is also found in Grasdahl (1998). Most research has been done on axial flow turbo machinery with gas turbines, but there are few studies on automotive size turbos, where most utilize the Moore-Greitzer model, e.g. Ammann et al. (2001); Leufvén and Eriksson (2008). Recent studies on surge in automotive applications combine the Moore-Greitzer model with 1D gas-dynamic model for the pipes around the compressor (Galindo et al., 2008, 2011). Studies on surge in parallel turbo systems are scarcer. Although the phenomena is mentioned already in Watson and Janota (1982), it has not received much research attention. Papers 4-5 in this thesis contribute to this area with studies on modeling and control of surge in a parallel turbo configuration for automotive applications.

Experimental setups

This chapter describes two of the experimental setups used for measurements in the thesis, the engine laboratory (used in Papers 1-3), and the vehicle propulsion laboratory (used in Paper 5), both located at Vehicular Systems, Linköping University. A few measurements in Paper 2 and the measurements in Paper 4 have been done on a test track, for more information on these, see the respective papers. The chapter also gives a description of the external sensors used, i.e. non ECU.

3.1 The engine laboratory

The engine laboratory at Vehicular System consists of one test cell with two engine test stands. The engines of each test stand are connected to individual Schenck Dynas3-LI250 electric dynamometers from 2002 (rated speed of 10 krpm, rated power of 250 kW, and rated torque of 480 Nm). The measurements in Papers 1-3 in this thesis mainly originate from one of the engines, but with two different turbo installations. The engine is a GM LNF engine, a 2l, four cylinder, spark ignited petrol engine, with dual variable cam phasing.

The first installation has a single twin-scroll turbo, BW K04-2277, and is rated at 260 hp, 350 Nm. The wastegate for the turbine is actuated by overpressure controlled by a solenoid valve connected to boost pressure. The second installation uses a series sequential two-stage turbo system extended with actively controlled high pressure stage compressor by-pass, BW K04-2270 + BW KP35-1574. Both wastegates and the compressor bypass are actuated by underpressure, controlled by solenoid valves connected to a vacuum tank. The measurements for the development of the actuator model in Paper 2 was performed on the first installation. The last measurement in Paper 2

and all measurements in Paper 3 are performed on the second installation. Measurements on the electronic throttle for Paper 1 has been performed on both, but the throttle did not change between the installations.

The control system consists of a dSpace MicroAutoBox (MABx) and a RapidPro (RP) architecture. The code for the system is generated from a large Simulink model that is compiled using Real Time Workshop, and then executed on the MABx. Interaction with the control system is handled by the dSpace program ControlDesk running on the lab computer, that has also been used for the measurements.

3.2 The vehicle propulsion laboratory

For the measurements in Paper 5 the test vehicle is mounted in a chassis dynamometer. The system used is Rototest Energy 230 4WD, which consist of four mobile electric dynamometer units, power electronics and control system. In this application only two dynamometers have been used mounted to the two driven wheels of the test vehicle. The system has been used in constant speed mode where the dynamometers keep the desired speed of the vehicle as long as the required torque is within the limitations of the system. In the speed range 0-1000 rpm the limit for each axle is 1180 Nm continuous torque and 2200 Nm momentarily. Above that speed the system is limited by 124 kW continuous power and 230 kW momentarily per axle. For more information on the chassis dynamometer installation, functionality and performance, see Öberg et al. (2013). The measurement and control system used in these measurements is the same as in the engine lab, that was described in the previous section.

3.3 Sensor equipment and installation

In this section, the sensors used for measurements during the thesis are presented, with some installation details main characteristics. A description of the sensor operation on a more detailed level with the underlying physics is outside the scope of this thesis, and the interested reader is referred to e.g. Westbrook and Turner (1994); Lindahl and Sandqvist (1996); Fraden (2010).

3.3.1 Pressure

To measure actuator pressure in Paper 2 a production manifold pressure sensor (part number 9132374) with a range of 25-175 kPa absolute pressure was used. The sensor was connected to the hose between the pressure control valve and the actuator by a T coupling and a 50 cm long hose, $d = 6$ mm. In Paper 3 the actuator pressures are measured by sensors from Kistler, of either the 4260-series (4260A50, 340 kPa and 4260A75, 500 kPa, piezoresistive absolute pressure sensors, 0.05% Full Scale (FS) accuracy, 0.1% FS stability per year, 3 x FS proof pressure, $f_{\max} = 2$ kHz) or the 4295-series (4295A2 and 4295A2V, 200 kPa absolute pressure sensors). The pressure sensors were connected between the pressure control valves and the actuators by T couplings and 50-100 cm long

hoses, with diameter $d = 6$ mm. The Kistler sensors are also used to measure all pressures in Paper 5 with the exception of the intake manifold pressure, that is measured by the standard production sensor and received from the CAN bus. The hoses connecting the measurement point and the sensors for those measurements are 1.5-3 m, $d = 6$ mm. A short time delay is expected due to the pipe length. The pressure will propagate with the speed of sound through the pipe, which for this pipe diameter is almost the same as the velocity of sound in free air, see for example Vance (1932); Iemoto and Watanabe (2004); Bajsić et al. (2007). This translates to a maximum delay of less than 10 ms for 3 m of pipe, which is the sampling time of the measurements in Paper 5.

3.3.2 Mass flow

For mass flow measurements in Paper 4 and Paper 5, three mass airflow (MAF) sensors of hot film type are used. The total flow is measured with a Bosch sensor (part number 0 280 128 055) placed 10 cm after the air filter, 30 cm before the air path is divided. The two other, that measure the flow in each path, are Hitachi sensors (part number 12788131 / AFH60M-18). They are placed 10 cm after the division of the air path, approximately 80 cm before the compressors. Hot film MAF sensors are fast sensors with time constants of around 10 ms (Westbrook and Turner, 1994).

3.3.3 Turbo speed

Turbo speeds in Paper 5 are measured with Acam PicoTurn-BM V6, rotational speed measurement system for turbochargers. The system has a range of 200-400000 rpm and has been used with digital output giving one pulse per revolution of the turbocharger, with a 50 % duty cycle. The specified frequency precision is 0.009 % of full scale.

3.3.4 Position

The wastegate position in Paper 2 and the bypass position in Paper 3 is measured with a Duncan 9615 linear position sensor, range 0-38 mm, linearity ± 2 %, 135°C max temperature. The wastegate positions for Paper 3 are measured with Gill Blade 25 non-contact position sensors, range 0-25 mm, range accuracy ± 0.1 mm, 125°C max temperature. Measurement of throttle position is covered in Section 2.1.

References

- Tankut Acarman, Umit Ozguner, Cem Hatipoglu, and Anne-Marie Igusky. Pneumatic Brake System Modeling for System Analysis. *SAE Trans. J. of Commercial Vehicles*, V109-2, September 2001.
- Salem Al-Assidi, Jens Breiting, and Nathan Murphy. Model-Based Friction and Limp Home Compensation In Electronic Throttle Control. *Electronic Engine Controls*, SP-2003, April 2006.
- D. G. Alciatore and M. B. Histand. *Mechatronics and measurement systems*. McGraw-Hill, 2nd edition, 2003.
- M. Ammann, N. P. Fekete, A. Amstutz, and L. Guzzella. Control-Oriented Modeling of a Turbocharged Common-Rail Diesel Engine. In *Proc. of the Int. Conference on Control and Diagnostics in Automotive Applications*, 2001.
- Ivan Bajsić, Jože Kutin, and Tomaž Žagar. Response time of a pressure measurement system with a connecting tube. *Instrumentation Science and Technology*, 36:399–409, 2007.
- Miroslav Barić, Ivan Petrović, and Nedjeljko Perić. Neural network-based sliding mode control of electronic throttle. *Engineering Applications of Artificial Intelligence*, 18(8):951–961, June 2005.
- Yurij G. Borila. A Sequential Turbocharging Method for Highly-Rated Truck Diesel Engines. In *SAE World Congr.*, Techn. Paper 860074, February 1986.
- C. Canudas de Wit, H. Olsson, and K. J. Åström. A New Model for Control of Systems with Friction. *IEEE Trans. on Automatic Control*, 40(3):419–425, 1999.

- Carlos Canudas de Wit, Ilya Kolmanovsky, and Jing Sun. Adaptive Pulse Control of Electronic Throttle. In *Proc. of the American Control Conference*, June 2001.
- A. Chasse, P. Moulin, A. Albrecht, L. Fontvielle, A. Guinois, and L. Doléac. Double Stage Turbocharger Control Strategies Development. *SAE Int. J. of Engines*, 1(1):636–646, 2008.
- Alain Chevalier, Martin Müller, and Elbert Hendricks. On the Validity of Mean Value Engine Models During Transient Operation. In *SAE World Congr.*, Techn. Paper 2000-01-1261, March 2000.
- Ivan Criscuolo, Oskar Leufvén, Andreas Thomasson, and Lars Eriksson. Model-based boost pressure control with system voltage disturbance rejection. In *Proc. of the IFAC World Congr.*, pages 5058–5063, August 2011.
- Bram de Jager. Rotating stall and surge control: A survey. In *Proc. of the IEEE Conference on Decision and Control*, volume 2, pages 1857–1862, December 1995.
- Claude Delarue and Paolino Tona. Éditorial. *Oil & Gas Science and Technology - Rev. IFP*, 66(4):541–547, 2011. doi: <http://dx.doi.org/10.2516/ogst/2011149>.
- Joško Deur, Danijel Pavković, Martin Janszand, and Nedjeljko Perić. Automatic Tuning of Electronic Throttle Control Strategy. In *Mediterranean Conference on Control and Automation*, 2003a.
- Joško Deur, Danijel Pavković, Nedjeljko Perić, and Martin Jansz. An Electronic Throttle Control Strategy Including Compensation of Friction and Limp-Home Effects. In *Proc of the IEEE Int. Electric Machines and Drives Conference*, volume 1, pages 200–206, June 2003b.
- Joško Deur, Danijel Pavković, Nedjeljko Perić, Martin Jansz, and Davor Hrovat. An Electronic Throttle Control Strategy Including Compensation of Friction and Limp-Home Effects. *IEEE Trans. on Industry Applications*, 40(3):821–834, 2004.
- Mario di Bernardo, Alessandro di Gaeta, Umberto Montanaro, and Stefani Santini. Synthesis and Experimental Validation of the Novel LQ-NEMCSI Adaptive Strategy on an Electronic Throttle Valve. *IEEE Trans. on Control Systems Technology*, 18(6):1325–1337, November 2010.
- K.-D. Emmenthal, G. Hagermann, and W.-H. Hucho. Turbocharging small displacement spark ignited engines for improved fuel economy. In *SAE World Congr.*, Techn. Paper 790311, February 1979.
- Lars Eriksson. Modeling and Control of Turbocharged SI and DI Engines. *Oil & Gas Science and Technology - Rev. IFP*, 62(4):523–538, 2007.
- Lars Eriksson and Lars Nielsen. Non-linear Model-Based Throttle Control. *Electronic Engine Controls*, SP-1500:47–51, March 2000.

- Lars Eriksson and Lars Nielsen. *Modeling and Control of Engines and Drivelines*. John Wiley & Sons, 2014.
- Lars Eriksson, Simon Frei, Christopher Onder, and Lino Guzzella. Control and Optimization of Turbo Charged Spark Ignited Engines. In *Proc. of the IFAC World Congr.*, Barcelona, Spain, July 2002a.
- Lars Eriksson, Lars Nielsen, Jan Brugård, Johan Bergström, Fredrik Pettersson, and Per Andersson. Modeling of a turbocharged SI engine. *Annual Reviews in Control*, 26(1):129–137, October 2002b.
- Lars Eriksson, Tobias Lindell, Oskar Leufvén, and Andreas Thomasson. Scalable Component-Based Modeling for Optimizing Engines with Supercharging, E-Boost and Turbocompound Concepts. In *SAE World Congr.*, Techn. Paper 2012-01-0713, April 2012a.
- Lars Eriksson, Tobias Lindell, Oskar Leufvén, and Andreas Thomasson. Scalable Component-Based Modeling for Optimizing Engines with Supercharging, E-Boost and Turbocompound Concepts. *SAE Int. J. of Engines*, 5(2):579–595, May 2012b.
- Jacob Fraden. *Handbook of Modern Sensors: Physics, Designs, and Applications*. Springer, 4 edition, 2010.
- J. Galindo, J.R. Serrano, H. Climent, and A. Tiseira. Experiments and modelling of surge in small centrifugal compressor for automotive engines. *Experimental Thermal and Fluid Science*, 32(3):818–826, 2008.
- J. Galindo, H. Climent, C. Guardiola, and J. Domenech. Strategies for improving the mode transition in a sequential parallel turbocharged automotive diesel engine. *Int. J. of Automotive Technology*, 10(2):141–149, 2009a.
- J. Galindo, H. Climent, C. Guardiola, and J. Doménech. Modeling the Vacuum Circuit of a Pneumatic Valve System. *J. of Dynamic Systems, Measurement and Control*, 131(3), May 2009b.
- J. Galindo, H. Climent, C. Guardiola, and A. Tiseira. Assessment of a sequentially turbocharged diesel engine on real-life driving cycles. *Int. J. of Vehicle Design*, 49(1/2/3):214–234, 2009c.
- Jose Galindo, Francisco Arnau, Andres Tiseira, Ricardo Lang, Hamid Lahjaily, and Thomas Gimenes. Measurement and Modeling of Compressor Surge on Engine Test Bench for Different Intake Line Configurations. In *SAE World Congr.*, Techn. Paper 2011-01-0370, April 2011.
- Patrick Gorzelic, Erik Hellström, Anna Stefanopoulou, Li Jiang, and Srinath Gopinath. A Coordinated Approach for Throttle and Wastegate Control in Turbocharged Spark Ignition Engines. In *Proc of the Chinese Control and Decition Conference*, pages 1524–1529, May 2012.

- Jan Tommy Gravdahl. *Modeling and Control of Surge and Rotating Stall in Compressors*. PhD thesis, Norwegian University of Science and Technology, 1998.
- E.M. Greitzer. Surge and rotating stall in axial flow compressors-Part I: Theoretical compression system model. *J. of Engineering for Power*, 98(2):190–198, April 1976.
- E.M. Greitzer. The Stability of Pumping Systems. *J. of Fluids Engineering*, 103(1):193–242, June 1981.
- L. Guzzella, U. Wenger, and R. Martin. IC-Engine Downsizing and Pressure-Wave Supercharging for Fuel Economy. *SAE World Congr.*, March 2000.
- Lino Guzzella and Alois Amstutz. Control of Diesel Engines. *Control Systems*, 18(5):53–71, 1998.
- K.E. Hansen, P. Jørgensen, and P.S. Larsen. Experimental and Theoretical Study of Surge in a Small Centrifugal Compressor. *J. of Fluids Engineering*, 103(3):391–395, 1981.
- Elbert Hendricks. The Analysis of Mean Value Engine Models. In *SAE World Congr.*, Techn. Paper 890563, February 1989.
- Elbert Hendricks and Spencer C. Sorenson. Mean value modelling of spark ignition engines. *SAE Trans. J. of Engines*, 99(3):1359–1373, 1990.
- Elbert Hendricks and Thomas Vesterholm. The Analysis of Mean Value SI Engine Models. In *SAE World Congr.*, Techn. Paper 920682, February 1992.
- Elbert Hendricks, Thomas Vesterholm, and Spencer C. Sorenson. Nonlinear, closed loop, SI engine control observers. In *SAE World Congr.*, Techn. Paper 920237, February 1992.
- John B. Heywood. *Internal Combustion Engine Fundamentals*. McGraw-Hill series in mechanical engineering. McGraw-Hill, 1988. ISBN 0-07-100499-8.
- Klas Håkansson and Mikael Johansson. Modeling and Control of an Electro-Pneumatic Actuator System Using On/Off Valves. Master’s thesis, Linköpings University, SE-581 83 Linköping, 2007.
- Werner Huber, Bernd Lieberoth-Leden, Wolfgang Maisch, and Andreas Reppich. New Approaches to Electronic Throttle Control. In *SAE World Congr.*, Techn. Paper 910085, February 1991.
- Yu Iemoto and Yoshiaki Watanabe. Measurements of Phase Velocity of a Sound Wave Propagating in a Tube in Low Frequency Region. *Japanese J. of Applied Physics*, 43(1):401–402, 2004.
- Mrdjan Jankovic, Miroslava Jankovic, and Ilya Kolmonovsky. Robust nonlinear controller for turbocharged diesel engines. In *Proc. of the IFAC Symposium on Advances in Automotive Control.*, pages 1389–1394, June 1998.

- J.-P. Jensen, A. F. Kristensen, S. C. Sorenson, N. Houbak, and E. Hendricks. Mean Value Modeling of a Small Turbocharged Diesel Engine. In *SAE World Congr.*, Techn. Paper 910070, February 1991.
- Shugang Jiang and Michael H. Smith James Kitchen. Automatic Tuning of Two-Degree-of-Freedom PID Control for Engine Electronic Throttle System. *Engine Control and Calibration*, SP-2285, April 2010.
- Ronald Jurgen. *Automotive Electronics Handbook*. McGraw-Hill, 1994.
- Allan J. Kotwicki and John Russell. Vacuum EGR Valve Actuator Model. *New Techniques in SI and Diesel Engine Modeling*, SP-1366, 1998.
- Amey Y. Kranik, Julia H. Buckland, and Jim S. Freudenberg. Electronic Throttle and Wastegate Control for Turbocharged Gasoline Engines. In *Proc. of the American Control Conference*, volume 7, pages 4434–4439, June 2005.
- Oskar Leufvén and Lars Eriksson. Time to surge concept and surge control for acceleration performance. In *Proc. of the IFAC World Congr.*, pages 2063–2068, Seoul, Korea, July 2008.
- Oskar Leufvén and Lars Eriksson. A Surge and Choke Capable Compressor Flow Model - Validation and Extrapolation Capability. *Control Engineering Practice*, 21(12):1871–1883, 2013.
- Per Erik Lindahl and William Sandqvist. *Mätgivare, mätning av mekaniska storheter och temperatur*. Studentlitteratur, 1996.
- R. N. K. Loh, T. Pornthanomwong, J. S. Pyko, A. Lee, and M. N. Karsiti. Modeling, Parameters Identification, and Control of an Electronic Throttle Control (ETC) System. In *Proc of the IEEE Int. Conference on Intelligent and Advanced Systems*, pages 1029–1035, November 2007.
- Eberhard S. Mausner and Manfred Pfalzgraf. The VDO Modular Throttle Body Concept for Electronic Engine Control. In *SAE World Congr.*, Techn. Paper 900782, February 1990.
- A. Mehmood, S. Laghrouche, and M. El Bagdouri. Nonlinear Modeling of the VNT Pneumatic Actuator with Aero-dynamic Force. In *Proc. of the IFAC Symposium on Advances in Automotive Control*, July 2010.
- A. Mehmood, S. Laghrouche, and M. El Bagdouri. Modeling identification and simulation of pneumatic actuator for VGT system. *Sensors and Actuators A: Physical*, 165(2):367–378, 2011.
- Paul Moraal and Ilya Kolmanovsky. Turbocharger Modeling for Automotive Control Applications. In *SAE World Congr.*, Techn. Paper 1999-01-0908, March 1999.
- P.E. Moraal, I.V. Kolmanovsky, and M-J. van Nieuwstadt. Modeling and Identification of a Current to Vacuum Transducer and VNT actuator. In *Proc. of the IEEE/ASME Int. Conference on Advanced Intelligent Mechatronics*, Atlanta, USA, September 1999.

- P. Moulin, J. Chauvin, and B. Youssef. Modelling and Control of the Air System of a Turbocharged Gasoline Engine. In *Proc. of the IFAC World Congr.*, pages 8487–8494, July 2008.
- Philippe Moulin and Jonathan Chauvin. Modeling and control of the air system of a turbocharged gasoline engine. *Control Engineering Practice*, 19(3):287–297, 2011.
- Martin Müller. Estimation and Control of Turbocharged Engines. In *SAE World Congr.*, Techn. Paper 2008-01-1013, April 2008.
- Martin Müller, ELbert Hendricks, and Spencer C. Sorenson. Mean Value Modelling of Turbocharged Spark Ignition Engines. *Modeling of SI and Diesel Engines*, SP-1330, 1998.
- Per Öberg, Peter Nyberg, and Lars Nielsen. A New Chassis Dynamometer Laboratory for Vehicle Research. *SAE Int. J. Passeng. Cars - Electron. Electr. Syst.*, 6(1):152–161, May 2013.
- H. Olsson, K.J. Åström, C. Canudas de Wit, M. Gäfvert, and P. Lischinsky. Friction Models and Friction Compensation. *European J. of Control*, 4(3): 176–195, 1998.
- Ümit Özgüner, Sulgi Hong, and Yaodong Pan. Discrete-time Sliding Mode Control of Electronic Throttle Valve. In *Proc. of the IEEE Conference on Decision and Control*, December 2001.
- Yaodang Pan, Ümit Özgüner, and Oğuz Hasan Dağci. Variable-Structure Control of Electronic Throttle Valve. *IEEE Trans. on Industrial Electronics*, 55(11): 3899–3907, 2008.
- Danijel Pavković and Joško Deur. *Modeling and Control of Electronic Throttle Drive*. LAP LAMBERT Academic Publishing, 2011. ISBN 978-3-8443-1628-5.
- Danijel Pavković, Joško Deur, Martin Janszand, and Nedjeljko Perić. Self-tuning Control of an Electronic Throttle. In *Proc. of the IEEE Conference on Control Applications*, pages 149–154, June 2003.
- Danijel Pavković, Joško Deur, Martin Jansz, and Nedjeljko Perić. Adaptive control of automotive electronic throttle. *Control Engineering Practice*, 14(2): 121–136, 2006.
- Dominique Petitjean, Luciano Bernardini, Chris Middlemass, S. M. Shahed, and Ronald G. Hurley. Advanced Gasoline Engine Turbocharging Technology for Fuel Economy Improvements. In *SAE World Congr.*, Techn. Paper 2004-01-0988, March 2004.
- K. J. Åström. Theory and applications of adaptive control – A survey. *Automatica*, 19(5):471–486, 1983.

- Edmond Richer and Yildirim Hurmuzulu. A High Performance Pneumatic Force Actuator System: Part I–Nonlinear Mathematical Model. *J. of Dynamic Systems, Measurement and Control*, 122(3):416–425, June 1999.
- R. Scattolini, C. Siviero, M. Mazzucco, S. Ricci, R. Poggio, and C. Rossi. Modeling and Identification of an Electromechanical Internal Combustion Engine Throttle Body. *Control Engineering Practice*, 5(9):1253–1259, 1997.
- Spencer C. Sorenson, Elbert Hendricks, Sigurjon Magnusson, and Allan Bertelsen. Compact and Accurate Turbocharger Modelling for Engine Control. In *SAE World Congr.*, Techn. Paper 2005-01-1942, April 2005.
- Richard Stone. *Introduction to internal combustion engines*. Palgrave Macmillan, 4th edition, 2012.
- Hans-Martin Strieb and Hubert Bischof. Electronic Throttle Control (ETC): A Cost Effective System for improved Emissions, Fuel, and Driveability. In *SAE World Congr.*, Techn. Paper 960338, February 1996.
- Viktor Szente and János Vad. Computational and Experimental Investigation on Solenoid Valve Dynamics. In *Proc. of the IEEE/ASME Int. Conference on Advanced Intelligent Mechatronics*, volume 1, pages 618–623, July 2001.
- Andreas Thomasson. Wastegate Actuator Modeling and Tuning of a PID Controller for Boost Pressure Control. Master’s thesis, Linköping University, SE-581 83 Linköping, 2009.
- Andreas Thomasson and Lars Eriksson. Model-Based Throttle Control using Static Compensators and IMC based PID-Design. In *Proc. of the E-COSM*, Paris, France, 2009.
- Andreas Thomasson and Lars Eriksson. Modeling and Control of Co-Surge in Bi-Turbo Engines. In *Proc. of the IFAC World Congr.*, Milano, Italy, 2011a.
- Andreas Thomasson and Lars Eriksson. Model-Based Throttle Control using Static Compensators and Pole Placement. *Oil & Gas Science and Technology - Rev. IFP*, 66(4):717–727, 2011b.
- Andreas Thomasson and Lars Eriksson. Co-Surge Detection and Control for Bi-Turbo Engines with Experimental Evaluation. In *Proc. of the IFAC Symposium on Advances in Automotive Control*, Tokyo, Japan, 2013.
- Andreas Thomasson and Lars Eriksson. Co-Surge in Bi-Turbo Engines - Measurements, Analysis and Control. *Submitted to Control Engineering Practice*, 2014.
- Andreas Thomasson, Lars Eriksson, Oskar Leufvén, and Per Andersson. Wastegate Actuator Modeling and Model-Based Boost Pressure Control. In *Proc. of the E-COSM*, Paris, France, 2009.

- Andreas Thomasson, Lars Eriksson, Tobias Lindell, James Peyton Jones, Jill Spelina, and Jesse Frey. Tuning and experimental evaluation of a likelihood-based engine knock controller. In *Proc. of the IEEE Conference on Decision and Control*, Florence, Italy, 2013a.
- Andreas Thomasson, Oskar Leufvén, Ivan Criscuolo, and Lars Eriksson. Modeling and validation of a boost pressure actuation system, for a series sequentially turbocharged SI engine. *Control Engineering Practice*, 21(12):1860–1870, 2013b.
- R. Tudor. Electronic Throttle Control as an Emission Reduction Device. In *SAE World Congr.*, Techn. Paper 930939, March 1993.
- R. B. van Varseveld and G. M. Bone. Accurate Position Control of a Pneumatic Actuator Using On/Off Solenoid Valves. *IEEE/ASME Trans. on Mechatronics*, 2(3):195–204, 1997.
- Charles B. Vance. Velocity of sound in tubes at audible and ultrasonic frequencies. *Physical Review*, 39:737–744, February 1932.
- M. Vašak, M. Baotić, M. Morari, I. Petrović, and N. Perić. Constrained optimal control of an electronic throttle. *Int. J. of Control*, 79(5):465–478, 2006.
- Mario Vašak, Ivan Petrović, and Nedjeljko Perić. State Estimation of an Electronic Throttle Body. In *IEEE Int. Conference on Industrial Technology*, volume 1, pages 472–477, December 2003.
- Mario Vašak, Mato Baotić, Ivan Petrović, and Nedjeljko Perić. Hybrid Theory-Based Time-Optimal Control of an Electronic Throttle. *IEEE Trans. on Industrial Electronics*, 54(3):1483–1494, 2007.
- Jihong Wang, Junscheng Pu, and Philip Moore. A practical control strategy for servo-pneumatic actuator systems. *Control Engineering Practice*, 12(12):1483–1488, 1999.
- N. Watson and M.S. Janota. *Turbocharging the Internal Combustion Engine*. The Macmillan Press ltd, 1982. ISBN 0-333-24290-4.
- M.H. Westbrook and J.D. Turner. *Automotive sensors*. IOP Publishing, 1994.
- Frank Willems and Bram de Jager. Modeling and Control of Compressor Flow Instabilities. *Control Systems*, 19, 1999.
- Fulin Xiang and Jan Wikander. Block-oriented approximate feedback linearization for control of pneumatic actuator system. *Control Engineering Practice*, 12(4):387–399, April 2004.
- G. Zito, P. Tona, and P. Lassami. "The Throttle Control Benchmark". In *Proc. of the E-COSM*, November 2009.

Papers

Model-Based Throttle Control using Static Compensators and Pole Placement[†]

Andreas Thomasson and Lars Eriksson

*Vehicular Systems, Department of Electrical Engineering,
Linköping University, SE-581 83 Linköping, Sweden.*

[†]This is a formatted version of “Model-Based Throttle Control using Static Compensators and Pole Placement” by Andreas Thomasson and Lars Eriksson, *Oil & Gas Science and Technology - Rev. IFP Energies nouvelles*, Volume 66, Number 4, pages 717-727. ©IFP Energies nouvelles 2011. Reproduced with the permission of IFP Energies nouvelles. The original paper can be found at ogst.ifpenergiesnouvelles.fr, <http://ogst.ifpenergiesnouvelles.fr>, and can be found using the Digital Object Identifier (DOI): 10.2516/ogst/2011137. The formatting is restricted to changing the article into a single-column format, adjusting sizes of figures and tables, and adjusting the referencing style.

Abstract

In modern spark ignited engines the throttle is controlled by the electronic control unit (ECU), which gives the ECU direct control of the air flow and thereby the engine torque. This puts high demands on the speed and accuracy of the controller that positions the throttle plate. The throttle control problem is complicated by two strong nonlinear effects, friction and limp-home torque. This paper proposes the use of two, simultaneously active, static compensators to counter these effects and approximately linearize the system. A PID controller is designed for the linearized system, where pole placement is applied to design the PD controller and a gain scheduled I-part is added for robustness against model errors. A systematic procedure for generating compensator and controller parameters from open loop experiments is also developed. The controller performance is evaluated both in simulation, on a throttle control benchmark problem, and experimentally. A robustness investigation pointed out that the limp-home position is an important parameter for the controller performance, this is emphasized by the deviations found in experiments. The proposed method for parameter identification achieves the desired accuracy.

Introduction

An electronic throttle is a DC-servo that controls the throttle plate in modern spark ignited (SI) engines. The position of the throttle plate controls the air-flow to the engine and hence the engine torque. As a consequence this servo is a very important component in a vehicle since it affects the vehicle driveability.

Throttle control design is challenging due to two non-linearities, friction and limp-home torque, which effects the throttle plate motion. Strategies for overcoming these difficulties have been addressed in several papers. A model based friction compensator was presented in Eriksson and Nielsen (2000) and a nonlinear control strategy with both friction and limp-home compensation is proposed in Deur et al. (2004). Another approach was made in Vařak et al. (2006), where a control law based on the solution of an optimal control problem was demonstrated.

This paper makes use of friction and limp-home compensators that are static functions of the measured throttle position and reference value, to remove most non-linearities. This is a combination of ideas presented in Eriksson and Nielsen (2000) and Deur et al. (2004). The proposed controller uses a Coulomb friction model, which is less complex than the friction models usually proposed in the literature, and a PID-controller with fewer degrees of freedom. This gives fewer parameters which simplifies the tuning procedure. With these simplifications the controller fulfills the requirements in the TC benchmark problem in Zito et al. (2009), similar to those in Deur et al. (2004).

A systematic tuning procedure is described that utilize ramp and step responses in control signal. The PD-controller is tuned using pole placement, to give a first order behavior with a desired rise time to the linearized system. A robustness investigation is made to analyze the sensitivity to parameter variations. This shows that an accurate estimation of the limp-home position is needed, and a calibration procedure to assure this is suggested.

In the next section a simplified model for an electronic throttle is presented with the aim of controller design. Section 2 describes the controller structure and its three main parts: friction compensator, limp-home compensator and PID-controller. In section 3, a procedure for identifying the controller parameters are discussed. The controller performance and robustness to parameter variations is verified in simulation on the benchmark model in section 4, and experimentally on a throttle in section 5.

1 Control oriented throttle model

In this section the throttle model that is used to design the controller in section 2 is presented. Figure 1 shows a sketch of the throttle system. The control signal is transformed to a PWM signal by the chopper that is connected to the DC motor. The motor torque is transferred to the throttle plate axle through a gearbox (not shown in figure). The return spring exercises a torque on the throttle plate that pulls it toward the limp-home position.

A process model for the electronic throttle body is shown in figure 2, see Scatoloni et al. (1997); Deur et al. (2004). The model is a standard linear electric

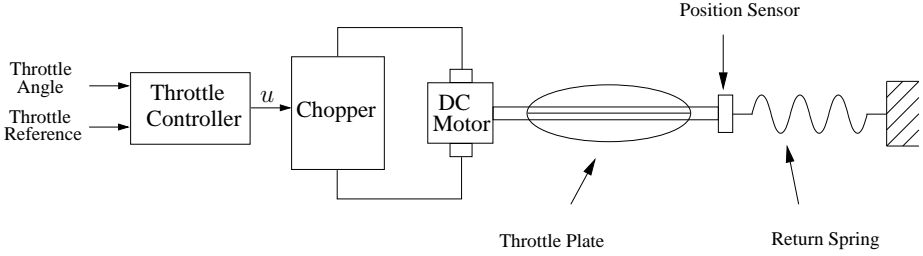


Figure 1: A schematic of the electronic throttle and controller. Main parts are the controller (which is part of the ECU), chopper, DC motor, throttle plate, return spring and position sensor.

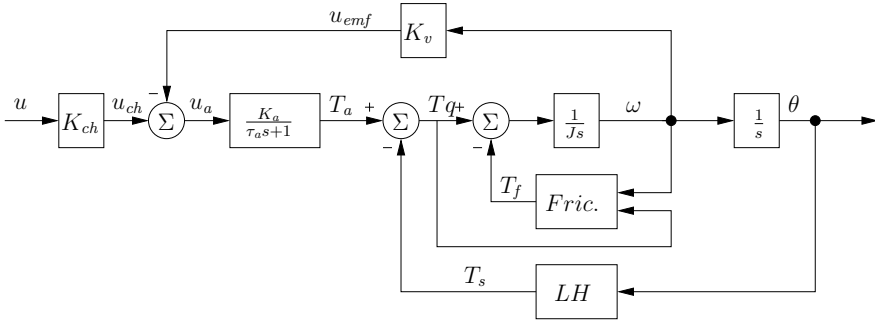


Figure 2: Process model for the electronic throttle. The torque contributions on the throttle plate are the armature torque, T_a , the friction torque, T_f , and the spring torque, T_s . The armature is modeled by a first order system with gain K_a and time constant τ_a . The chopper and back electromotive torque are modeled with the proportional gains, K_{ch} and K_v , from the control signal and throttle plate angular velocity, u and ω , respectively.

dc-motor, augmented with friction and limp-home torque components. The chopper is modeled with a proportional gain. The armature time constant, τ_a , is typically very small, approximately 1 ms (Deur et al., 2004). This effect is therefore neglected for the purpose of controller design. The armature torque can then be divided in

$$T_a = K_a K_{ch} u - K_a K_v \omega = T_u - T_{emf}$$

The torque acting on the throttle plate is thus composed of four main parts. The driving torque from the DC motor, T_u , the spring torque, T_s , the friction torque, T_f , and the back electromotive torque, T_{emf} . The friction torque is further divided into a static and dynamic part, T_{fs} and T_{fv} . After modeling the separate torque contributions, the equations of motion for the throttle plate are given by Newtons second law.

$$\dot{\theta} = \omega \quad (1a)$$

$$J\dot{\omega} = T_u - T_s - T_{fs} - T_{fv} - T_{emf} \quad (1b)$$

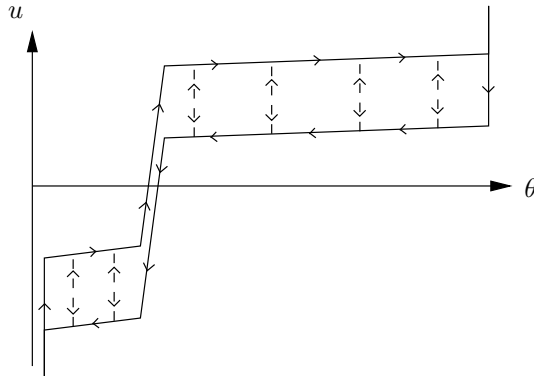


Figure 3: Sketch of the static nonlinearities for the electronic throttle. Arrows indicate the direction of movement. The influence of friction and the nonlinear spring torque is clearly seen. Compare with the measured curve shown in figure 8.

Both the static friction and limp-home nonlinearity can be seen from the process static curve illustrated in figure 3. This curve can be estimated by performing a slow ramp in the control signal while measuring the response in throttle position. The influence of friction is clearly seen from the difference in the ramp up and down in control signal. The static friction is modeled using the classical Coulomb friction model (2), Olsson et al. (1998). The friction torque is equal to the applied torque, T , when $\omega = 0$ and the applied torque is less than the Coulomb friction, T_c . Otherwise the friction torque is equal to Coulomb friction in the opposite direction of motion.

$$T_{fs}(T, \omega) = \begin{cases} T & \text{if } \omega = 0 \text{ and } |T| < T_c \\ T_c \text{sgn}(\omega) & \text{otherwise} \end{cases} \quad (2)$$

Several papers suggest the use of more complex, dynamic friction models, and to include Stribeck effect. The Coulomb friction model is chosen because it is simpler and has fewer parameters, whilst it proved to be sufficient for the controller design to meet all benchmark requirements in Zito et al. (2009), similar to those in Deur et al. (2004).

The limp-home nonlinearity comes from the springs that pull the throttle plate toward the limp-home position. The spring torque is piecewise linear but the spring constant differs greatly, depending on whether the throttle plate is inside or outside of the limp-home region. The slope of the $u(\theta)$ curve is almost flat above and below the limp-home region, with a very sharp transition between them. There is approximately 30% increase in the control signal from fully closed to fully open throttle, where about 20% is in a narrow region of $0.5\text{-}2^\circ$ around the limp-home position. The spring torque is therefore described as the

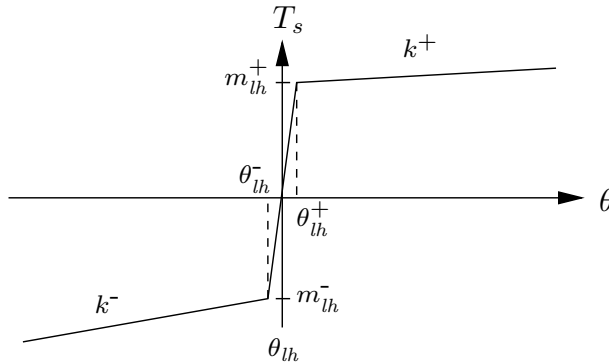


Figure 4: A graphical representation of the model for the spring torque, which is a piecewise linear function of the throttle position.

piecewise linear function in the equation below and is illustrated in figure 4.

$$T_s(\theta) = \begin{cases} m_{lh}^+ + k^+(\theta - \theta_{lh}^+) & \text{if } \theta > \theta_{lh}^+ \\ m_{lh}^+(\theta - \theta_{lh}) / (\theta_{lh}^+ - \theta_{lh}) & \text{if } \theta_{lh}^- < \theta \leq \theta_{lh}^+ \\ m_{lh}^-(\theta_{lh} - \theta) / (\theta_{lh} - \theta_{lh}^-) & \text{if } \theta_{lh}^- < \theta \leq \theta_{lh} \\ m_{lh}^- - k^-(\theta_{lh}^- - \theta) & \text{if } \theta \leq \theta_{lh}^- \end{cases} \quad (3)$$

The models for viscous friction and electromotive torque are both linear functions in angular velocity acting in the opposite direction of motion. They are lumped into a single torque model.

$$T_{fv} + T_{emf} = K_{fv}\omega \quad (4)$$

Combining (1), (2), (3), and (4), gives the differential equation for the throttle plate angular velocity.

$$J\dot{\omega} = -K_{fv}\omega - T_s(\theta) - T_{fs}(T, \omega) + Ku \quad (5)$$

The complete model is shown as a block diagram in figure 5. This model captures most essential parts of the throttle dynamics and form the basis for the controller structure.

2 Controller structure

To linearize the system in (5), a nonlinear compensator block that modifies the control signal u is proposed. The main idea is to choose the control signal as

$$u = \frac{T_s(\theta)}{K} + \frac{T_{fs}(T, \omega)}{K} + \tilde{u} \quad (6)$$

which would be an exact linearization of (5). This is not possible due to several reasons, but can be done approximately by the compensator blocks described in the two following sections. The linearized system is then controlled by a slightly modified PID-controller described in sections 2.4 and 2.5.

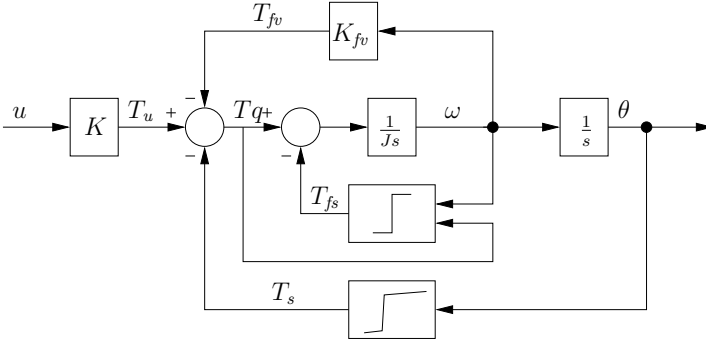


Figure 5: A block diagram showing the simplified process model. The model captures the most important throttle dynamics and is the basis for the controller structure.

2.1 Limp-home compensator

To exactly counter the limp-home torque this block would use (3) directly. Small variations in the measured output close to the limp-home position would then result in severe chattering of the control signal due to the large slope in the static curve in this region. To overcome this, the commanded throttle reference, θ_{ref} , is used as input to (3) instead of the measured position. As long as the reference itself does not vary rapidly around the limp-home position this will prevent the limp-home compensator from causing chattering in the control. Effectively this is a feedforward with the inverse static gain of the system as output.

2.2 Friction compensator

Based on (2) the compensator would be an ideal relay that switches sign around $\omega = 0$. This creates a problem with estimating the speed and direction of the throttle plate motion based on the position measurements. It is also not beneficial if the throttle plate currently is moving away from the reference value and the friction compensator add to that motion. Instead the friction compensator is based directly on the tracking error and compensation is made in the direction that reduces the tracking error. An ideal relay function would be very sensitive to noise around $e_\theta = 0$ and would also cause undesirable oscillations around the reference value. This problem is solved with a small dead zone around the reference value and a smooth transition when e_θ increases. The dead zone radius is denoted θ_d and the width of the transition θ_r , see figure 6 and equation (7).

$$\tilde{T}_f(e_\theta) = \begin{cases} 0 & \text{if } |e_\theta| \leq \theta_d \\ \tilde{T}_c \frac{\theta - \theta_d}{\theta_r} \text{sgn}(e_\theta) & \text{if } \theta_d < |e_\theta| \leq \theta_r + \theta_d \\ \tilde{T}_c \text{sgn}(e_\theta) & \text{if } |e_\theta| > \theta_r + \theta_d \end{cases} \quad (7)$$

When the throttle plate is close to the reference value a large part of the control signal comes from the friction compensator block. If the Coulomb friction were underestimated the rise time could get unnecessary long after small changes in

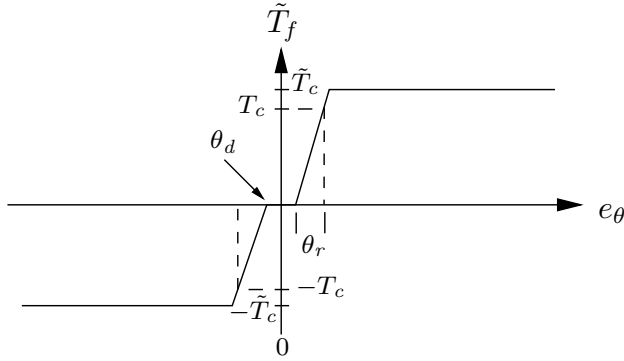


Figure 6: The friction compensation is implemented as a static function of the tracking error. A small dead zone and a smooth transition is used around $e_\theta = 0$ to make the compensation less sensitive and avoid oscillations close to the reference value.

reference position. To make sure that the friction compensator overcomes the Coulomb friction the maximum amplitude of the compensator block is increased to $\tilde{T}_c = T_c * k$, where k is slightly larger than one. Also the Coulomb friction is different above and below the limp-home position and its values are distinguished by T_c^+ and T_c^- respectively.

The limp-home and friction compensators are used to modify the control signal according to (8), where \tilde{u} is the output from the PID-controller described next.

$$u = \frac{T_s(\theta_{ref})}{K} + \frac{\tilde{T}_f(e_\theta)}{K} + \tilde{u} \quad (8)$$

2.3 The linearized system

With the control signal selected according to (8) and the compensators in section 2.1 and 2.2, the system is approximately linear and given by the equation

$$J\dot{\omega} = -K_{fv}\omega + K\tilde{u} \quad (9)$$

To simplify notation the equation is normalized by K_{fv} and the parameters $T_0 = \frac{J}{K_{fv}}$ and $K_0 = \frac{K}{K_{fv}}$ are introduced. The resulting differential equation is

$$T_0\dot{\omega} = -\omega + K_0\tilde{u} \quad (10)$$

and the resulting transfer function from \tilde{u} to θ is

$$\theta(s) = \frac{K_0}{s(T_0s + 1)}\tilde{u}(s) \quad (11)$$

The throttle position is normalized to $[0, 100]$ and the control signal is normalized to $[-100, 100]$.

2.4 PID design using pole placement

To avoid hitting the mechanical stops at the end positions, the response to a reference step should have no overshoot. The parameter T_0 in equation (11) is typically small, in the order of a few samples of the controller, and the system is simplified to

$$\theta(s) = \frac{K_0}{s} \tilde{u}(s) = G(s) \tilde{u}(s) \quad (12)$$

with $G(s) = K_0/s$ for synthesis. To avoid overshoot we desire the closed loop system to have a first order behavior, and use pole placement to design the controller (Rivera et al., 1986; Åström and Hägglund, 2006). For the system in (12) this results in a P-controller. The the closed loop system is given by

$$G_c(s) = \frac{1}{\frac{1}{K_p K_0} s + 1} = \frac{1}{\lambda s + 1} \quad (13)$$

with $K_p = \frac{1}{K_0 \lambda}$, where the tuning parameter λ is the desired rise time. This rise time will of course only be achieved when the control signal does not saturate. If the product $K_0 \cdot \lambda$ is smaller than about one this will unfortunately be the case for larger reference steps.

Using only a P-controller have however shown to give overshoots, most likely due to the approximate linearization and model uncertainties. A derivative part is included in the feedback loop to overcome this. The controller equation and corresponding closed loop system becomes

$$\tilde{u}(s) = K_p(\theta_{ref}(s) - \theta(s)) - K_d s \theta(s) \quad (14a)$$

$$G_c(s) = \frac{1}{\frac{1+K_d K_0}{K_p K_0} s + 1} = \frac{1}{\lambda s + 1} \quad (14b)$$

$$\lambda = \frac{1 + K_d K_0}{K_p K_0} \quad (14c)$$

This is the same closed loop system as with only a P-controller, but with an extra degree of freedom that can be used to adjust the trade-off between the sensitivity function, S , and complementary sensitivity function, T , according to

$$S(s) = \frac{\frac{1}{K_p K_0} s}{\frac{1+K_d K_0}{K_p K_0} s + 1} = \frac{\frac{1}{K_p K_0} s}{\lambda s + 1} \quad (15a)$$

$$T(s) = \frac{\frac{K_d}{K_p} s + 1}{\frac{1+K_d K_0}{K_p K_0} s + 1} = \frac{\frac{K_d}{K_p} s + 1}{\lambda s + 1} \quad (15b)$$

For a given desired rise time λ , increasing K_d will increase K_p due to (14c), which will decrease the sensitivity function. At the same time the complementary sensitivity function will increase since $S + T = 1$. The strategy for tuning the PD-controller is discussed in section 3.2.

In the control system the position derivative in (14a) has to be estimated from discrete measurements. To reduce the sensitivity to measurement noise

the derivative is approximated with the filtered difference

$$D_y(z) = \frac{(1 - \gamma)(1 - z^{-1})}{1 - \gamma z^{-1}} Y(z) \quad (16)$$

where $D_y(z)$ is the derivative approximation and $Y(z)$ is the measured output. The filter coefficient, γ , has to be chosen to give the filter a cut-off frequency that is above the frequency range where a reduction in the sensitivity function is desired.

2.5 A modified I-part

A prerequisite to get the closed loop system behavior in (13) is that the model is correct. Even with a correct model the approximations in the linearization or input disturbances etc. could result in a stationary tracking error. To compensate for this an I-part is added to the controller. The integrator gain K_i is gain scheduled. It is small when the error is large and increases with decreasing error. This helps to quickly overcome model errors for small changes in reference and prevent overshoot for relatively small steps, that could otherwise result from the large integrator gain.

To prevent wind-up the integrator is turned off when the control signal saturates. One reset condition is also used, that is for reference steps larger than 0.5%. This was introduced because a nonzero integrator before a small reference step, where the control signal does not saturate, was causing overshoot. For this controller, with a sampling rate of 1 ms, a ramp in reference with a change of 0.5% per sample corresponds to a change from fully closed to fully open throttle in 0.2 s, which is on the edge of what is possible to achieve in a step (see figure 11). The integrator would not improve tracking for this rapid change in reference, implying that the reset condition will not have a negative effect on tracking performance. For a lower sampling rate this threshold would have to be increased accordingly. Other standard anti-windup schemes, e.g. tracking Åström and Hägglund (2006), were tried for this controller with slightly worse result, but could be an alternative.

The error input to the integrator is also modified. When the tracking error is smaller than half the resolution of the position measurement, the error is set to zero. A block diagram of the implemented controller structure is shown in figure 7.

3 Identification and controller tuning

In order to be able to automate the controller parametrization, two experiments are proposed. The experiments are designed to identify the model parameters that directly give the controller parameters in the model-based controller. Both compensator blocks are identified from a ramp response in control signal described in section 3.1, while the PD-parameters are determined using open and closed loop step responses, described in section 3.2.

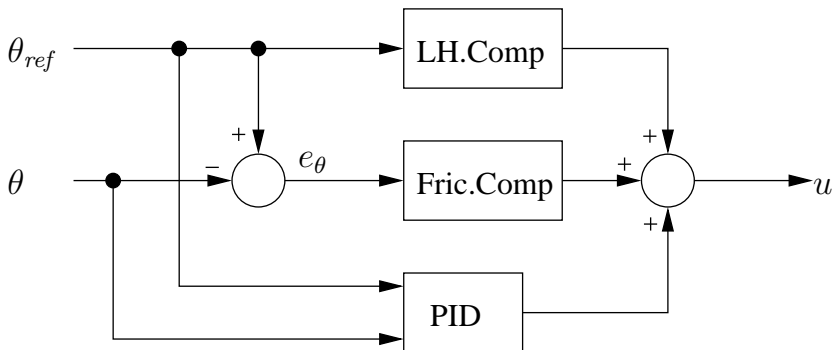


Figure 7: A block diagram of the controller structure. The control signal u is the sum of the outputs from the compensator blocks and the PID-controller.

3.1 The static compensators - ramp response

Both the friction and limp-home nonlinearities are estimated from the process static curve that was illustrated in figure 3. This characteristic can be measured by doing a slow ramp response up and down in the throttle control signal, see figure 8. The proposed method for calculating the limp-home and friction compensators identifies the points A_1 - A_4 and B_1 - B_4 marked in the figure by fitting a piecewise linear function to each ramp.

The coulomb friction in the friction compensator block is estimated as half the distance between the two curves. The values above and below the limp-home position are calculated as

$$T_c^- = \frac{u(A_1) - u(B_1) + u(A_2) - u(B_2)}{4} \quad (17a)$$

$$T_c^+ = \frac{u(A_3) - u(B_3) + u(A_4) - u(B_4)}{4} \quad (17b)$$

The dead zone and transition in the friction compensator should be made small to get precise control for small changes in reference. Making them too small however can cause oscillations around the reference value. In simulation and experimentally $\theta_d \approx 0.1\%$ and $\theta_r \approx 0.5\%$ have proved to work satisfactory.

The equations for calculating the parameters in the limp-home compensator are given in (18). For this specific throttle the slope below the limp home position is only slightly higher than the slope above, but this difference can be

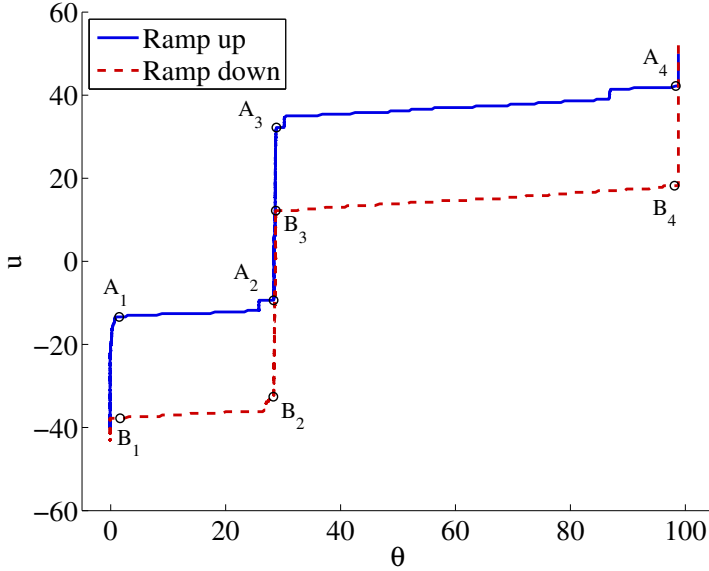


Figure 8: Measured ramp response in throttle position, the solid line (blue) is when u is increasing and the dashed line (red) when u is decreasing. The marked points A1-A4 and B1-B4 are used in the calibration procedure when calculating the friction and limp-home compensators.

larger, see for example Scattolini et al. (1997); Pavković et al. (2006).

$$\theta_{lh} = \frac{\theta(A_2) + \theta(A_3) + \theta(B_2) + \theta(B_3)}{4} \quad (18a)$$

$$\theta_{lh}^- = \frac{\theta(A_2) + \theta(B_2)}{2} \quad (18b)$$

$$\theta_{lh}^+ = \frac{\theta(A_3) + \theta(B_3)}{2} \quad (18c)$$

$$m_{lh}^- = \frac{u(A_2) + u(B_2)}{2} \quad (18d)$$

$$m_{lh}^+ = \frac{u(A_3) + u(B_3)}{2} \quad (18e)$$

$$k^- = \frac{u(A_2) - u(A_1)}{\theta(A_2) - \theta(A_1)} \quad (18f)$$

$$k^+ = \frac{u(A_4) - u(A_3)}{\theta(A_4) - \theta(A_3)} \quad (18g)$$

3.2 P and D parameters - step response

After the static curve has been determined a step response is made to identify the linear process dynamics. Starting with the throttle in the limp-home position the control signal is ramped up until the position is slightly larger than θ_{lh}^+ . Then

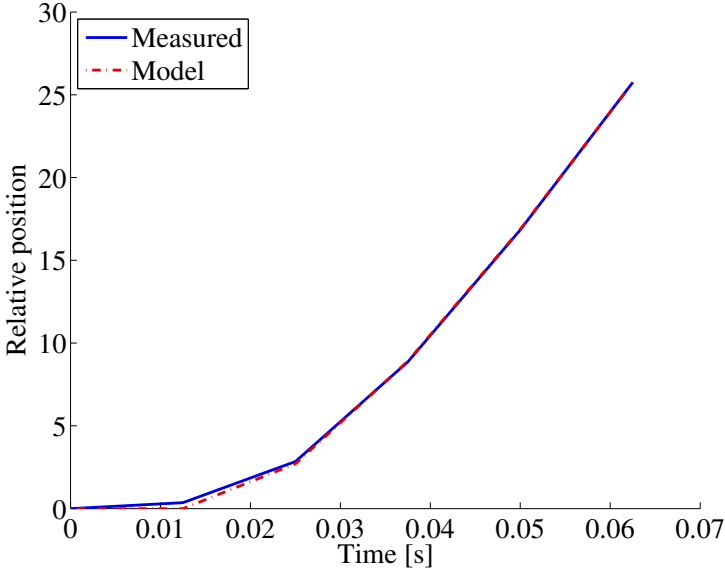


Figure 9: A measured step response together with simulation of the adapted process model. The initial position before the step has been set to zero.

a step in control signal is applied and the position response is measured. The parameters in (11) are fitted with the least mean squares method to the step response. A measured step response and the adapted model can be seen in figure 9.

How to choose λ

The tuning parameter λ gives the rise time of the closed loop system. This can be translated into an arbitrary demand of the form “within X % in t seconds” by considering the step response of the system in (13) to a unit step.

$$y(t) = 1 - e^{-t/\lambda} \quad (19)$$

Setting $y(t) = 1 - X$ and solving for λ gives

$$\lambda = \frac{-t}{\ln(X)} \quad (20)$$

As was previously mentioned, this is only true when the control signal does not saturate. The increase in rise time due to signal saturation during large reference steps could be somewhat compensated for by decreasing λ . This will saturate the control signal for a longer period of time than with the original setting, thereby making up for lost time at the end of the step response, but is limited by the shortest possible rise time achieved with a saturated signal. Making λ too small will make the PD-controller sensitive to measurement noise and make it use unnecessary large controller output.

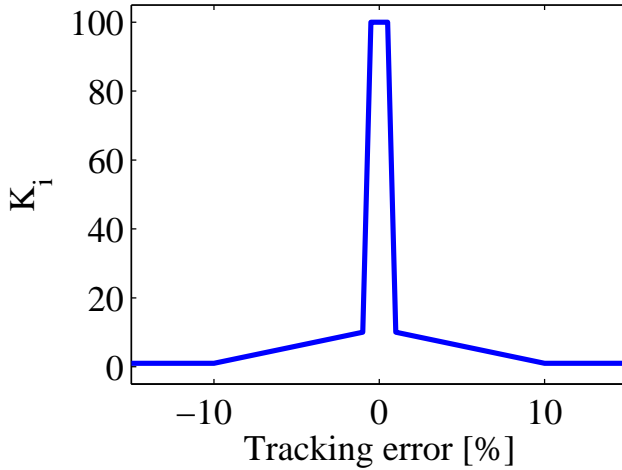


Figure 10: The integrator gain as a function of the tracking error. The large integrator gain close to zero tracking error help to quickly overcome modeling errors for small reference steps.

The K_p and K_d parameters

Once λ is fixed, the relation between K_p and K_d is given by equation (14c) from section 2.4, restated here

$$\lambda = \frac{1 + K_d K_0}{K_p K_0} \quad (21)$$

Start by setting $K_d = 0$ and do a reference step. Increase K_d until an acceptable response is achieved, fine tuning can be done but is not necessary for the cases studied here. If λ is too low, the desired rise time might not be achievable without overshoot. In that case λ has to be increased and the process of selecting K_p and K_d restarted.

The filter coefficient γ

The filter coefficient in (16) depend on the desired bandwidth of the filter and the sampling time of the controller. In the implementation $\gamma = 0.7$ is used, which for a sampling time of 1 ms gives the filter a settling time (within 5% of end value) of less then 10 ms. This has proved to work satisfactory in simulations and experiments.

3.3 The I-part

As described in section 2.5 the I-part of the controller is gain scheduled, using the tracking error to determine the integrator gain K_i . When $|e_\theta|$ is larger than 10%, the integrator gain is small, $K_i = 1$. As $|e_\theta|$ decreases from 10% to 1%, K_i increases linearly from 1 to 10. From that point K_i increases to 100 at $|e_\theta| = 0.5\%$ and remains constant when $|e_\theta| \leq 0.5\%$, se figure 10.

Table 1: Controller parameters identified with the two experiments on the throttle control benchmark model.

K_p	7.36	θ_{lh}	11.1	m_{lh}^-	-10.9
K_d	0.03	θ_{lh}^+	11.3	k^+	0.051
T_c^+	8.76	θ_{lh}^-	10.9	k^-	0.065
T_c^-	6.83	m_{lh}^+	9.03		

Table 2: Performance measures for the tests defined in the TC benchmark (integral square error).

A1.1	A1.2	A1.3	A2.1	A2.2	A3.1	A3.2
835	150	20.0	0.17	0.13	1113	507

4 Simulation results on TC benchmark model

The procedure described in section 3 has been performed on the benchmark model provided by E-COSM'09, Zito et al. (2009), and resulted in the controller parameters in table 1.

The controller performance is evaluated using the different reference signals provided by the benchmark model. These include a series of steps, ramps, and more arbitrary signals. Two different sized step responses are shown in figure 11. For the large step the controller saturates the control signal until almost within 10% of the reference which indicates that the step response could not get much faster and the overshoot is less then 0.25%. For the small step the throttle position is within the quantization error from the reference value in less than 20 ms. The small chattering in the control signal originates from the PD-controller when the measurement oscillates rapidly around the measurement value. A ramp response (part of signal A2.2) and corresponding tracking error are shown in figure 12. A small stick slip motion of the throttle is evident in the figure but the error does not exceed 0.3% during the ramp, which is small. All these results must be considered good and meet the demands on an automotive throttle controller.

The integral square error for all provided test signals in the throttle benchmark with the presented controller are given in table 2. The initial throttle position was set equal to the initial reference value for each test.

4.1 Robustness investigation

One critical parameter in the controller is the accuracy of the limp-home position. Due to the step-like characteristic of the static curve, incorrect information in the controller could lead to degraded controller performance around this position. Another important parameter is the amplitude of the friction compensator. During operation with only small changes in reference around a nominal value, a large part of the control signal comes from the friction compensator block. A bad estimate of the Coulomb friction could have large effect on the controller performance for small reference changes. To investigate the influence of incorrect limp-home and friction compensation a series of test have been made.

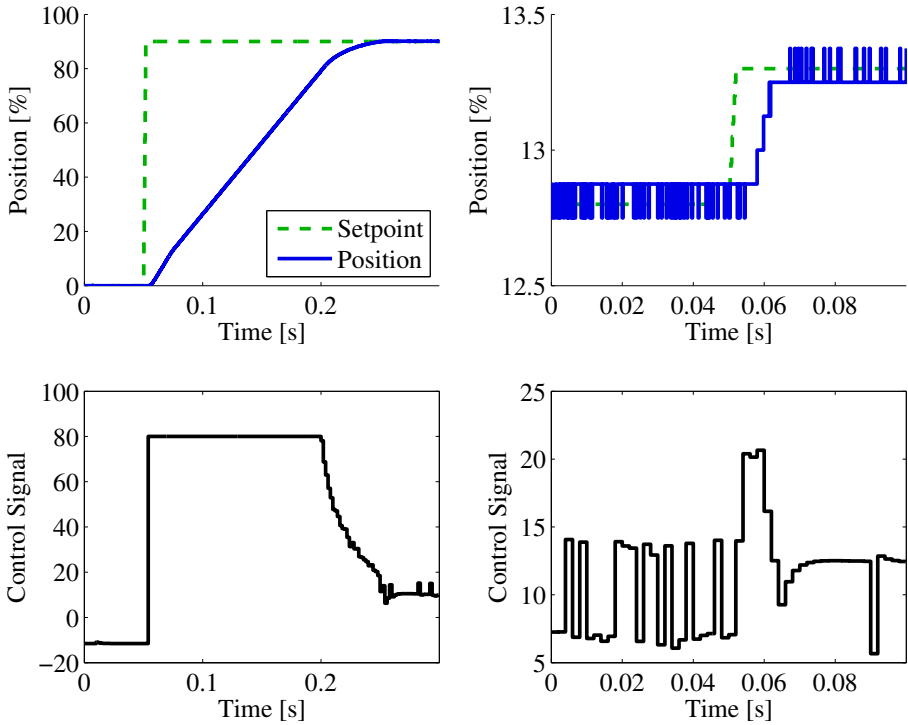


Figure 11: Two different sized step responses in θ_{ref} (part of signals A1.1 and A3.2) simulated on the benchmark model and the corresponding control signals. Settling time for the large step are less than 170 ms and the overshoot smaller than 0.25%. The small step is within the quantization error from the reference in less than 20 ms. A small chattering in the controls signal originating from the PD-controller occur when the measurement oscillates rapidly around the reference value.

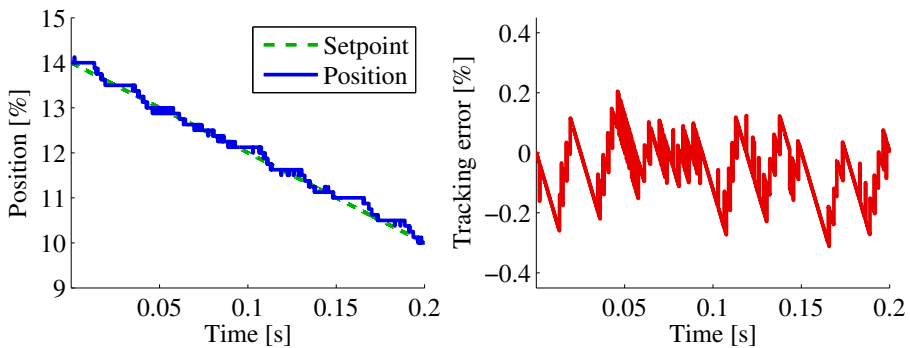


Figure 12: Simulated ramp response (the end of signal A2.2) and corresponding tracking error while passing through the limp-home position, which is around 11.1%. Peak tracking error is approximately 0.3%.

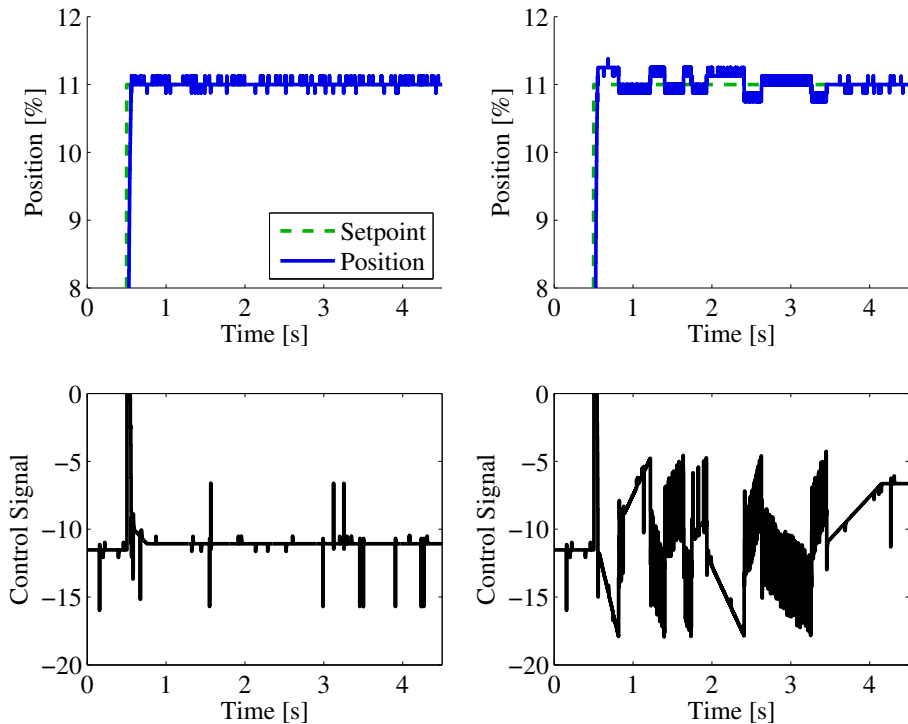


Figure 13: *Left:* The controller has correct information of the limp-home position. *Right:* The controller has a 2% error in limp-home position. The limp-home compensator starts to compensate below the limp-home position, resulting in an overshoot and small oscillations.

Error in limp-home position

Figures 13, 14, 15 and 16 show comparisons between the nominal controller and controllers that have an error in the limp-home compensator. In the figures to the left the limp-home compensator has the limp-home position at 11% which is the same as the actual position. In the figures to right the actual limp-home position is set to 13% in the model while the controller still believes it to be at 11%.

In figure 13 the controller starts to compensate for the limp-home position when the reference step to 11% is made, resulting in an overshoot. Small oscillations occur due to the stick slip motion of the throttle when the integral part have to overcome the limp-home torque to correct the position. In figure 14 a ramp response through the limp-home position is compared. For the controller with incorrect limp-home position the throttle position deviates slightly from the reference ($\leq 1.5\%$) both where the controller believes the limp-home position is, and at the actual limp-home position.

Figure 15 shows step responses around the limp-home position with both the correct and the incorrect controller. The incorrect controller compensates

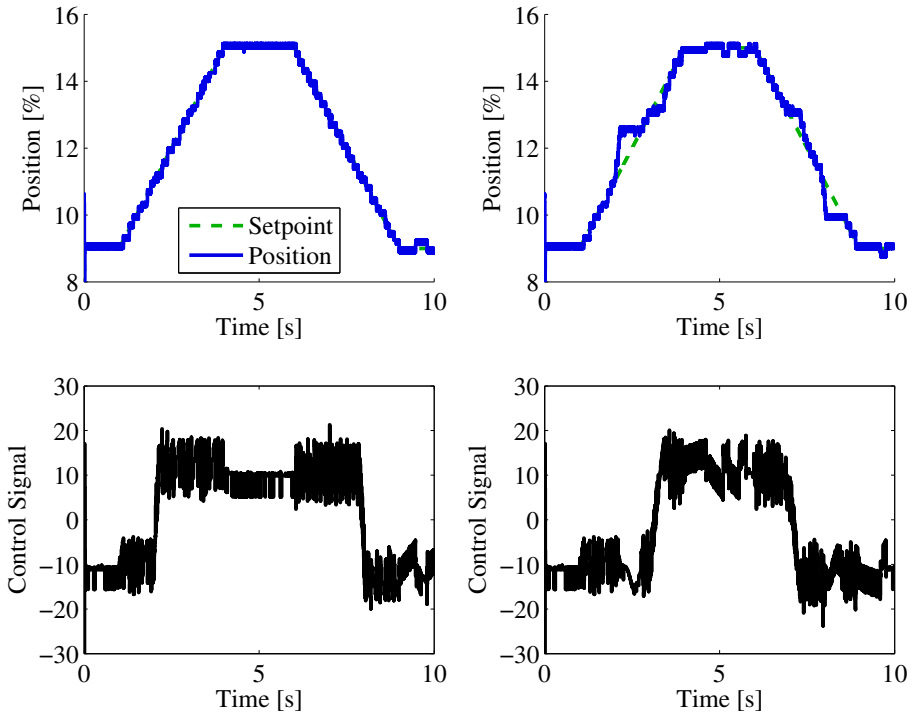


Figure 14: *Left:* The controller has correct information of the limp-home position. *Right:* The controller has a 2% error in limp-home position. When the reference passes the actual limp-home position (13%) and where the controller believes the limp-home position is (11%), the tracking error rises to about 1% before the integrator compensates for the error.

for the limp-home position before it has been reached, leading to relatively large overshoot compared to the step size. In figure 16 the behavior when doing steps into the limp-home position is shown. With an error in the controller, the position over- or undershoots of about 0.5%.

An error in the limp-home compensator has a large effect on the controller performance when operating between the limp-home position in the controller and the actual limp-home position. The largest impact is seen in figure 15 and could lead to oscillations in the engine air flow that would result in oscillations in torque. This would be unacceptable in a production vehicle and thus this controller requires good precision in the parameter θ_{lh} in the limp-home compensator, within a few tenths of a percent. The significance of this is further strengthened by experiments with real throttles, that have shown that there can be significant differences in the limp-home position between individual throttles. In particular a deviation larger than 2 % has been found between an engine in an engine test cell and an identical engine in a vehicle. As a result of the incorrect calibration, torque variations could be felt by the driver in an operating point with a throttle reference in the proximity of the limp-home position. However, the desired

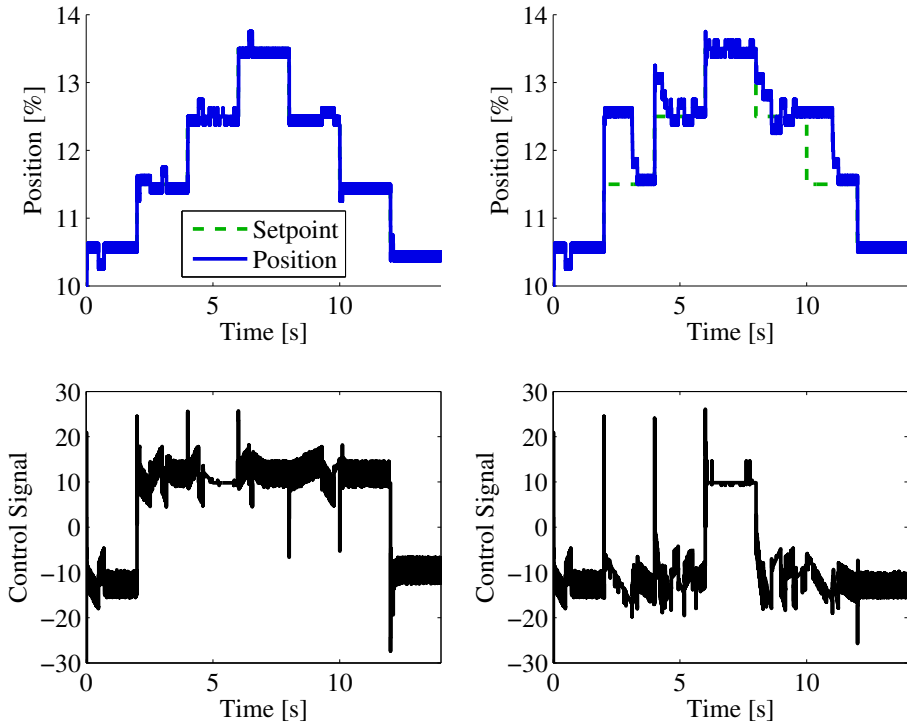


Figure 15: *Left:* The controller has correct information of the limp-home position. *Right:* The controller has a 2% error in limp-home position. The worst case scenario with limp-home position error. Small steps between the expected and actual limp-home position will cause over and undershoots of about 1%.

accuracy is achieved with the presented tuning method. Effects like aging of the throttle and position sensor or production deviations could be handled by running a calibration at start up. If a full calibration is not possible, it is suggested that the system performs a simpler diagnosis and calibration by measuring the throttle position with zero control signal, which gives an accurate enough measurement of the limp-home position.

To further improve the robustness of the controller it could be extended with on-line adaptation of the limp-home position and the static curve. This would amend problems that could arise due to parameter variations during a single engine run, for example due to variations in battery voltage and external temperature. These variations has been thoroughly discussed in Pavković et al. (2006) where an adaptive control is proposed, and is not treated here.

Error in friction compensator

Figure 17 compare the controller performance with correct friction estimation and where the friction has been underestimated of 30%. Small oscillations around the reference value are introduced. An overestimated friction of 30% also

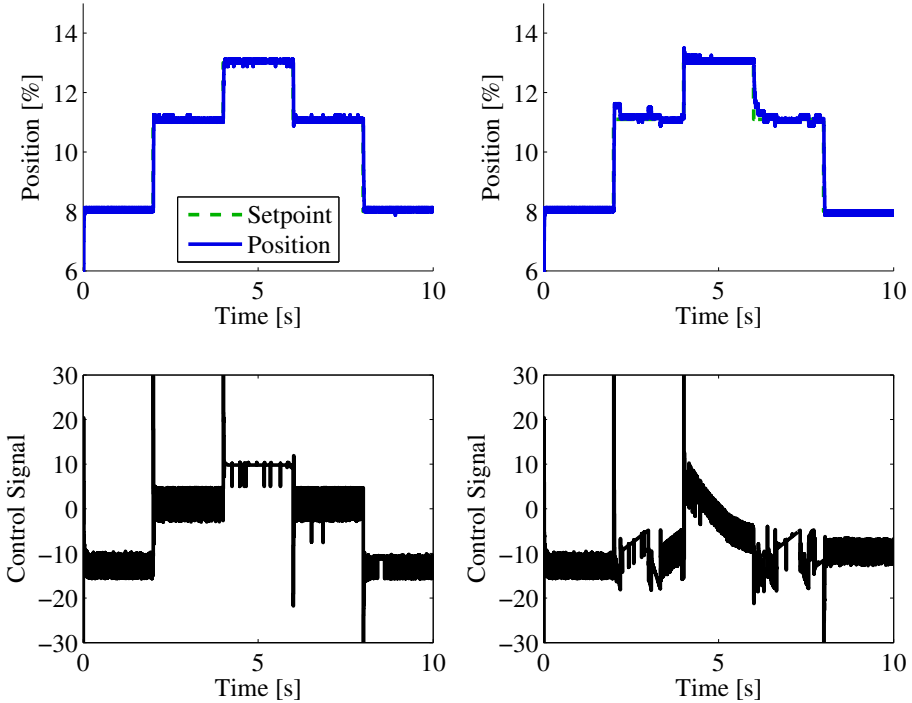


Figure 16: *Left:* The controller has correct information of the limp-home position. *Right:* The controller has a 2% error in limp-home position. The effect of the error in the controller is a small overshoot and undershoot.

tends to increase the position overshoot. These deviations are however fairly small and do not have a large effect on vehicle driveability. The controller is not very sensitive to friction compensator errors of this magnitude.

5 Experimental results

The control design and tuning procedure have also been applied to the throttle in an engine test cell. The controller was evaluated using similar input signals as the benchmark model. A large and a small step response are shown in figure 18, and a ramp with the corresponding tracking error are shown in figure 19. The step response is slightly slower in the experimental tests but also has less overshoot. The control signal does not saturate during the step so the response time could be decreased by a lower value of λ . A creeping effect is visible for the small step, which could be explained by the higher measurement resolution, approximately 0.033%, for this experimental setup compared to the TC benchmark model and standard production throttles. The error after the initial step is less than 0.1%.

The tests show that the controller achieves satisfactory results also in experiments. These experimental results further strengthens the conclusion that

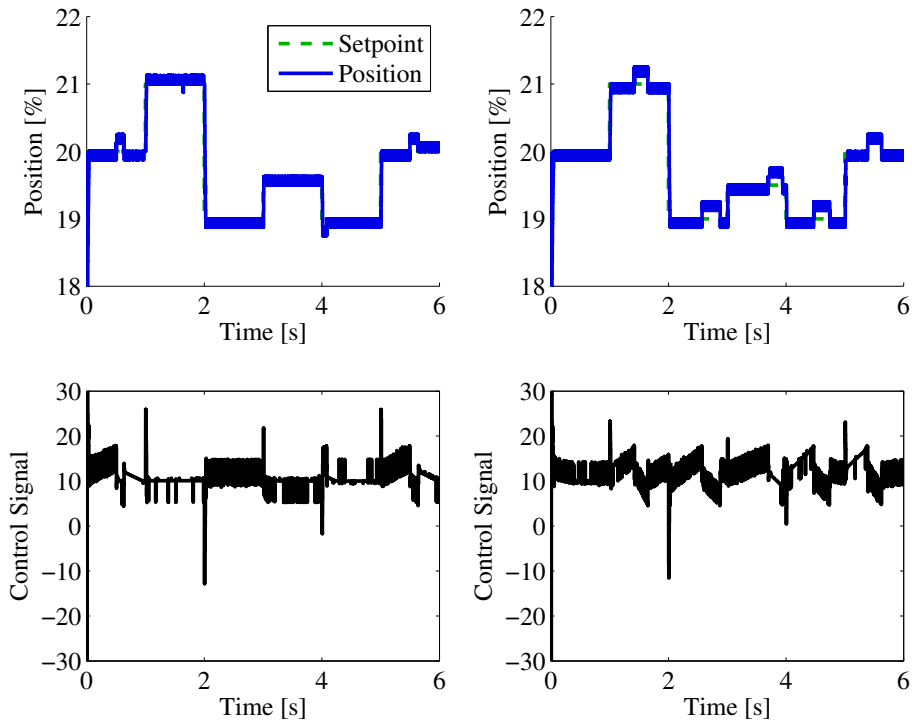


Figure 17: *Left:* The controller friction compensation is correct. *Right:* The friction compensator underestimates the friction of 30%. Visible but small deviations from the reference value are introduced. The controller is not very sensitive to friction estimation errors of this magnitude.

the developed throttle controller gives good performance. The tuning method is straightforward to apply, and the controller performance is easy to tune with the aid of the tuning parameter λ and the procedure described in section 3.2.

6 The throttle control benchmark

During E-COSM'09 the controller was evaluated together with five other participants, Vidal et al. (2009); Pozo et al. (2009); Colin and Chamailard (2009); Reynoso-Meza et al. (2009) and one other contributor, during a series of tests in both SiL and HiL environment. The HiL evaluation showed that with the proposed calibration procedure, the controller met all specifications set by the benchmark in Zito et al. (2009). The results are presented in Zito and Tona (2009).

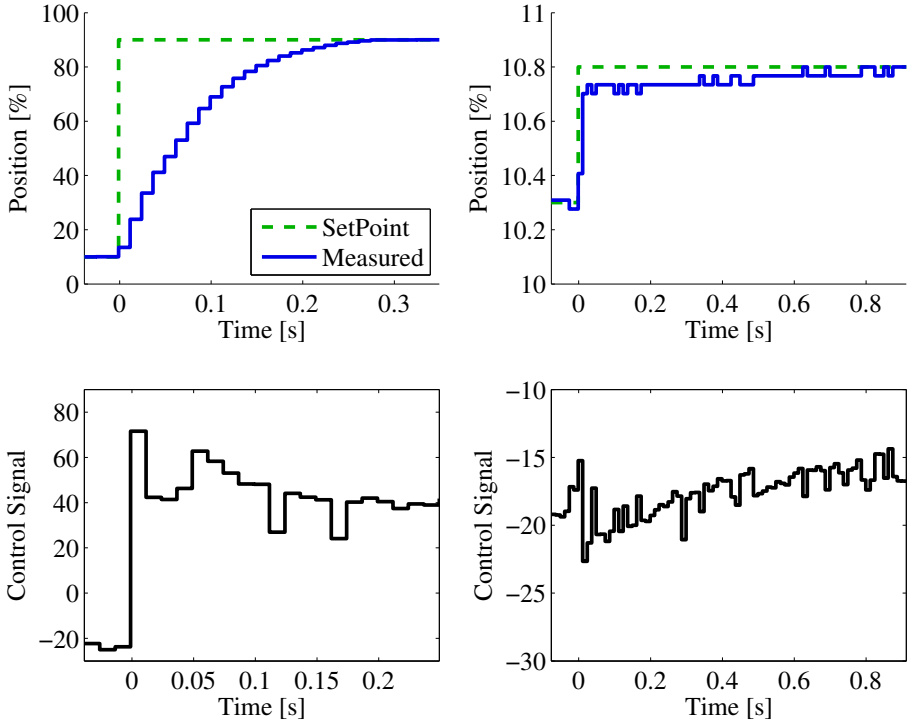


Figure 18: Two experimental step responses of different magnitude. The settling time for the large step is less than 200 ms and the overshoot is smaller than 0.1%. The creeping effect seen in the small step could be explained by the higher measurement resolution for the experimental setup, approximately 0.033%. The error after the initial step is less than 0.1%.

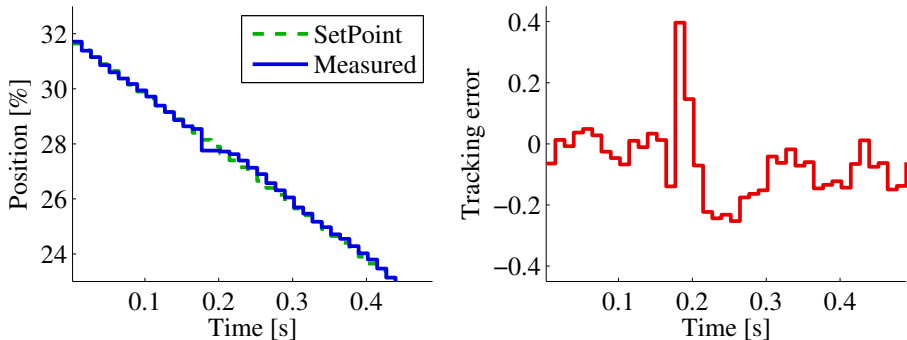


Figure 19: An experimental ramp response and corresponding tracking error which is slightly larger than on the simulation model. The error peaks at 0.4% when passing through the limp-home position but is otherwise below 0.2%

Conclusions

A throttle control strategy based on two static compensators and a PID controller has been presented. A tuning method for the parameters in both the compensator blocks and the PID controller has been developed. The relatively simple controller has been shown to give good performance both in simulation and in experiments. A robustness investigation has also been performed with respect to the friction and limp-home nonlinearities. An important result is that the controller is sensitive to how well the limp-home position is known. The accuracy of this controller parameter must be within a few tenths of a percent of the actual position in order to give a satisfactory control behavior in the neighborhood of the limp-home position. Experimental data have shown that deviations of a few percent between individual throttles can occur, which thus can pose a problem if this is not accounted for. The proposed design method and calibration procedure achieves a sufficiently accurate calibration. However, a simpler strategy for diagnosing and amending possible problems is to calibrate the limp-home position at each start up by registering and storing the throttle position with zero control signal.

Acknowledgements

This research was supported by the VINNOVA Industry Excellence Center LINK-SIC and by the Strategic Research Center MOVIII, funded by the Swedish Foundation for Strategic Research.

References

- Guillaume Colin and Yann Chamaillard. PI and RST controllers for throttle actuator. In *Proc. of the E-COSM*, November 2009.
- Joško Deur, Danijel Pavković, Nedjeljko Perić, Martin Jansz, and Davor Hrovat. An Electronic Throttle Control Strategy Including Compensation of Friction and Limp-Home Effects. *IEEE Trans. on Industry Applications*, 40(3):821–834, 2004.
- Lars Eriksson and Lars Nielsen. Non-linear Model-Based Throttle Control. *Electronic Engine Controls*, SP-1500:47–51, March 2000.
- H. Olsson, K.J. Åström, C. Canudas de Wit, M. Gäfvert, and P. Lischinsky. Friction Models and Friction Compensation. *European J. of Control*, 4(3): 176–195, 1998.
- Danijel Pavković, Joško Deur, Martin Jansz, and Nedjeljko Perić. Adaptive control of automotive electronic throttle. *Control Engineering Practice*, 14(2): 121–136, 2006.
- Francesc Pozo, Leonardo Acho, and Yolanda Vidal. Nonlinear Adaptive Tracking Control of an Electronic Throttle System: Benchmark Experiments. In *Proc. of the E-COSM*, November 2009.

- Karl J. Åström and Tore Hägglund. *Advanced PID Control*. ISA-The Instrumentation, Systems, and Automation Society, 2006. ISBN 1-55617-942-1.
- Gilberto Reynoso-Meza, Javier Sanchis, and Xavier Blasco. Multiobjective Design of a Digital Controller for the Throttle Control Benchmark. In *Proc. of the E-COSM*, November 2009.
- Daniel E. Rivera, Manfred Morari, and Sigurd Skogestad. Internal Model Control. 4. PID Controller Design. *Ind. Eng. Chem. Process. Des. Dev.*, 25:252–265, 1986.
- R. Scattolini, C. Siviero, M. Mazzucco, S. Ricci, R. Poggio, and C. Rossi. Modeling and Identification of an Electromechanical Internal Combustion Engine Throttle Body. *Control Engineering Practice*, 5(9):1253–1259, 1997.
- M. Vašak, M. Baotić, M. Morari, I. Petrović, and N. Perić. Constrained optimal control of an electronic throttle. *Int. J. of Control*, 79(5):465–478, 2006.
- Yolanda Vidal, Leonardo Acho, and Francesc Pozo. Robust Control of an Electronic Throttle System Via Switched Chattering Control: Benchmark Experiments. In *Proc. of the E-COSM*, November 2009.
- G. Zito and P. Tona. The throttle control benchmark. Presentation at E-COSM'09, 2009. <http://ecosm.nokiweb.fr/images/TC%20Benchmark.pdf>.
- G. Zito, P. Tona, and P. Lassami. "The Throttle Control Benchmark". In *Proc. of the E-COSM*, November 2009.

Wastegate Actuator Modeling and Model-Based Boost Pressure Control[†]

Andreas Thomasson^a, Lars Eriksson^a, Oskar Leufvén^a,
and Per Andersson^b

^a*Vehicular Systems, Department of Electrical Engineering,
Linköping University, SE-581 83 Linköping, Sweden.*

^b*GM Powertrain Sweden AB, Per Andersson, SE1-A04-007,
SE-461 80 Trollhättan*

[†]This is a formatted version of “Wastegate Actuator Modeling and Model-Based Boost Pressure Control” by Andreas Thomasson, Lars Eriksson, Oskar Leufvén, and Per Andersson, IFAC Workshop on Engine and Powertrain Control Simulation and Modeling 2009, Paris, France. ©IFAC 2009. Reproduced with the permission of IFAC. The original version was published in ifac-papersonline.net, <http://ifac-papersonline.net>, and can be found using the Digital Object Identifier (DOI): 10.3182/20091130-3-FR-4008.00012. The formatting is restricted to changing the article into a single-column format, adjusting sizes of figures and tables, and adjusting the referencing style.

Abstract

The torque response of an engine is important for driver acceptance. For turbocharged spark ignited (TCSI) engines this is tightly connected to the boost pressure control, which is usually achieved with a wastegate. A challenging scenario is when the throttle is fully open and the load is essentially controlled by the wastegate. First a model for the pneumatic wastegate actuator and air control solenoid is developed. The wastegate model consists of three submodels; the actuator pressure, the static position, and an additional position dynamics. A complete engine model is constructed by including the actuator model in a Mean Value Engine Model (MVEM) for a TCSI engine. This model describes the transient boost pressure response to steps in wastegate control inputs. The subsystems and complete MVEM are validated on an engine test bench and it explains the overshoot seen in the step responses.

The model is used to study the system response and give insight into the dominating phenomena and it points out that the engine speed is important for the response. Further, for each speed it is sufficient to model the system as a second order linear system, that captures an overshoot. A controller consisting of a mapped feedforward loop and a gain scheduled feedback loop is developed together with a tuning method based on the IMC framework for the feedback loop. The controller and tuning method is shown to achieve the desired boost pressure behavior both on the complete MVEM and on real engines. The experimental validation is carried out both in an engine test cell and in a vehicle.

1 Introduction

Turbocharging is a common way of increasing the power density of both spark ignited and diesel engines. Combining turbocharging with downsizing gives a cost effective way for improving the fuel economy of a vehicle (Emmenthal et al., 1979; Guzzella et al., 2000; Soltic, 2000; Petitjean et al., 2004). To achieve good engine performance and driveability over the full operating range it is necessary to control the turbocharger, and this is usually done with an actuator on the turbine (Watson and Janota, 1982). The most frequently used actuator is the wastegate. Boost pressure control and wastegate control has been studied in many publications, see e.g. Wakeman and Wright (1986); Kranik et al. (2005); Moulin et al. (2008); Müller (2008). A flexible wastegate system enables more advanced strategies, for example it is favorable to open the wastegate as much as possible in order to reduce pumping losses and thus fuel consumption (Eriksson et al., 2002a). For engine operating points with intake pressures above atmospheric this leads to a control strategy with fully open throttle and where the wastegate alone is used to control the boost pressure and engine torque. In general the demand for good performance combined with more advanced system configurations put higher demands on the design of boost pressure controllers.

The wastegate is normally opened by a pressure actuator connected to a pressure blender solenoid valve controlled by the ECU. The position is not measured and the static and dynamic response to control inputs depend on engine operating conditions. A complete physical model of the pressure actuator and pressure feed system is challenging since several parameters such as membrane areas, flow coefficients, valve areas and how they vary with control signal and actuator position, have to be determined. Physical modeling gives valuable insight into the system and it has been successfully applied in Moraal et al. (1999) and Galindo et al. (2009). This paper tackles the problem from another angle. A novel model for the wastegate actuator is developed, using fewer parameters that are easily tuned from measured data and that is suitable for control design evaluation. The model is divided into three submodels and captures the stationary and dynamic behavior of the system, which are needed to predict the system behavior and controller performance. With the aid of a complete Mean Value Engine Model (MVEM), a model-based tuning method for a boost controller structure is developed. The tuning method is based on linearizations of the boost pressure response to control signal. The developed wastegate actuator model is used to simulate the performance of the controller, which is then implemented and experimentally evaluated on an engine. In the development and experimental validation the emphasis is on cases where the throttle has a large opening area, i.e. where the wastegate control has a big impact on the torque response.

1.1 Outline and experimental setup

The development of the controller and its tuning is based on a complete MVEM of a TCSI engine, that has been developed and validated in Eriksson et al. (2002b); Andersson (2005); Eriksson (2007). This MVEM provides a gas flow

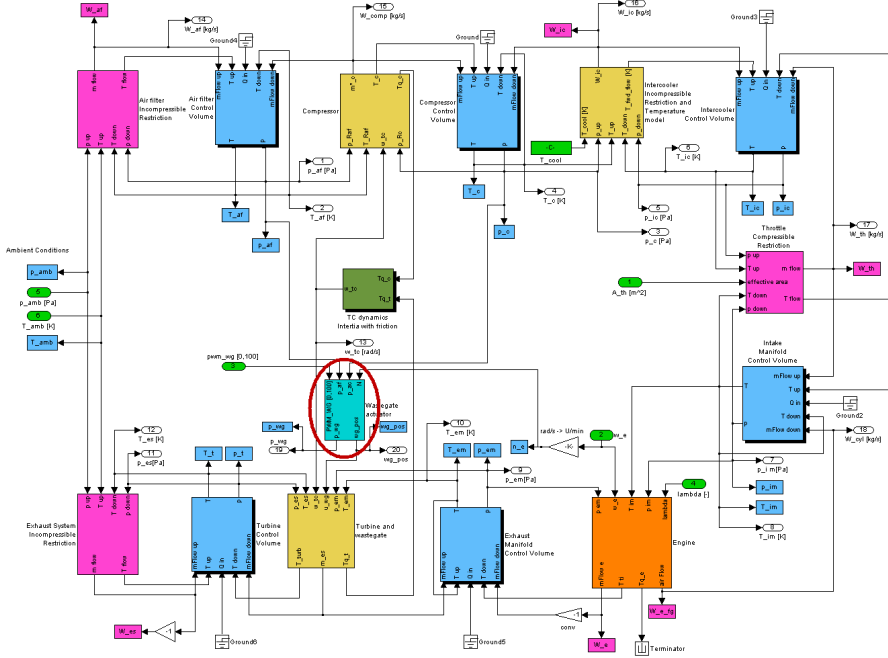


Figure 1: The MVEM implemented in Simulink. The encircled block contains the wastegate actuator model developed in this paper.

model of the engine, shown in Figure 1, that is extended with the new wastegate actuator model, encircled in the figure. Section 2 describes the development of the actuator model where engine test cell data is used to build and validate this actuator model.

In Section 3 a boost pressure controller is designed. It consists of feedforward and feedback loops that fit well into the structure that is current industrial practice. The main effort is on the feedback loop. It is designed based on the IMC framework where the plant model consists of several linearizations of a reduced order MVEM for the TCSI engine. The feedforward loop is a static map that is determined in stationary experiments. It is shown that the feedback loop is not able to compensate for large errors in the feedforward during transients, hence the accuracy of the feedforward is important for performance. Controller validation is first performed on the non-linear model, in Section 4.1, and then on a vehicle, both on the road and on a vehicle dynamometer, in Section 4.2.

The wastegate model identification experiments have been performed in the engine lab of the Division of Vehicular Systems at Linköping University. The engine is a four cylinder two liter turbocharged gasoline engine with direct injection. The control system from dSPACE consists of a RapidPro system and MicroAutoBox connected to a PC running Control Desk. Two extra sensors are added to the test cell setup, a linear position sensor to measure the actuator position and a pressure sensor for the pressure in the actuator. The extra sensors are used for modeling and analysis while the sensors used for control are those of a standard production engine.

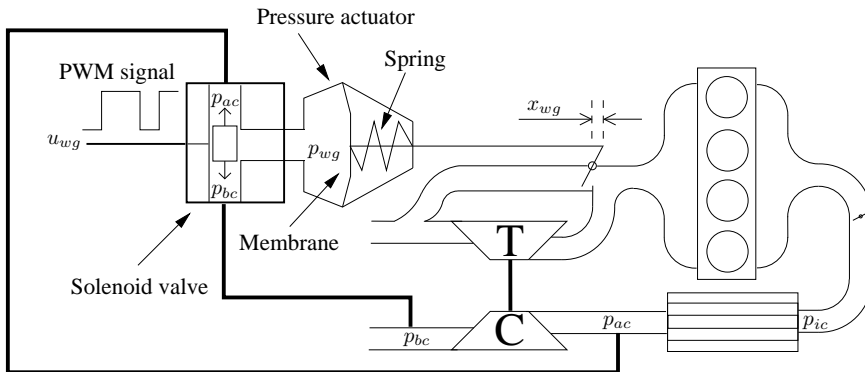


Figure 2: A sketch of the complete system but with special emphasis on wastegate actuator and pressure blender solenoid valve.

The test vehicle used for controller tuning and evaluation is powered by a two liter turbocharged engine, similar to the engine in the test cell. This vehicle also uses a development control system instead of a production system.

2 Wastegate actuator modeling

The wastegate actuator is a little studied topic in the literature but it has a significant influence on the controller performance. In particular, the transient response to changes in control signal shows an overshoot in boost pressure. This is not predicted by the MVEM without extending it with a model for the connections between the control signal and the effective area of the wastegate valve. If such a model is available then the pressure oscillations, that can be introduced by the controller, can be predicted and accounted for already in simulation, which reduces the time needed for engine calibration.

A sketch of the wastegate actuation system is shown in Figure 2. The wastegate valve is opened by a pressure actuator which is mechanically connected to the valve. The position of the actuator is denoted x_{wg} and measured in percent of full opening. The pressure in the actuator p_{wg} is generated by a pressure blender solenoid that is connected to the pressures before and after the compressor. The blender solenoid has as input the wastegate duty cycle u_{wg} , which is a pulse-width modulated signal. The wastegate actuator model has u_{wg} as input and gives the wastegate position x_{wg} as output and the main components are the pressure blender solenoid valve, the pressure chamber, and the actuator rod with a spring.

2.1 Model identification experiments

For model identification several ramp and step responses in wastegate duty cycle were made. These were done with fully open throttle and for different engine speeds. Figure 3 shows ramp responses for two different engine speeds. The ramp responses are very slow and are used to identify the static behavior of the actuator. The step responses are used in section 2.6 where the actuator dynamics are treated.

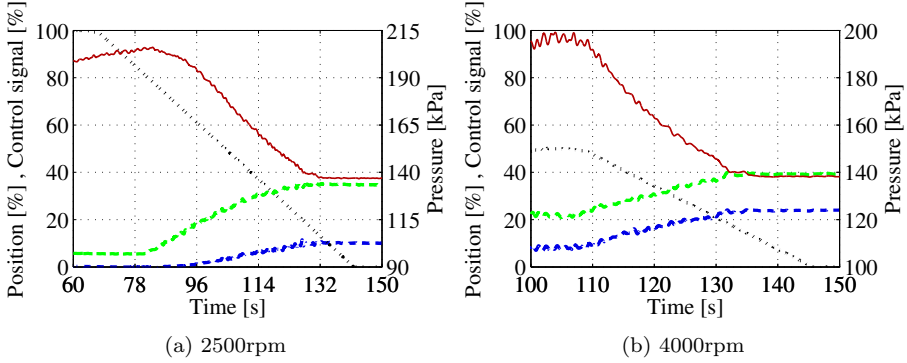


Figure 3: Ramp response measured in test cell. The wastegate duty cycle (u_{wg} - black dotted) is ramped from the maximum allowed by the control system during normal operation and down to zero. As u_{wg} decreases the pressure in the actuator (p_{wg} - green dashed) rises. Eventually p_{wg} overcomes the spring force, the wastegate opens (x_{wg} increases - blue dash-dot) and the boost pressure decreases (red solid).

2.2 Wastegate position model - static behavior

The wastegate actuator position is mainly affected by the pressure in the actuator. The actuator pressure generates a force in the actuator $F = p_{wg} A$, where A corresponds to the actuator membrane area. This force is in its turn balanced by the spring force, described with a linear expression $F = -k_s x$. Assuming all other forces constant for a given speed results in the following static model

$$\bar{x}_{wg} = k(N) \cdot (p_{wg}(u_{wg}) - p_0(N)) \quad (1)$$

where k and p_0 represent the static gain from actuator pressure to position and the opening pressure, respectively. Naturally there are other forces that also act on the wastegate, coming from the gas motion and pressure difference around the valve. To model this physically from the geometry of the valve, the surrounding pressures and gas motion is difficult. However the experiments have shown that sufficiently good accuracy can be achieved by allowing k and p_0 to vary with engine speed only. However, if other applications necessitate the addition of other forces that act on the wastegate valve, they could also be fitted into the model structure.

2.3 Wastegate position model - small openings

It has been noted that there is a deviation between model (1) and measurements for small openings. It is believed that these deviations are due to oscillations in the wastegate position that have been observed in the measurements. In the experimental data oscillations can be seen both in the chamber pressure and in the wastegate position and they have the same frequency as the opening and closing of the intake and exhaust valves. Whether the oscillations in position are due to pressure pulsations on the intake side that propagate through the valve

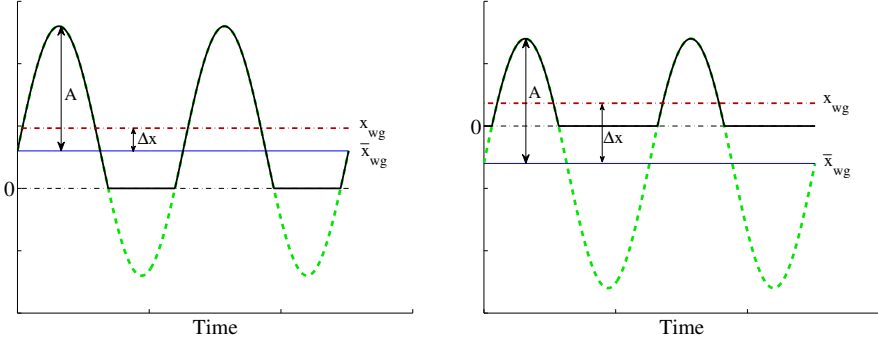


Figure 4: Illustration of position modification for small wastegate positions. Unsaturated oscillation (green dashed) and saturated oscillation (black solid). The mean value for the saturated oscillation (red dash-dot) is larger than the mean value for the unsaturated oscillation (blue solid).

to the actuator chamber and to the waste gate position, or if they are caused by the pulsating flow around the valve in the exhaust, is still an open question.

Regardless of the source, if the movement follows an oscillation that is saturated then this will lead to a deviation in the mean value \bar{x}_{wg} , which is what (1) describes. Specifically, when the mean value of the oscillation is in the range of $[-A, A]$, where A is the amplitude of oscillation, the mean value for the free oscillation will be lower than that of the clipped, see Figure 4 for an illustration.

A simple model can be received by assuming that the oscillations follow a sinusoidal with amplitude A that is saturated. The offset in mean value, Δx , due to the saturation is given by

$$\begin{cases} m = \min(\max(\bar{x}_{wg}, -A), A) \\ \phi = \cos^{-1}(-m/A) \\ \Delta x = \frac{1}{\pi}(A \sin(\phi) + m\phi) - m \end{cases} \quad (2)$$

where \bar{x}_{wg} is given by (1) and A has been chosen as the maximum amplitude of oscillation for the unfiltered signal. It is worth to note that a similar effect is expected at the maximum, where the actuator also saturates. This is not included in the model since the upper saturation is seldom reached, if it is necessary it can be modeled analogously as above. Thus the resulting model for the corrected position becomes

$$x_{wg} = \bar{x}_{wg} + \Delta x \quad (3)$$

Figure 5 compares the position model (3) to measurement data and shows that the model gives a good description of the behavior. In some cases it might not be necessary to include this sub-model, but it simply improves the model agreement in the region near where the wastegate is closed.

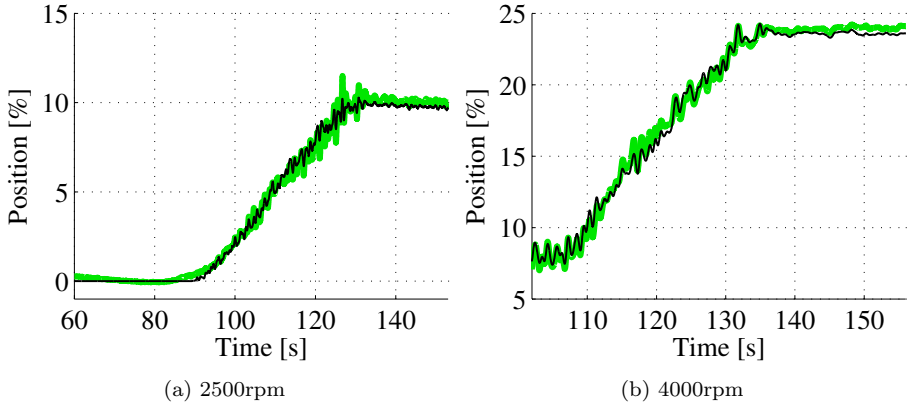


Figure 5: Comparison between the wastegate position model (black thin) and measurements (green thick) for two different engine speeds.

2.4 Wastegate pressure model - static behavior

The pressure model describes the relationship between the wastegate duty cycle and the two feeding pressures to the actuator pressure. A linear interpolation between the two feeding pressures with the duty cycle as argument has proved to be insufficient. The proposed model is a second order polynomial in wastegate duty cycle, with coefficients that depend on the feeding pressures and the saturation limits of the control signal, u_{min} and u_{max} . The resulting pressure model is defined by

$$p_{wg} = \begin{cases} p_{ac} & \text{if } u_{wg} < u_{min} \\ a u_{wg}^2 + b u_{wg} + c & \text{if } u_{min} \leq u_{wg} \leq u_{max} \\ p_{bc} & \text{if } u_{wg} > u_{max} \end{cases} \quad (4)$$

The parameters a , b , c , u_{min} and u_{max} have been estimated with the least squares method under the following two algebraic constraints

- $a u_{min}^2 + b u_{min} + c = p_{ac}$
- $a u_{max}^2 + b u_{max} + c = p_{bc}$

that ensure that p_{wg} in (4) is continuous at $u_{wg} = u_{min}$ and $u_{wg} = u_{max}$. The resulting pressure model is validated in Figure 6 and it is shown that it gives a good description of the measured actuator pressure.

2.5 Complete static model

Combining (3) and (4), gives the complete model for the wastegate position as a function of duty cycle and the two pressures fed to the pressure blender solenoid. Figure 7 shows a validation of the model where it is seen that the model gives a good description of the measured position.

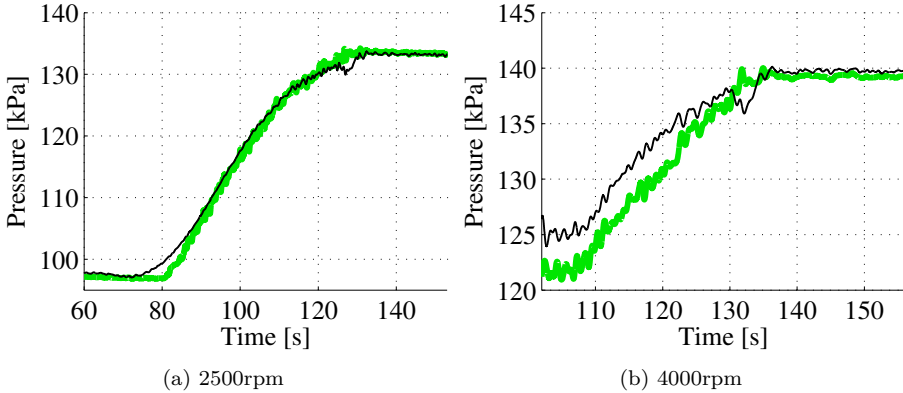


Figure 6: Modeled actuator pressure (black thin) and measured actuator pressure (green thick) during a ramp in the control signal. Estimated parameters for the second model are $u_{min} = 12.5$, $u_{max} = 94.5$.

2.6 Wastegate actuator dynamics

Step responses in wastegate duty cycle show that there are overshoots both in actuator pressure, Figure 8, and wastegate position, Figure 9. The overshoot in pressure is expected and is sufficiently well described by the static model. This is due to the following. An increase in wastegate duty cycle lowers the actuator pressure, which closes the wastegate. This gives more air flow through the turbine and increases the energy to the compressor. The pressure after the compressor thus increases and since it is connected to the pressure blender solenoid it thereby increases the actuator pressure once again.

The large position overshoots, seen in Figure 9, are not fully explained by the static models. These overshoots have an impact on the transient response which motivates an introduction of dynamics in the wastegate position. This is done by observing that the system in Figure 2 is similar to a mass-spring-damper system, which is a second order system. It turns out that the large position overshoot seen in the measurements can not be described by the regular mass-spring-damper model (5), without adding a zero to the transfer function.

$$H(s) = \frac{1}{T^2s + 2\zeta Ts + 1} \quad (5)$$

Adding the term βTs to the numerator and setting the damping coefficient to 1 results in the dynamic model

$$H_{x_{wg}}(s) = \frac{\beta Ts + 1}{(Ts + 1)^2} \quad (6)$$

with a double pole in $s = -1/T$ and a zero in $s = -1/(\beta T)$, $\beta > 1$. An interpretation of the term βTs is that the position dynamics is dependent on both the pressure and the pressure derivative. The parameters β and T have

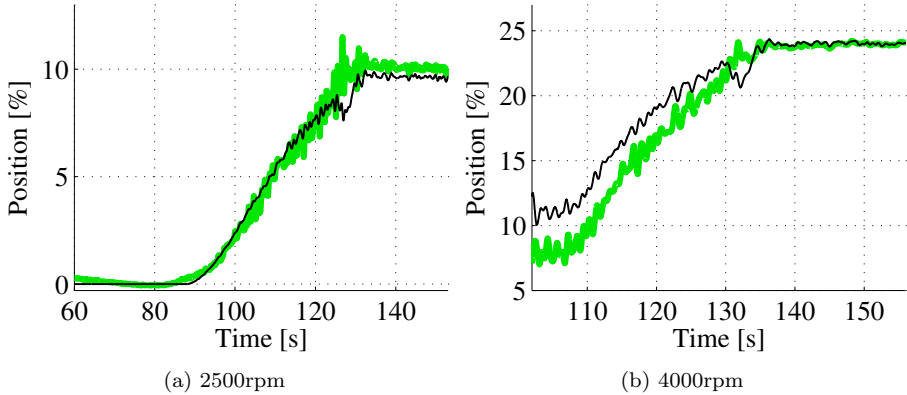


Figure 7: Plots for the static model from duty cycle to wastegate position (black thin) and the measured position (green thick). As a result of the pressure model being a little less accurate for the higher engine speeds, so is also the combined model.

been tuned manually to match the overshoot in the measurements. Comparisons between the measured position and the static and dynamic models, for steps in wastegate duty cycle, are shown in Figure 9, and it is seen that the model gives a good description of the system behavior.

2.7 Full MVEM with wastegate model

To evaluate the developed model and use it for controller tuning the actuator model was implemented in the available MVEM. To be useful when evaluating the controller tuning method the model needs to capture the wastegate duty cycle response on an engine. Figure 10 compares the boost pressure for two step responses in u_{wg} measured in engine test cell with simulations made with the extended MVEM.

When first comparing the measured and simulated values there is a small bias error in pressure. In Figure 10 the bias error has been removed (the maximum offset was 4 kPa). This is done to be able to better compare the pressure transients which is important for control. This bias error will not affect the control design and tuning, presented in section 3, but will be handled by the feedforward.

The developed model, consisting of three simple submodels, captures the dynamic behavior of the wastegate actuator. More importantly, together with the MVEM it captures the boost pressure response, including the overshoot, for changes in wastegate duty cycle. A good agreement in the dynamic response between the simulation environment and the engine improves the chances that a design based on the model will work in practice. In the next section the model is used in the development of a controller tuning method.

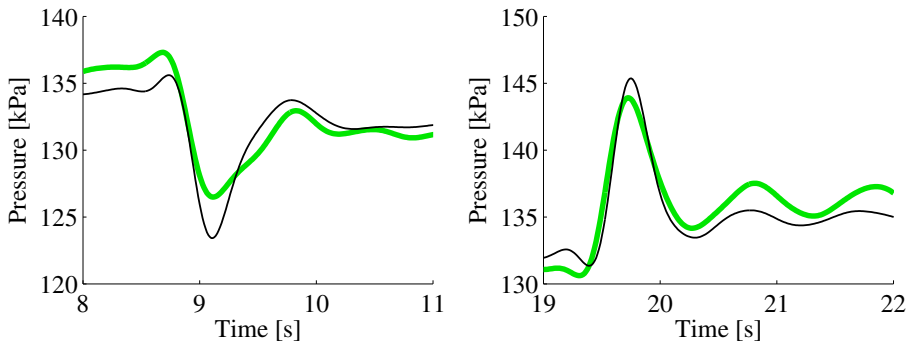


Figure 8: Measured wastegate pressure (green thick) and calculated wastegate pressure (black thin) with the static model during two steps in wastegate duty cycle at 4000 rpm. The pressure overshoot during steps in duty cycle is described satisfactorily by the static model.

3 Boost pressure controller

The controller structure studied in this paper is in industrial use today and consists of a static feedforward and a gain scheduled PID controller, see Figure 11. The feedforward gives the desired boost pressure at stationary conditions. It is determined by running the engine at stationary conditions and recording the duty cycle u_{wg} needed for desired boost pressures. The task of the PID controller is to shape the dynamic response of the system while minimizing the response time during steps in desired boost pressure and eliminating stationary error. This should also be achieved without introducing oscillations. The focus of the following sections is to present and evaluate a systematic method for tuning the PID controller.

3.1 PID tuning method

From industrial perspective it is desirable for a tuning method to be simple, fast and easy to automate. To tune the PID controller some experiments for gathering process knowledge is needed. The complete MVEM together with the wastegate actuator model developed in the previous section is a nonlinear model with 15 states. Using this model as the starting point for tuning the PID controller, by linearizing and deriving transfer functions between u_{wg} and p_{ac} , would be cumbersome and a simpler model is searched for.

Experimental results indicate that at least a second order system is needed to describe the system behavior for steps in input signal. Several simulations with the MVEM and wastegate model have been performed for different speed and load conditions showing that a second order behavior seems to be sufficient for capturing the important dynamics. For this reason step responses in u_{wg} are suggested for model identification experiments. The behavior of the system changes significantly with engine speed and thus the step responses are done for several engine speeds in the range of interest, resulting in the process model

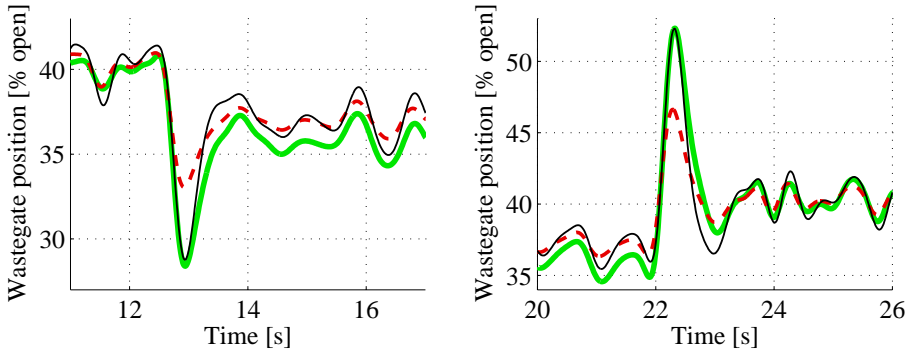


Figure 9: Measured wastegate position for step responses in duty cycle (green thick) at 4500 rpm. With the static model (red dashed) the overshoot in wastegate position is not accurately described by the model. Adding the dynamics (6) to the wastegate position (black thin) improves the model.

in (7). Plots for two engine speeds measured in a test vehicle are shown in Figure 12.

$$G(s) = \frac{K(N)}{T^2(N)s^2 + 2T(N)\zeta(N)s + 1} \quad | \quad \zeta \leq 1 \quad (7)$$

When identifying the process model the zero level should be set to the boost pressure before the step. Based on the measured step responses with the adjusted zero level, the parameters in the process model can be identified one at a time with the algorithm below, alternatively an LSQ problem over all parameters can be solved.

1. K is given by the static gain: $K = \frac{\Delta p_{boost}}{\Delta w_{gdc}}$
2. ζ is a function of the pressure overshoot: $\zeta = f\left(\frac{p_{overshoot}}{\Delta p_{boost}}\right)$
3. T only scales the step response in time and is chosen to best fit the measured step response.

Figure 12 shows a measured step response and the step response for the adapted process model for two engine speeds. The second order model, with different parameters for different engine speeds, gives a good description of the pressure behavior.

The suggested parameter tuning is based on the IMC-framework for controller design or Q-parametrization (Garcia and Morari, 1982). Consider the controller structure in Figure 13. The idea is to use the process model to predict the output and only use the new information in the feedback loop. If $G(s) = G_0(s)$ the feedback term is zero and the transfer function from reference to output becomes $Y(s) = G(s)Q(s)R(s)$. This means that $Q(s)$ can be used to design the transfer function from $R(s)$ to $Y(s)$ by choosing $Q(s) = G_d(s)G^{-1}(s)$ where G_d is the desired closed loop transfer function. The IMC structure could be

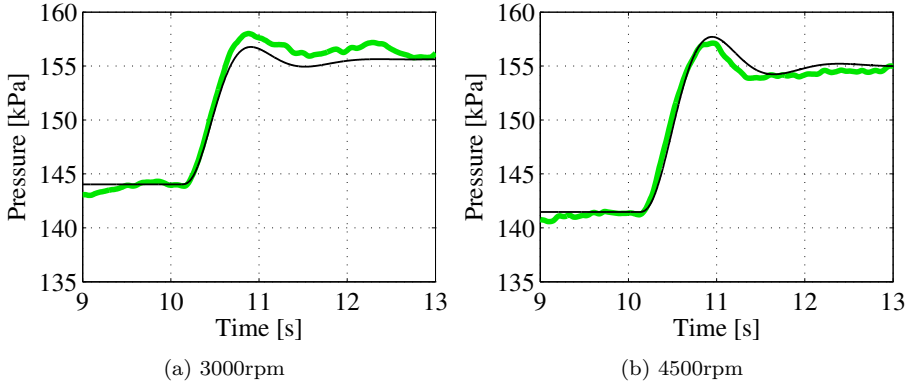


Figure 10: A comparison between measured (green thick) and simulated (black thin) boost pressure during a step in wastegate duty cycle. For both engine speeds the simulated pressure behavior is similar to the measured step.

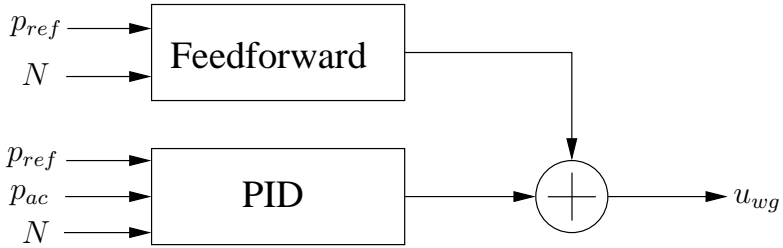


Figure 11: The controller structure for the boost pressure controller. The feedforward is a static map from desired boost pressure and engine speed to u_{wg} . The PID controller parameters depend on engine speed.

implemented as it is, but can also be transformed into the standard feedback controller with the equation $F(s) = Q(s)(1 - G(s)Q(s))^{-1}$.

In general the controller $F(s)$ is not a PID controller, but for many simple process models it is (Rivera et al., 1986). In this case when $G(s)$ is a second order system, and with the choice $G_d(s) = 1/(\lambda s + 1)$ a PID controller is the result. This choice of $G_d(s)$ as a first order system is motivated by the desire to suppress disturbances without introducing oscillations. The parameter λ is a tuning parameter that can be interpreted as the time constant for how fast the controller will react to a control error. Deriving $F(s)$ for the suggested choice of $Q(s)$ gives the ideal PID controller and parameters in (8).

$$F(s) = \frac{T^2 s^2 + 2\zeta T s + 1}{\lambda K s} \quad (8a)$$

$$K_p = \frac{2T\zeta}{\lambda K} \quad K_i = \frac{1}{\lambda K} \quad K_d = \frac{T^2}{\lambda K} \quad (8b)$$

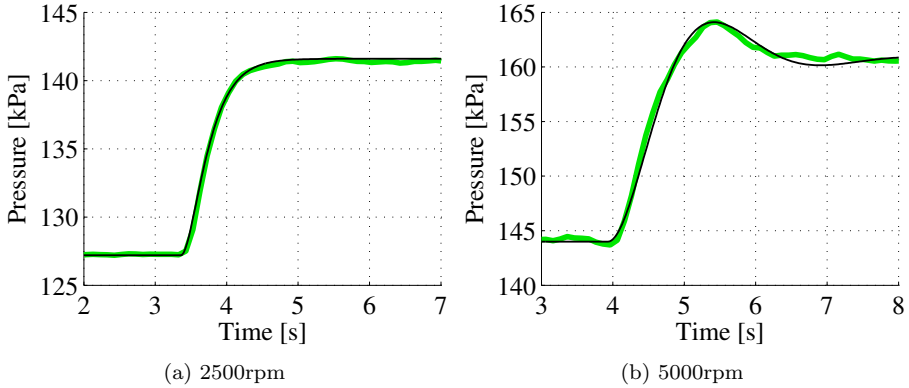


Figure 12: Measured boost pressure response in test car to steps in u_{wg} (green thick) together with the adapted process model (black thin) for two different engine speeds. The adapted model shows very good fit to measured data. For 5000rpm the pressure peak is slightly sharper compared to the adapted model, but the difference is very small.

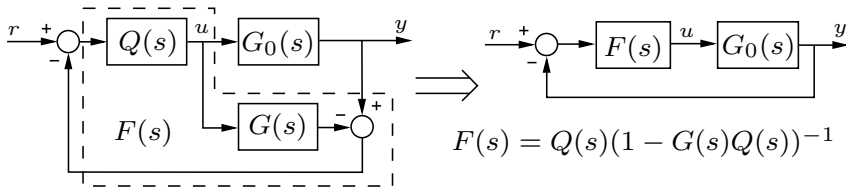


Figure 13: The standard IMC controller structure and how it can be interpreted as a standard feedback controller.

Since the parameters in the second order model are engine speed dependent then also the PID parameters will depend on the engine speed, in the equations above this dependence has been omitted. The choice of the tuning parameter λ effects the speed of the controller and will be discussed in section 4.

3.2 PID implementation aspects

A direct implementation of the ideal PID controller, with an unfiltered derivative, is not appropriate due to high frequency measurement noise. The D part of the controller has been filtered with a low-pass filter with a cut off frequency of 20 rad/s.

The low pass filtering of the derivative introduce another problem if steps in reference signal occur. If the derivative act on the control error, $e = r - y$, this results in large transients for sudden changes in reference value. For an unfiltered signal this would only be one sample but when the derivative is filtered it can sustain for several samples. One solution described in Åström and Hägglund (2006) is to let the derivative act on $e_d = \beta r - y$ where β is chosen between 0

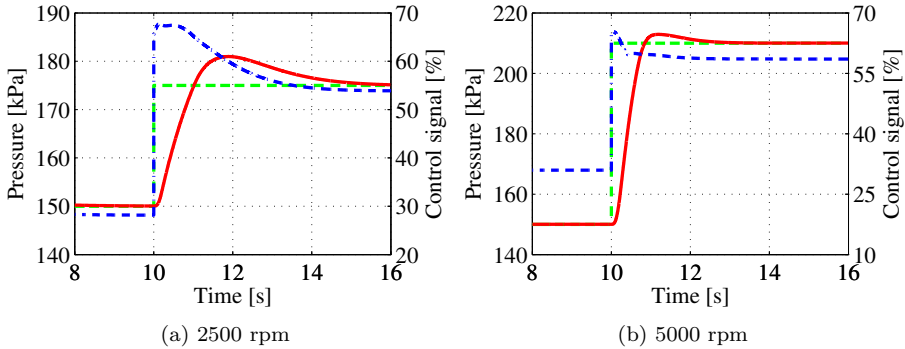


Figure 14: Simulated pressure step responses (red solid) and control signal (blue dash-dot) with a step in reference pressure (green dashed). For the two engine speeds the overshoot is, 7 *kPa* and 3 *kPa* respectively, which is not far from the desired overshoot of 5 *kPa*.

and 1. In this controller $\beta = 0$ is chosen because the derivatives main task is to decelerate the pressure increase after a step in desired boost pressure, when the reference value is reached. For slower and smoother changes in boost pressure reference, where a derivative acting on the $e = r - y$ would be preferred, the derivative action is fairly small.

Having integrator engaged when the control signal saturates will cause undesirably large overshoots due to wind-up. Therefore conditional integration is used to prevent integrator wind-up.

4 Controller tuning and results

Evaluation of the controller and the tuning method is first performed on the complete MVEM with the actuator model developed in Section 2. If the controller performs well in simulation, and the engine model used is accurate, the chance of failure on the engine is small. When the tuning method is proved to work in simulation, it is tested and evaluated on an engine. The response in boost pressure to a step in reference value should be as fast as possible with a small overshoot (around 5 *kPa*) and no oscillations. The small overshoot is desired because you do not want a shortage of power but rather a small excess.

The tuning parameter λ should be chosen so that the transient behavior described above is achieved. If a too small value for λ is used, the controller will be too aggressive, and introduce oscillations during transients. With too large value for λ , disturbances will not be suppressed fast enough and the transient response will be slow. A value of around $\lambda = 2$ has proved to be a good starting point for calibration. Engine test cell experiments have shown that engines with a comparatively bigger turbos, and thus slower and smoother response, can tolerate a smaller value of λ . This can also be needed to achieve the desired closed loop response. Furthermore, a system with fast step response and larger overshoots need larger λ -values.

4.1 Controller performance in simulation with the MVEM

In the simulation evaluation of the control design the steps for the open system, that are utilized in the tuning procedure, were performed on the complete MVEM. Based on these the controller parameters were determined and step responses in desired boost pressure were performed with the boost pressure controller acting on the complete MVEM. Figure 14 shows such step responses for two different engine speeds. The proposed controller gives a smooth pressure transient with an overshoot close to the desired 5 *kPa*. With an accurate model for the engine and especially the boost pressure behavior, this is a good indication that the tuning method will work on the engine.

4.2 Controller performance in test vehicle

In the next step the controller is evaluated in a test vehicle and these were done in a vehicle dynamometer. The step responses used for parameter identification have already been presented in Figure 12. Figures 15 and 16 show responses for the closed loop system for different engine speeds and step sizes. Both figures show that the controller successfully achieves the desired performance, i.e. a fast transient response with a small overshoot in boost pressure, not exceeding 5 *kPa*, without any significant oscillations.

Even though this paper focuses on the feedback loop it must be noted that the feedforward loop has a profound effect on the performance. Figure 17 illustrates a potential problem if the feedforward is poorly calibrated. In this example the step response is slower and it takes longer time for the controller to converge to the desired set point. The converse, with a too big overshoot can also occur. The integrator part of the controller removes the stationary error but slow convergence or big overshoots in the transient response are undesirable.

4.3 Controller performance for a slower system

An engine setup with a much larger turbo fitted on the engine is used to further investigate the applicability of the control design. Experiments from that engine configuration on a dynamometer, are shown in Figure 18. With the bigger turbo this system has a much slower step response compared to the previous ones, and the same closed loop performance can therefore not be achieved. However as can be seen in the figure the qualitative behavior of the closed loop system is still achieved, i.e. with as fast response as possible balanced against a small overshoot. In this case a smaller λ -value is used, as was indicated in the discussion of the controller tuning. These results further strengthens the conclusion that the proposed control design successfully achieves the desired behavior.

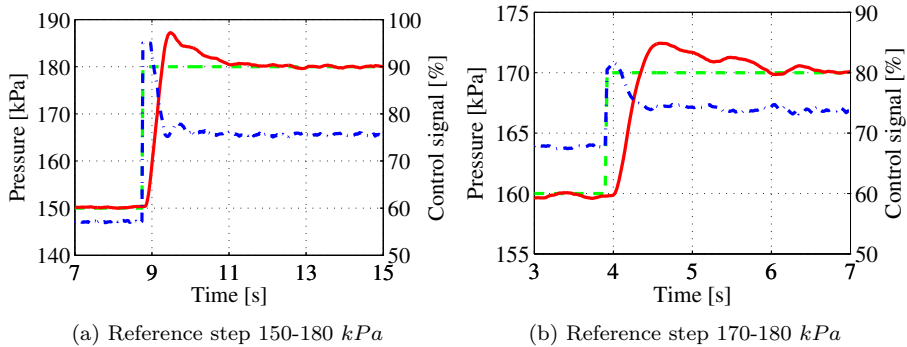


Figure 15: Boost pressure step responses for 2500 rpm measured in test car. The overshoot is close to 5 kPa for the larger step response and around 3 kPa for the smaller. There are no significant oscillations present, the small tendency seen in (b) is too small to be felt by the driver.

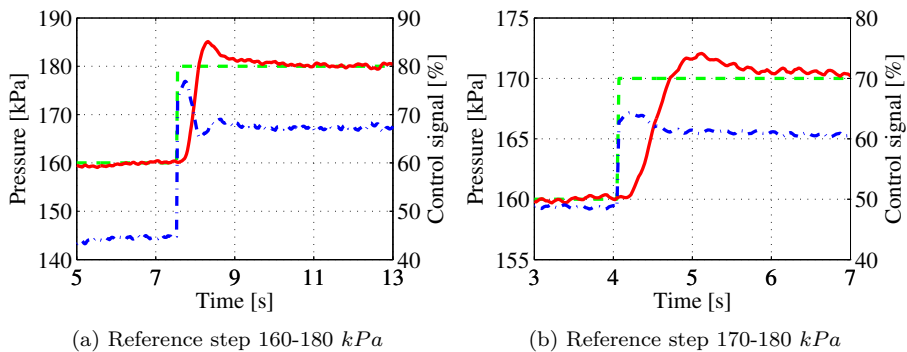


Figure 16: Boost pressure step responses for 4500 rpm measured in test car. As for 2500 rpm the overshoot is about 5 kPa for the larger step response and around 3 kPa for the smaller.

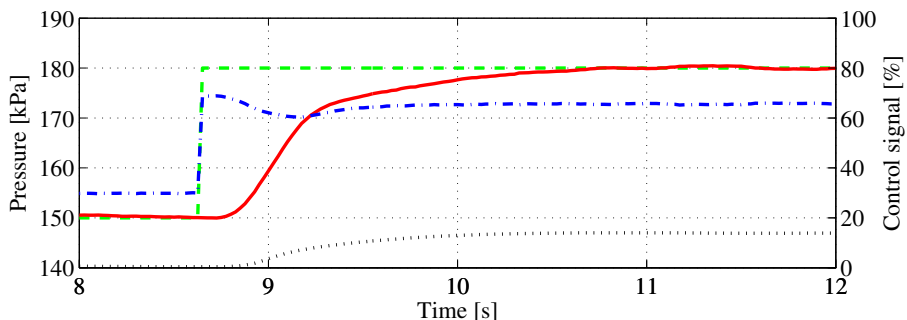


Figure 17: Boost pressure step response measured in test car that illustrates the importance of accurate feedforward calibration. In this example there is a 13 % error in the feedforward for 180 kPa reference pressure. The error is suppressed by the integrator part of the PID controller but the desired shape of the step response is not achieved. The same signals are used as in previous figures with the addition of the integrator in the controller (black dotted).

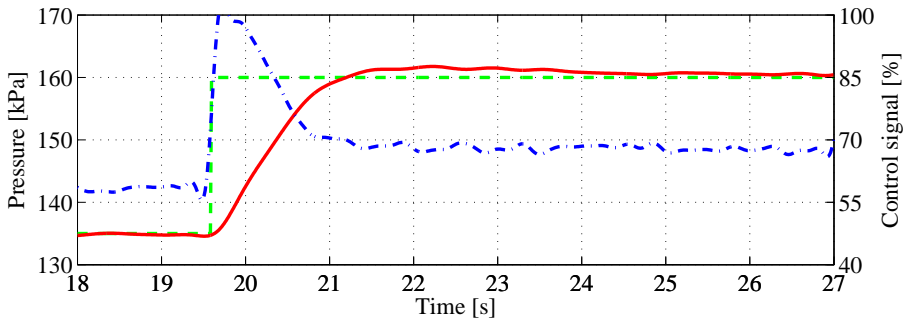


Figure 18: Boost pressure step response measured in an engine test cell with a bigger turbo fitted to the same engine, hence a slower system. It is seen that the control design gives the desired behavior with a fast control response that is balanced against a small overshoot.

5 Conclusions

Wastegate modeling and boost pressure control in a TCSI engine has been studied. A new and simple wastegate actuator model has been developed that captures the main behavior of the actuator. The actuator model is composed of three simple submodels: the actuator pressure, the static position, and an additional position dynamics. The dynamics of the actuator turns out to be important for the transient boost pressure behavior. In particular there is an overshoot in the boost pressure for step changes in the actuator control input that is caused by the actuator characteristics.

The actuator model is inserted in an existing MVEM, that describes the gas flows of the engine, and the complete model is used to predict the transient behavior of the wastegate and boost pressure. These transient responses are studied for different conditions and give insight into the properties of the system and thus valuable input to the boost pressure controller. With the aid of the complete MVEM a boost pressure controller, consisting of a feedforward and a gain scheduled PID controller, is developed together with a tuning method based on the IMC framework. Evaluations are performed both on the complete MVEM and on engines where the proposed controller and tuning method is shown to achieve the desired transient behavior in boost pressure. The applicability of the control design and tuning method is experimentally demonstrated, both on an engine in a vehicle and in a test cell where a larger turbo is fitted to the engine. In the latter evaluation the design method is put to test on a slower system and still achieves the desired behavior.

References

- Per Andersson. *Air Charge Estimation in Turbocharged Spark Ignition Engines*. PhD thesis, Linköpings Universitet, December 2005.
- K.-D. Emmenthal, G. Hagermann, and W.-H. Hucho. Turbocharging small displacement spark ignited engines for improved fuel economy. In *SAE World Congr.*, Techn. Paper 790311, February 1979.
- Lars Eriksson. Modeling and Control of Turbocharged SI and DI Engines. *Oil & Gas Science and Technology - Rev. IFP*, 62(4):523–538, 2007.
- Lars Eriksson, Simon Frei, Christopher Onder, and Lino Guzzella. Control and Optimization of Turbo Charged Spark Ignited Engines. In *Proc. of the IFAC World Congr.*, Barcelona, Spain, July 2002a.
- Lars Eriksson, Lars Nielsen, Jan Brugård, Johan Bergström, Fredrik Pettersson, and Per Andersson. Modeling of a turbocharged SI engine. *Annual Reviews in Control*, 26(1):129–137, October 2002b.
- J. Galindo, H. Climent, C. Guardiola, and J. Doménech. Modeling the Vacuum Circuit of a Pneumatic Valve System. *J. of Dynamic Systems, Measurement and Control*, 131(3), May 2009.
- Carlos E. Garcia and Manfred Morari. Internal Model Control. 1. A Unifying Review and Some New Results. *Ind. Eng. Chem. Process. Des. Dev.*, 21: 308–323, 1982.
- L. Guzzella, U. Wenger, and R. Martin. IC-Engine Downsizing and Pressure-Wave Supercharging for Fuel Economy. *SAE World Congr.*, March 2000.
- Amey Y. Kranik, Julia H. Buckland, and Jim S. Freudenberg. Electronic Throttle and Wastegate Control for Turbocharged Gasoline Engines. In *Proc. of the American Control Conference*, volume 7, pages 4434–4439, June 2005.
- P.E. Moraal, I.V. Kolmanovsky, and M-J. van Nieuwstadt. Modeling and Identification of a Current to Vacuum Transducer and VNT actuator. In *Proc. of the IEEE/ASME Int. Conference on Advanced Intelligent Mechatronics*, Atlanta, USA, September 1999.
- P. Moulin, J. Chauvin, and B. Youssef. Modelling and Control of the Air System of a Turbocharged Gasoline Engine. In *Proc. of the IFAC World Congr.*, pages 8487–8494, July 2008.
- Martin Müller. Estimation and Control of Turbocharged Engines. In *SAE World Congr.*, Techn. Paper 2008-01-1013, April 2008.
- Dominique Petitjean, Luciano Bernardini, Chris Middlemass, S. M. Shahed, and Ronald G. Hurley. Advanced Gasoline Engine Turbocharging Technology for Fuel Economy Improvements. In *SAE World Congr.*, Techn. Paper 2004-01-0988, March 2004.

Karl J. Åström and Tore Hägglund. *Advanced PID Control*. ISA-The Instrumentation, Systems, and Automation Society, 2006. ISBN 1-55617-942-1.

Daniel E. Rivera, Manfred Morari, and Sigurd Skogestad. Internal Model Control. 4. PID Controller Design. *Ind. Eng. Chem. Process. Des. Dev.*, 25:252–265, 1986.

Patrik Soltic. *Part-Load Optimized SI Engine Systems*. PhD thesis, Swiss Federal Institute of Technology, Zürich, 2000.

Russel J. Wakeman and Danny O. Wright. Closed Loop Turbocharger Control with Transient Wastegate Functions. *SAE World Congr.*, March 1986.

N. Watson and M.S. Janota. *Turbocharging the Internal Combustion Engine*. The Macmillan Press ltd, 1982. ISBN 0-333-24290-4.

Modeling and validation of a boost pressure actuation system, for a series sequentially turbocharged SI engine[†]

Andreas Thomasson^a, Oskar Leufvén^a, Ivan Criscuolo^b,
and Lars Eriksson^a

^a*Vehicular Systems, Department of Electrical Engineering,
Linköping University, SE-581 83 Linköping, Sweden.*

^b*Department of Mechanical Engineering, University of Salerno,
Fisciano 84084 Italy*

[†]This is a formatted version of “Modeling and validation of a boost pressure actuation system, for a series sequentially turbocharged SI engine” by Andreas Thomasson, Oskar Leufvén, Ivan Criscuolo, and Lars Eriksson, *Control Engineering Practice*, Volume 21, Issue 12, pages 1860-1870. ©Elsevier 2013. Reproduced with the permission of Elsevier. The original paper can be found at [sciencedirect.com](http://www.sciencedirect.com) <http://www.sciencedirect.com/>, and can be found using the Digital Object Identifier (DOI): 10.1016/j.conengprac.2013.01.004. The formatting is restricted to changing the article into a single-column format, adjusting sizes of figures and tables, and adjusting the referencing style.

Abstract

An actuation system for flexible control of an advanced turbocharging system is studied. It incorporates a vacuum pump and tank that are connected to pulse width modulation controlled vacuum valves. A methodology for modeling the entire boost pressure actuation system is developed. Emphasis is placed on developing component models that are easily identified from measured data, without the need for expensive measurements. The models have physical interpretations that enable handling of varying surrounding conditions. The component models and integrated system are evaluated on a two stage series sequential turbo system with three actuators having different characteristics. Several applications of the developed system model are presented, including a nonlinear compensator for voltage disturbance rejection where the performance of the compensator is demonstrated on an engine in a test cell. The applicability of the complete system model for control and diagnosis of the vacuum system is also discussed.

1 Introduction

The trend towards downsizing of internal combustion engines in the automotive industry has increased in recent years. The main goal is to decrease fuel consumption and emissions, while keeping the performance of the engine constant. A way of achieving this goal is the introduction of turbocharging Emmenthal et al. (1979); Guzzella et al. (2000); Petitjean et al. (2004). Lately, more than one turbo has been added to increase flexibility. Both series sequential Zhang et al. (2009); Chasse et al. (2008); Galindo et al. (2009a) and parallel sequential Borila (1986) systems have been developed, and even three stage systems Nitta et al. (2011) have been evaluated. As turbocharging develops, the demand on the wastegate and bypass valve control strategies increases. Coordinated control of throttle, and compressor and turbine bypass valves is important, since the control affects engine performance and efficiency (Eriksson and Nielsen, 2000; Eriksson et al., 2002a). Boost control flexibility can be increased by including a vacuum tank and vacuum controlled actuators, that unlike pressure controlled actuators are unaffected by the current boost pressure. Both types are however affected by other surrounding conditions, like system voltage and ambient pressure. This leads to an increasing need for good knowledge about the complete vacuum system and how surrounding conditions affect boost control performance. Unnecessary operation of the high power vacuum pump, naturally also affects fuel efficiency, due to its increased electrical load.

1.1 Related research and contributions

A control strategy for a pneumatic system, based on using actuator acceleration feedback is presented in Wang et al. (1999). No air leakages, constant supply pressure and measurement of actuator position to estimate acceleration was assumed. A self-tuning LQG pressure regulator for a pneumatic pressure load systems is presented in Wang et al. (2007). Compared to the control strategy in Wang et al. (1999), the requirement of acceleration feedback is removed. The valve flow is modeled with valve position dependent effective flow areas, and the actuator is modeled using an emptying and filling approach. Constant supply pressure and no leakage are assumed in these papers, while this paper contributes by considering varying pressure and models the leakage flow.

To increase controller response, a Pulse Width Modulation (PWM) peak and hold control strategy is proposed in Amirante et al. (2008). The approach presented removes the requirement for a control valve position sensor, but instead requires a special power driver, and is shown to increase the performance of the control valve.

A switching valve is developed and modeled in Topçu et al. (2006), describing the underlying electromagnetic subsystems of the control valve. The very rapid valve switching times, and thus PWM frequency, is emphasized, as well as the good linearity between PWM frequency and valve position. Physical modeling of the electromagnetic solenoid system is further presented. The pneumatic actuator system of an automotive VGT system is modeled and simulated in Mehmood et al. (2011), emphasizing and modeling the aerodynamic forces due to the exhaust

gas and friction hysteresis effects. The model assumes no leakages, isothermal processes and then describes the mass flow between system components. The modeling makes use of force sensors. The aerodynamic forces are also discussed in Naseradinmousavi and Nataraj (2011), along with physical modeling of the electromagnetic properties.

These referenced papers contribute with in depth knowledge of the physical properties of the valves and pneumatic actuator. This paper builds upon these results, and develops a novel model connecting the subsystems while reducing the need for detailed solenoid measurements, geometric data, and magnetic properties. In particular it extends the results of Criscuolo et al. (2011), and the main contribution is a physically based system model for the pneumatic actuator system that is easy to tune from measurements. The model balances model complexity and capability to describe the system, from a boost pressure control perspective. Compared to Criscuolo et al. (2011) the analysis is extended, and a generalized modeling methodology is developed. The methodology is shown to be applicable to all three actuators of a series sequential two stage charging system, and thus also includes the compressor bypass valve. Further, the paper contributes with knowledge about the spread among components. The modeling covers the full boost pressure actuator system, and therefore also includes models for the vacuum pump and tank subsystems. The vacuum pump is especially important since it consumes high power, and therefore affects the system supply voltage and thereby the boost pressure control. The model structure and parametrization methods are applicable for complex boost pressure control development.

The proposed system model can be integrated in an MVEM structure. MVEM was coined in Hendricks (1989), and component based MVEM of Turbo Charged (TC) Spark Ignited (SI) engines is outlined in Eriksson et al. (2002b). The baseline model is developed and validated in Andersson (2005); Eriksson (2007).

1.2 Outline

The engine and system components are described in Section 2, together with the experimental setup. The data collected for modeling, together with the development of a model for the actuator and solenoid valves, including parameter identification and model validation, are described in Section 3. Section 4 describes the vacuum tank and vacuum pump model, including validation of the models for the different mass flows to and from the tank. In Section 5 several application examples of the developed system model are presented. A nonlinear compensator for voltage disturbance rejection is presented and validated on an engine in a test cell. The possibility to use the model for diagnosis of the vacuum system is discussed, and the contribution to a model based boost control system are pointed out. Conclusions are presented in Section 6. A nomenclature is included in Appendix A.

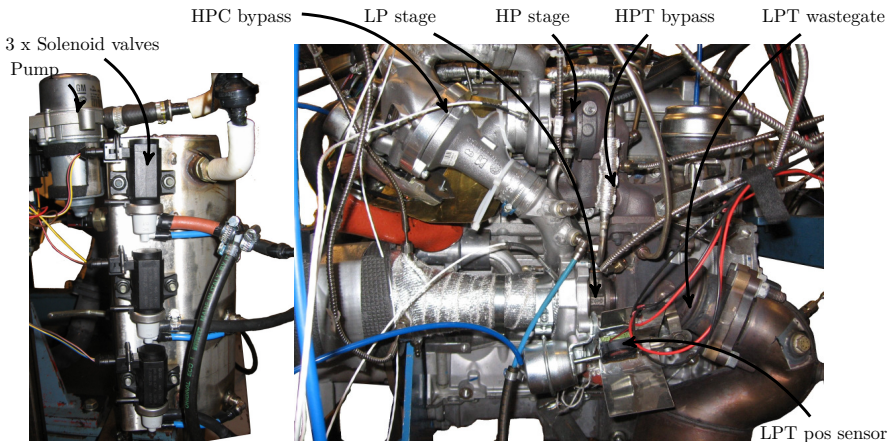


Figure 1: Engine test stand installation pictures. The left picture shows the vacuum tank with the three solenoid valves fitted. The vacuum pump is located on top of the tank, and the tank is further positioned just outside of the lower left corner of the engine picture. The right picture shows the two stage turbo system, with the larger LP stage and the smaller HP stage, as well as the position sensors.

2 Experimental setup

This section describes the series sequential two stage turbocharged engine, its actuation system and the experimental setup.

2.1 Engine and control system

The measurements have been performed in the engine laboratory at the division of Vehicular Systems, Linköping University. A 2.0 liter GM four cylinder direct injection spark ignition engine, equipped with an experimental series sequential two stage system was used for the experiments. The advantage of this layout comes from the different sizes of the turbochargers, where the turbo of the low pressure (LP) stage is larger than the one of the high pressure (HP) stage. In this way, it is possible to utilize each turbocharger in its region of maximum efficiency.

The engine uses a rapid prototyping system from dSpace (RapidPro and MicroAutoBox), connected to a PC running ControlDesk. An overview of the actual two stage system installation, and the vacuum tank with its pump and the three solenoid valves used for control, is shown in Figure 1. System voltage disturbances are injected into the system using an array of light bulbs, controlled by the ECU. A schematic overview of the components and signals is given in Figure 2.

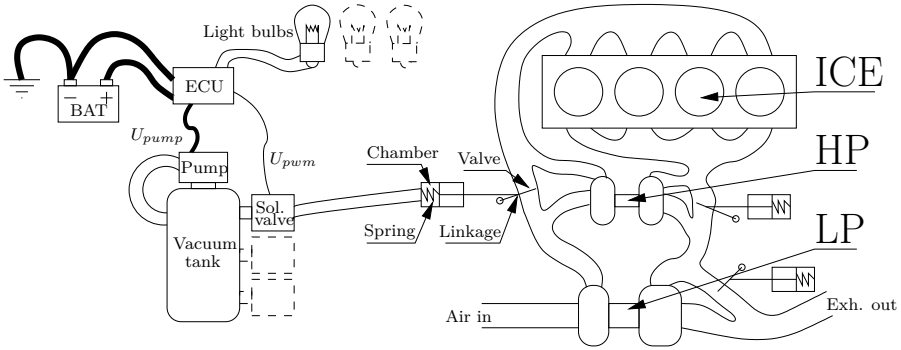


Figure 2: Schematic overview of the systems studied, highlighting important components. The engine control unit (ECU) controls the high power vacuum pump, and the PWM signals to the three solenoid valves. Each solenoid valve controls the an actuator chamber pressure. The force balance on the chamber membrane, set up by pressure difference on either side of the membrane, friction on the linkage and the spring force, gives the valve position. The valve position controls the air flow of the internal combustion engine (ICE). There are in total three gas flow control valves; two on the high pressure (HP) stage, and one on the low pressure (LP) stage. Switching on the high power pump affects the supplied voltage to the ECU from the battery (BAT).

2.2 Boost pressure actuation system

The actuation system consists of three different pneumatic actuators, each supplied by a PWM controlled solenoid valve. In this work, the frequency of the PWM signal was 300 Hz, and the PWM duty cycle is updated by the controller at 80 Hz. The high pressure stage can be by-passed both on the compressor and the turbine side, and a waste gate valve is used for the low pressure stage turbine. All three actuators consist of a membrane sealed chamber, where a controllable vacuum pressure acts on one side of the membrane, and ambient pressure on the other. The pressure difference creates a force. A spring is further used to control the membrane to a safe default position. The membrane is connected via a rod, to the actual valve controlling the engine flow. The geometries of both the rod linkage, as well as the membrane and actuator chamber differ between the three actuators. The solenoid valve contains a plunger, which position is controlled by a PWM signal. The plunger position then controls the pressure in the other pneumatic components. All three actuators use the same solenoid valve type.

The system further consists of a vacuum tank with a high power vacuum pump. The pressure in the vacuum tank should be kept low enough, to allow the membrane force to overcome the other actuator forces, and thereby allowing fully opened and closed valves. The vacuum tank pressure is controlled by the control system, which switches on the vacuum pump when the pressure becomes too high. The reasons for tank pressure rises are leakages and plunger movement in the valve. Leakages are due to air infiltration through the ducts of the system and the elastic membrane in the solenoid valve. Further, when the plunger is in

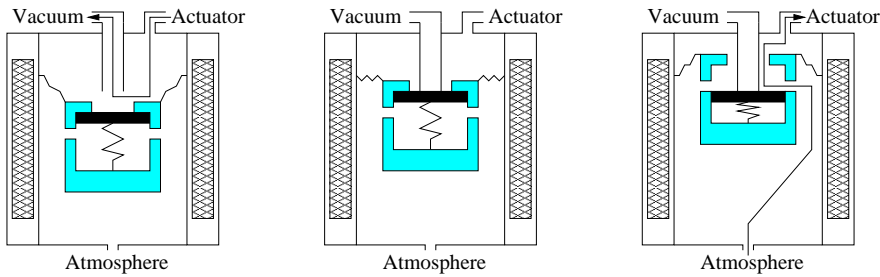


Figure 3: Plunger movement inside the solenoid valve for the three possible working positions. The plunger is drawn in blue color, while the component drawn with squared black-white at the extremities of the figure is the solenoid. The thin arrow show the mass flow direction. In the left figure air flows from the actuator to the vacuum tank, lowering the pressure in the actuator. In the middle figure the plunger is in equilibrium, the pressure in the actuator is constant. In the right figure a mass flow from the atmosphere to the tank is established, raising the actuator pressure.

the down position, a mass flow from actuator to tank is established increasing the tank pressure, see Figure 3. More information on plunger behavior can be found in Galindo et al. (2009b) and Mehmood et al. (2010).

The dSpace equipment was used to both measure the relevant signals (position and pressure) and generate the PWM valve control signals, and to control the system supply voltage using external circuits. Blade 25 position sensors from Gill instruments were used for the two waste gate valves on the turbine side, and a model 9610 linear position sensor from BEI sensors was used for the HP stage compressor bypass. The sensors used to measured actuator pressures were Kistler models 4260 and 4295. The tank pressure was measured using the built in production sensor, which was calibrated using the Kistler cell sensors.

3 Actuator modeling

This section presents a modeling methodology for vacuum controlled actuators, commonly used to control turbochargers in the automotive industry. The characteristics of these actuators can vary significantly but their common physical structure allows the same method and model structure to be applied.

The models structure is divided in three parts, the pressure solenoid model i.e. the relationship between control signal and actuator pressure, a model for the actuator pressure to position and a model for the mass flow leakage to the vacuum tank. The last part is important for a complete system understanding, since the vacuum pump consumes high power, affecting the supply voltage and thereby the solenoid valve characteristic. The models require neither detailed knowledge of electrical and magnetic properties of the solenoid nor the plunger movement inside it, but are easily identified from measurements and applicable to control design. The only extra sensors used are actuator chamber pressure and position of the connecting rod.

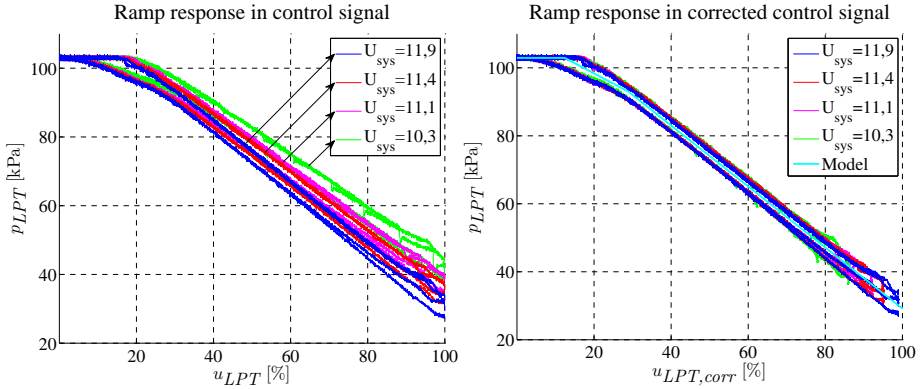


Figure 4: Actuator pressure from ramp responses up and down in control signal. In the right figure control signal have been normalized with the current system voltage. When this is done the control signal to pressure relation align into two curves, determined by whether the pressure is increasing or decreasing.

To demonstrate the methodology, each submodel are identified for all three vacuum actuators on a series sequential turbocharging system. In each subsection the model are presented together with identification for one wastegate actuator, followed by the corresponding plots for the other wastegate and bypass actuator, and discussion of similarities and differences. The nomenclature used in the following sections is found in A.

3.1 Control signal to pressure

The actuator pressure is governed by a solenoid valve connected to the vacuum tank, ambient pressure, and the actuator, see Figure 3. The solenoid is controlled by the ECU with a PWM signal. Depending on the duty cycle the solenoid will strive for a certain pressure drop from the atmosphere to the actuator. This is done by either leading air form the actuator to the vacuum tank, lowering the pressure in the actuator, or by leading air from the atmosphere to the actuator, raising the actuator pressure.

A slow ramp response up and down in control signal is shown to the left in Figure 4. It is evident that different system voltages gives different characteristics of the control signal to pressure relation. Normalizing the control signal with the system voltage results in a control signal with the same average value for different supply voltage. The corrected control signal, u_{corr} , becomes

$$u_{corr} = \frac{U_{syst}}{U_{ref}} u \quad (1)$$

where u is the control signal, U_{syst} is the system voltage and U_{ref} is a reference voltage. The right figure shows the actuator pressure plotted against corrected control signal, u_{corr} . The difference between the curves depends on whether the pressure is increasing or decreasing. The mean value of the two curves is

identified as the static control signal to pressure relation. For this actuator the relationship is almost linear in control signal, with a change in proportionality constant around $u_{corr} = 25$. It is therefore described as a piecewise linear function in control signal, saturated above and below by the ambient pressure, p_{amb} , and the vacuum tank pressure, p_{vac} , respectively.

$$p_{LPT}^* = \min(k_1 u_{corr} + p_{01}, k_2 u_{corr} + p_{02})$$

$$p_{LPT,stat} = \begin{cases} p_{amb} & \text{if } p_{LPT}^* \geq p_{amb} \\ p_{LPT}^* & \text{if } p_{vac} \leq p_{LPT}^* \leq p_{amb} \\ p_{vac} & \text{if } p_{LPT}^* \leq p_{vac} \end{cases} \quad (2)$$

Model parameters are the proportionality constants, k_1 and k_2 , and the offsets p_{01} and p_{02} , for the linear functions. The model output is the static pressure, $p_{LPT,stat}$. In the right plot of Figure 4 this model has been fitted to the corrected control signal to pressure data, and it can be seen that the agreement is good.

The actuator pressure does not change instantaneously as the control signal changes. The pressure rise depends on the mass flow between ambient, actuator and vacuum tank, and can be modeled as

$$\dot{m} = \frac{p_u}{\sqrt{RT_u}} C_d A \Psi(\Pi_{lim})$$

$$\Psi(\Pi_{lim}) = \sqrt{\frac{2\gamma}{\gamma-1} \left(\Pi_{lim}^{\frac{2}{\gamma}} - \Pi_{lim}^{\frac{\gamma+1}{\gamma}} \right)}$$

$$\Pi_{lim} = \max \left(\Pi, \left(\frac{2}{\gamma+1} \right)^{\frac{\gamma}{\gamma-1}} \right) \quad (3)$$

where \dot{m} is the mass flow, p_u and T_u are the pressure and temperature upstream, R is the specific gas constant, C_d is the discharge coefficient, A is the flow area, p_d is the pressure downstream and $\Pi = p_d/p_u$ is the pressure ratio, see e.g. Taghizadeh et al. (2009). This model requires detailed knowledge about the solenoid and how the effective area $A_{eff} = C_d A$ varies with control signal and pressures.

Analyzing the operating principles and interaction between the solenoid valve and the actuator pressure, presented in e.g. Topçu et al. (2006); Mehmood et al. (2010); Galindo et al. (2009b), an opportunity for model reduction is identified. It is recognized that the solenoid valve acts as a controller for the actuator pressure, where the reference in this controller is $p_{LPT,stat}$. This is motivated by the property that the solenoid controls the pressure toward the static pressure in equation (2) and Figure 4. Studying measurements, it is seen that a first order system is a good approximation for the pressure dynamics, see Figure 5. A simple model for this is therefore

$$\tau \dot{p}_{LPT,dyn} = -p_{LPT,dyn} + p_{LPT,stat} \quad (4)$$

where $p_{LPT,stat}$ is the input pressure, $p_{LPT,dyn}$ is the output pressure and τ is the time constant for the first order dynamic system. This model is easily identified

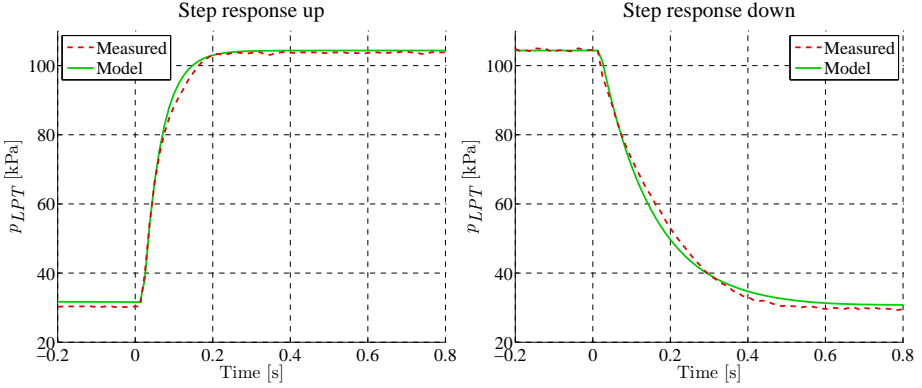


Figure 5: Actuator pressure for a step responses up and down in control signal. The response is well described by a first order dynamic system, but with different time constants for increasing and decreasing pressure.

from measured data with few extra sensors, using ramps and step responses in control signal.

Figure 5 shows two step responses in control signal, together with a step response for a first order system. The pressure response to a step is well described by the first order system, but different time constants have to be used for increasing and decreasing pressure. This difference is due to different effective areas and pressures for the mass flow from ambient to actuator, compared to actuator to vacuum tank.

Ramp responses for the other two actuators are shown in Figure 6, where measured and modeled pressure is plotted against corrected control signal. The characteristics of the HPC solenoid is very different, compared to that of the other two. This requires another function to be used for the static pressure, but the same model structure can be used.

$$\begin{aligned}
 p_{HPC}^* &= \min(k_1 u_{corr} + p_{01}, p_{amb} + k_2 \max(0, u_{corr} - u_0)^3) \\
 p_{HPC,stat} &= \begin{cases} p_{amb} & \text{if } p_{HPC}^* \geq p_{amb} \\ p_{HPC}^* & \text{if } p_{vac} \leq p_{HPC}^* \leq p_{amb} \\ p_{vac} & \text{if } p_{HPC}^* \leq p_{vac} \end{cases} \quad (5)
 \end{aligned}$$

The parameters u_0 and k_2 describes the decrease from ambient pressure at $u_{corr} = u_0 \approx 40\%$ until $u_{corr} \approx 90\%$, and k_1 and p_{01} describes the linear region with $u_{corr} \approx 90 - 100\%$, see the right plot of Figure 6.

The pressure dynamics for the other two actuators are shown in Figure 7. As for the LPT actuator solenoid the dynamics is well captured by a first order dynamical system.

3.2 Pressure to position

The pressure in the actuator chamber exercises a force on the membrane in the actuator. The other forces are the spring force, the friction force and forces

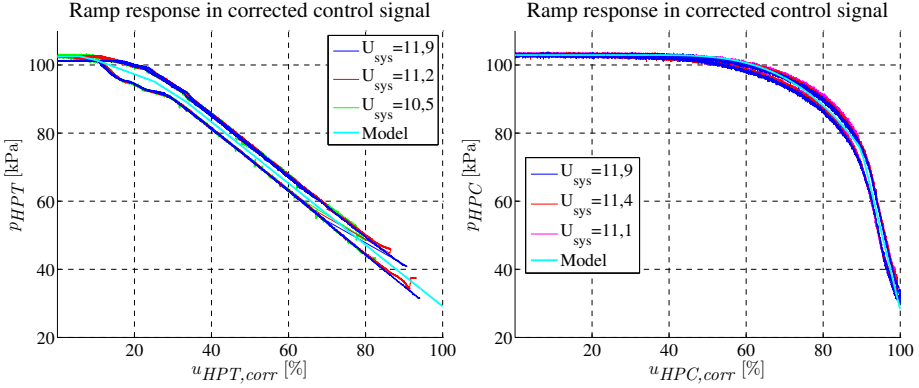


Figure 6: Actuator pressure from ramp response up and down in control signal for the HPT and HPC actuator. The pressure solenoid for the HPC actuator has a very different characteristic than the other two actuators. The model structure remains the same, but a different function for the static pressure is used.

resulting from the gas in the exhaust or intake acting on the wastegate or bypass valve respectively, see Figure 8. This means that the model does not only depend on the actuator itself, but is also affected by the mounting on the engine. The sum of the forces on the actuator accelerates the connecting rod of the actuator and the valve it is connected to, according to Newtons second law of motion

$$m \ddot{x} = F_{amb} - b \dot{x} - F_{act} - F_{fr} - F_{sp} - F_{aero} \quad (6)$$

where x is the displacement, m is the mass of the moving parts, b is the dynamic friction coefficient, F_{act} is the force from the actuator pressure on the membrane, F_{amb} is from the ambient pressure on the other side of the membrane, F_{sp} is the spring force, and F_{aero} is the aerodynamic force. To accurately identify the relation between the forces F_{amb} , F_{act} , F_{sp} , F_{fr} it is recommended to run the experiments without the engine running. To model F_{aero} , one can e.g. follow the approach presented in Mehmood et al. (2010).

A slow ramp response in pressure can be used to identify the spring and static friction forces. Figure 9 shows position plotted against pressure for ramp responses in control signal for the LPT actuator, previously used to identify the static pressure relation. The ramp responses are very slow and approximates the static relation given by setting $\ddot{x} = 0$ and $\dot{x} = 0$ in (6). To further simplify identification, since $F_{amb} = p_{amb}A_{act}$ and $F_{act} = p_{act}A_{act}$ where A_{act} is the membrane area, the force balance is normalized with A_{act} to get the relation

$$0 = p_{amb} - p_{act} - p_{sp}(x_{act}) - p_{fr} \quad (7)$$

Assuming that the friction has the same magnitude in both directions, p_{fr} can be estimated as the difference between the ramps up and down, and the mean of the two ramps with $p_{fr} = 0$ gives $p_{sp}(x_{act})$. In the right plot of Figure 9 the following linear model for the LPT actuator position is included

$$x_{LPT} = k p_{LPT} + x_0 \quad (8)$$

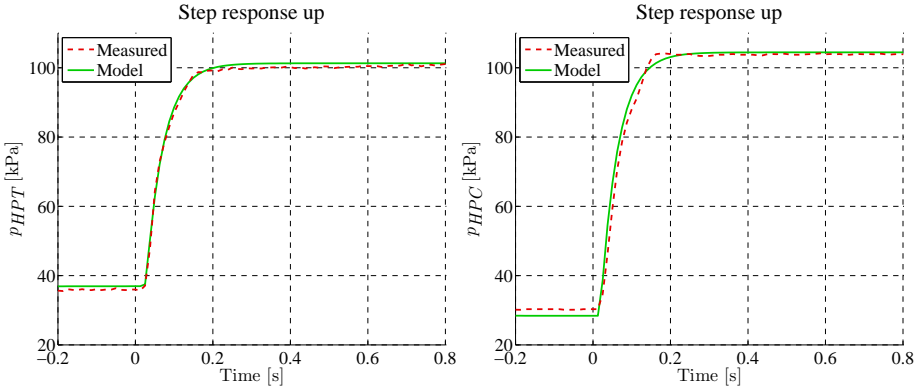


Figure 7: Actuator pressure for a step response in control signal for the HPT and HPC actuator. As for the LPT actuator, the responses are well described by a first order dynamic system.

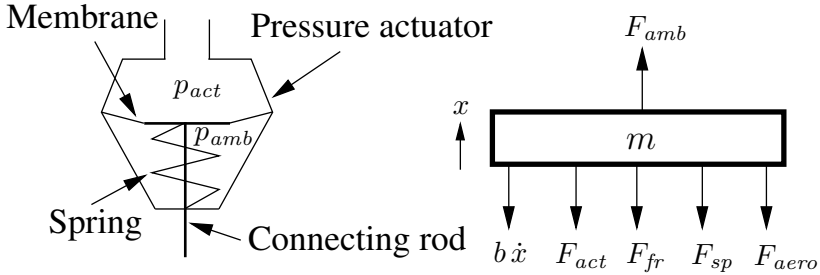


Figure 8: Actuator working principle and the forces acting on the mechanical system.

where k and x_0 are model parameters. From (7) and (8), $p_{sp}(x_{act})$ is easily determined ($x_{act} = x_{LPT}$ for this actuator).

Ramp responses for the other two actuators are shown in figure 10. Two differences compared to the LPT actuator are evident. The relationship is not linear and the distance between the ramp up and down, corresponding to the friction force, is greater and varies with position.

Measurements from ramps up and down are used to parametrize two static relations from pressure to position, see Figure 10. The mean value is then used as the spring force (or pressure) and half the distance between them as a position dependent friction. To parameterize the pressure position relation for the two curves, for both actuators an arctan function has been used.

$$x_{act} = a_1 + a_2 \arctan \frac{a_3 - p_{act}}{a_4} \quad (9)$$

The parameters a_1 and a_3 determines the xy-position of the curve and a_2 and a_4 controls the shape. All parameters are estimated from measurements using least squares. In the same manner as for the LPT actuator, given a position this

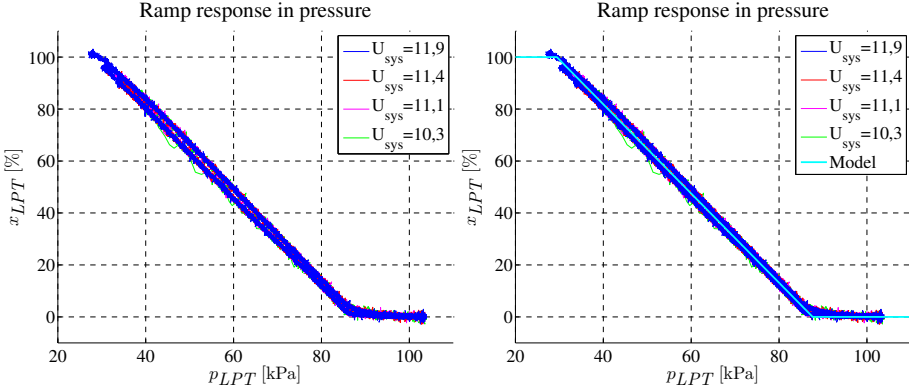


Figure 9: Position vs. pressure for ramps up and down in control signal, for the LPT actuator. The relationship between pressure and position is linear, with a small difference between ramps up and down due to friction. In the right figure a linear model with saturation is included.

is used to calculate the resulting spring force or pressure. The difference being that two pressures are calculated and the mean is used for the spring force and half the difference as the coulomb friction.

To model the friction force the popular Dahl's model is used, proposed by Dahl (1968) and used also by e.g. Singh and Kunt (1990); Armstrong-Hélouvy et al. (1994); Mehmood et al. (2010):

$$\frac{dF_{fr}}{dt} = \sigma \left(1 - \frac{F_{fr}}{F_c} \operatorname{sgn}(\dot{x}) \right)^\alpha \dot{x} \quad (10)$$

where F_c , σ and α are model parameters that determine the shape of the curve. Further, the common choice of $\alpha = 1$ is used, see Olsson et al. (1998).

The position dynamics are determined by the parameters m and b in (6). These are identified using the least squares method from measured pressure and position for steps in control signal. The dynamic friction for the step responses up and down are different, roughly by a factor of two. Measured and modeled LPT actuator positions, for steps up and down in control signal, are shown in Figure 11. It is seen that the mass spring damper model gives a good description of the measured data.

The same procedure can be applied to identify the parameters of the dynamic position response for the other two actuators. Step responses for these actuators are shown in Figure 12. The step response for the HPT actuator follows the measured position, except at the end of the step where the modeled position is lower. In the step for the HPC actuator a non modeled phenomena is present, the actuator almost comes to a halt soon after the step starts. This is due to small linkage clearance of the prototype system, causing the HPC actuator to stick at 10% for closing steps. This results in an error in the static friction force and is also evident in the ramp response in the right plot in Figure 10.

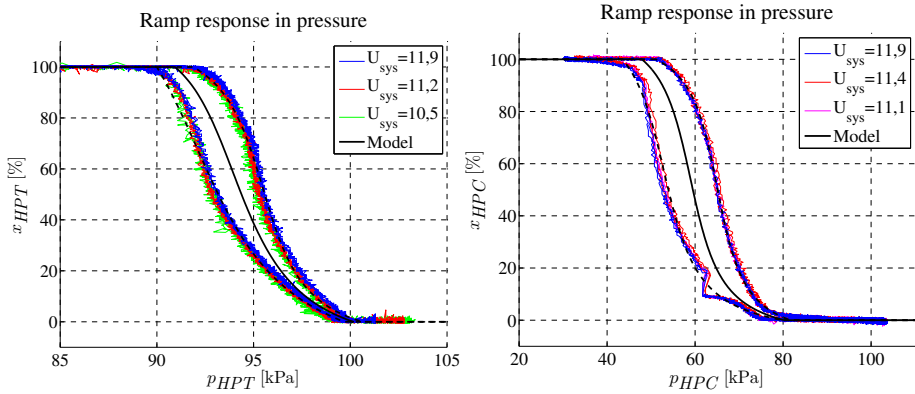


Figure 10: Position vs. pressure for ramps up and down in control signal for the HPT and HPC actuators. For both these actuators, a larger friction is present.

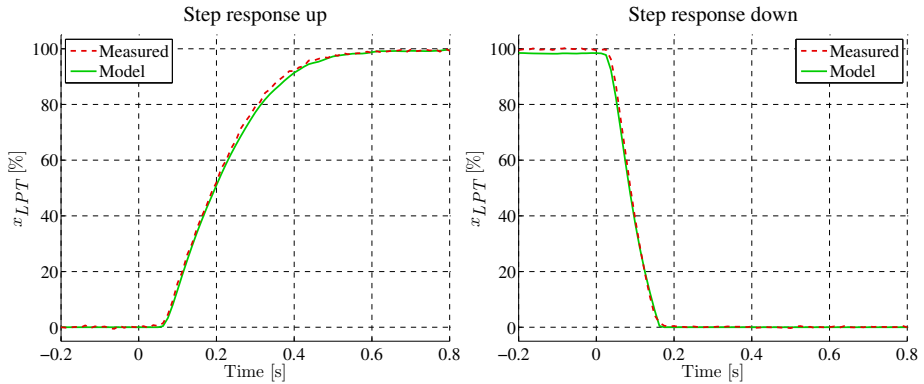


Figure 11: Measured and modeled pressure response for a step up and down in control signal for the LPT actuator.

3.3 Mass flow

To model the complete vacuum system, the mass flow leakage from the actuators and surrounding to the vacuum tank needs to be estimated. This is divided into different parts. First a base leakage is determined by only looking at the pressure rise in the vacuum tank without operating the solenoid valves. The leakage flow is modeled with the orifice equation for compressible flow (3), and an effective leakage area is determined.

Ideally there should be no more leakage than this for constant control signal when the actuator pressure has stabilized, and the plunger in the solenoid has reached equilibrium. The plunger will however oscillate and allow some flow through the solenoid valve. The left plot of Figure 13 shows that the leakage flow for constant control signal increases with increasing control signal. The right plot of Figure 13, shows the effective area for the leakage flow from actuator to vacuum tank plotted against control signal. The area increases linearly until

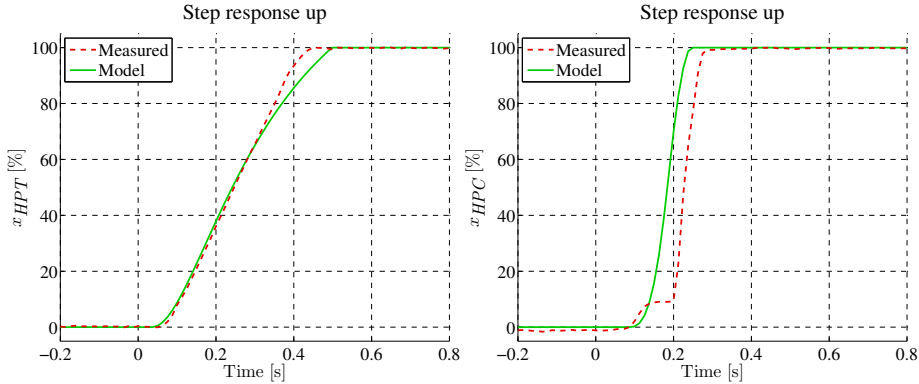


Figure 12: Measured and modeled pressure response for a step in control signal for the HPT and HPC actuators. The HPT model describes the measured response good except for the end of the step where the model undershoots the measurement. In the step for the HPC actuator an error originating from a non modeled phenomena in the static friction or spring force is present. This is due to small linkage clearance of the prototype system, causing the HPC actuator to stick at 10% for closing steps. This is also seen in Figure 10.

approximately 80% control signal, a linear model is also included in the figure. In the next section it is shown that this model is sufficient to give an accurate enough estimate of the leakage flow for constant control signal. If more accuracy is needed, a more complicated function or look-up table can be used.

The last part of the mass flow from actuator to tank is due to changes in pressure and volume of the actuator. To reduce the pressure in the actuator a mass flow is established from the actuator to the tank. In addition when the pressure decreases the actuator volume is reduced which also contributes to the mass flow to the tank. Starting from the ideal gas law

$$p_{act} V_{act} = m_{act} R T_{act} \quad (11)$$

constant temperature is assumed, $T_{act} = T_{amb}$. Differentiating and saturating the result at zero from below, since negative mass flow will mean mass flow from ambient to actuator, gives the following equation for the mass flow from actuator to tank

$$\frac{dm}{dt} = \max \left(0, \frac{1}{RT_{amb}} \left(\frac{dp_{act}}{dt} V_{act} + \frac{dV_{act}}{dt} p_{act} \right) \right) \quad (12)$$

The procedure for identifying the mass flow leakage from the other two actuators are identical and are not included here. Validation of the mass flow leakage models for all actuators are done together with the vacuum tank model in the next section.

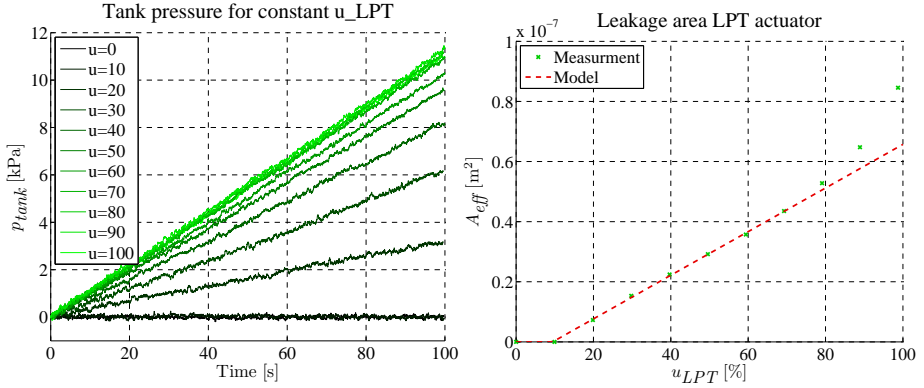


Figure 13: *Left:* Vacuum tank pressure, with offset to start at zero, for different constant control signals for the LPT actuator. The base leakage for zero control signal have been subtracted from each curve. The trend toward increasing leakage with increasing control signal is clear. *Right:* Effective area for the leakage flow and a linear model for the effective area. The model is very accurate up to 80% control signal.

4 Vacuum tank and pump model

The vacuum tank provides a low pressure reservoir needed to operate the vacuum actuators. This part is important for the complete system, since it determines how often the vacuum pump will be used. The vacuum pump is used to lower the vacuum tank pressure. When the pump is turned on it consumes high power and can lower the overall system voltage, affecting boost control. Since it consumes power it also contributes to the overall fuel consumption and it is therefore of interest to include in a complete system model.

4.1 Vacuum tank model

The vacuum tank is modeled as an isothermal volume, with $T_{tank} = T_{amb}$, and one state for the tank pressure. The pressure change in the tank are determined from the ideal gas law (11) and becomes

$$\frac{dp_{tank}}{dt} = \frac{R T_{amb}}{V_{tank}} (\dot{m}_{in} - \dot{m}_{out}) \quad (13)$$

The mass flow to the tank is the sum of the base leakage and the mass flow from each actuator. Mass flow out of the tank is achieved by the vacuum pump described in the next section. In Figure 14, the measured and modeled tank pressures are shown for different operation of the three actuators. The left plots are from a series of steps in control signal and the right plots are from ramp responses. The pressure deviates slightly over time, but this is hard to avoid since the mass flow is integrated to get the tank pressure. A small error in flow will therefore result in an increasing pressure error. The leakage flow is overestimated in some operating points. This is not of major importance and the accuracy is enough to give a realistic behavior. If a more accurate estimate of the

leakage flow during operation is required, an observer should be implemented. This model agreement is acceptable for a controls application, since there is a tank pressure sensor.

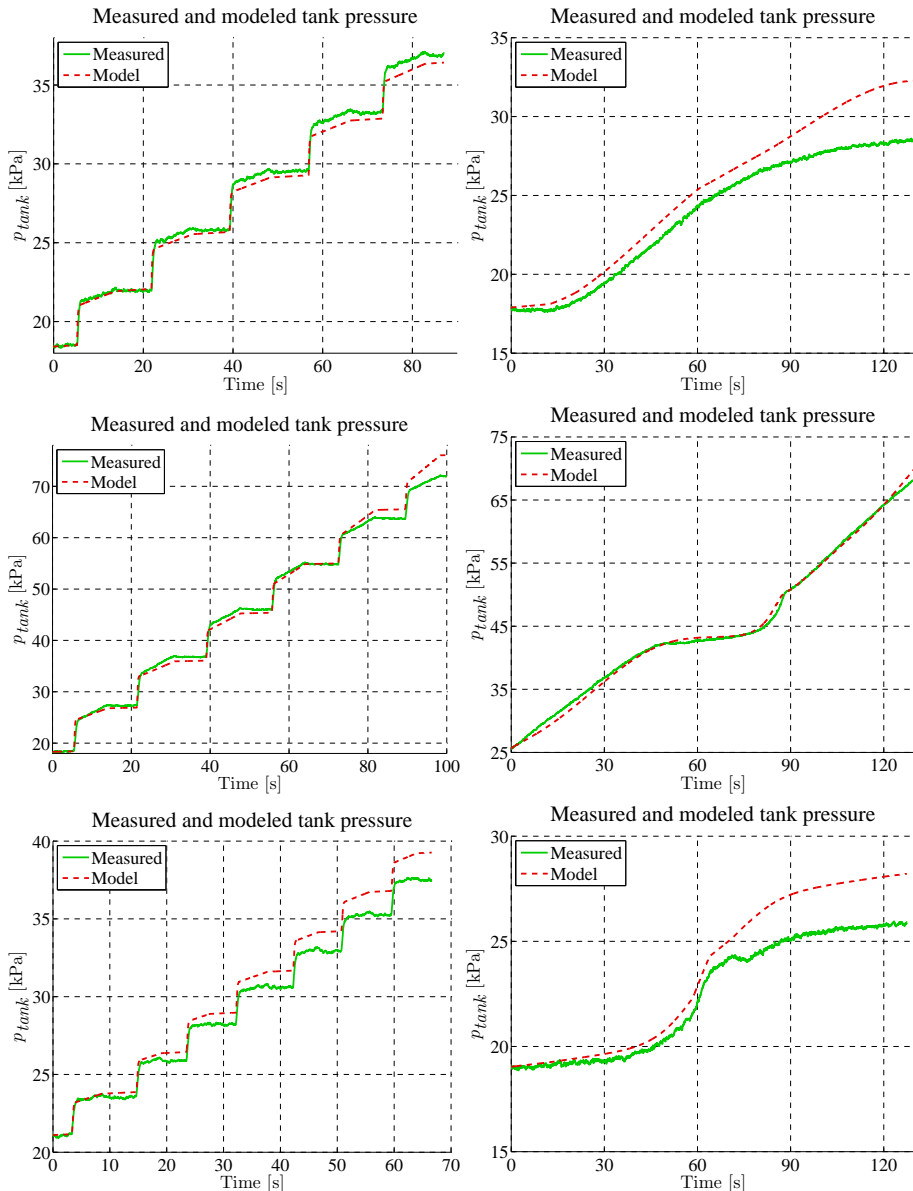


Figure 14: Measured and modeled vacuum tank pressures for steps and ramps in all actuators. The model gives a good estimation of the tank pressure change for both the step and ramp responses. The slight deviation over time in some operating points is not of major importance for a realistic behavior of the vacuum system during operation, and is hard to avoid since the system is integrating.

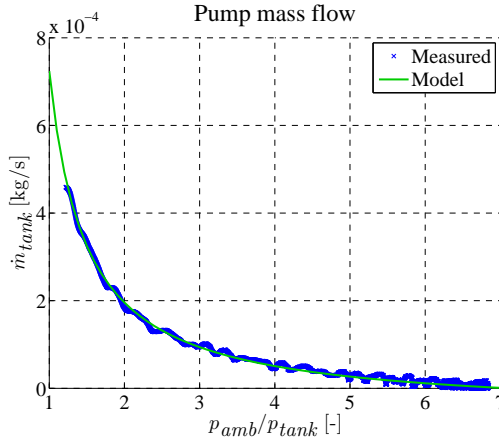


Figure 15: Pump mass flow plotted against pressure ratio from ambient to vacuum tank. Also in the figure is a three parameter model of the pump flow as function of pressure ratio.

4.2 Vacuum pump model

The mass flow that the pump is able to produce is strongly connected to the pressure ratio over the pump, see Figure 15. The data was collected by switching on the pump with close to ambient pressure in the tank and wait until the vacuum settled on the lowest possible pressure. The total mass flow was then calculated from the pressure trace and the base leakage flow to get the pump flow.

$$\dot{m}_{tank} = \frac{a_1}{\frac{p_{amb}}{p_{tank}} + a_2} + a_3 \quad (14)$$

This three parameter model captures the mass flow as function of pressure ratio with good accuracy and its validation is included in Figure 15.

5 Model applications

One important practical problem for control engineering, is that the system voltage can vary several Volts during operation. This can directly influence the boost pressure controller performance. System voltage changes can for example be caused by switching on the vacuum pump. An example of the measured effect from a supply voltage disturbance (switching on light bulbs), is shown in Figure 16. The change in the high pressure turbine actuator pressure, and the corresponding change in boost pressure before the throttle and high pressure stage turbo shaft speed is shown. The engine speed and throttle position were held constant during the experiment. During the first 2.5 seconds and after 20 seconds of the measurement, no light bulbs were lit. The difference in system supply voltage seen here is due to the high power vacuum pump being switched on initially in the measurement, resulting in different boost pressure.

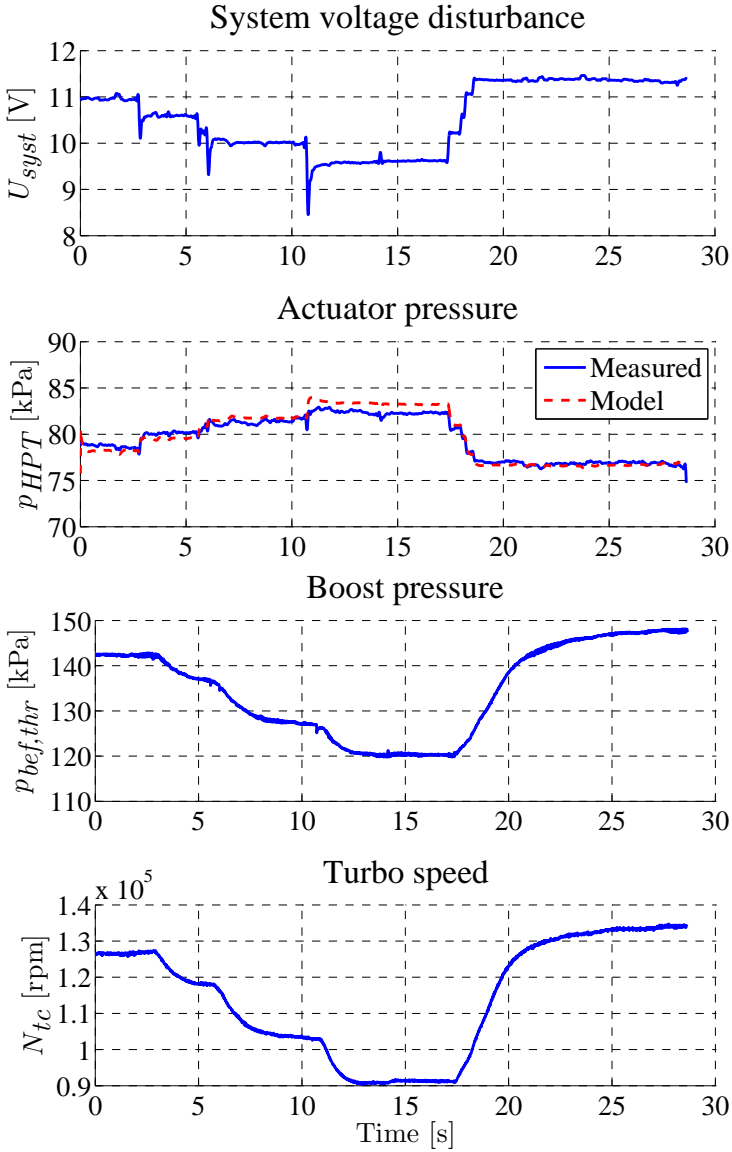


Figure 16: The effect of a system voltage disturbance for a constant speed operating point, 1800 rpm, with fixed throttle position. Boost pressure is controlled by the smaller high pressure stage, and a series of voltage steps are applied. When the system voltage drops, the actuator pressure increases, the wastegate valve opens and the boost pressure decreases. The dashed line in the second plot shows that the developed model captures both the static and the dynamic behavior well.

5.1 Actuator pressure model

In Figure 16, it can be seen that the system voltage variations of roughly 1.5 V, lead to an actuator pressure change of 5 kPa. This pressure change causes the boost pressure to drop from 145 kPa to 120 kPa, and turbo speed to drop from 125 krpm to 90 krpm.

Also shown in the second plot of Figure 16, is the simulated output of the high pressure stage turbine actuator model developed in the previous section, showing good agreement both during transients and stationary. The high pressure turbine actuator was chosen here, since this actuator was the most sensitive to supply voltage disturbances, due to steepness of the pressure to position curves, see Figure 10. The behavior however, is representable also for the low pressure stage turbine actuator as well as the high pressure stage compressor bypass actuator.

5.2 Supply voltage compensation

The system voltage affects the magnetic field controlling the plunger position in the solenoid valve. This is supported by the measurements and the developed control signal to pressure model in Section 3.1. It was shown that the dispersion due to system voltage could be removed by normalizing the control signal with the current system voltage. Based on the model and (1), the following modification to the boost controller output is proposed to handle deviations in supply voltage

$$u_{ctrl,corr} = \frac{U_{ref}}{U_{syst}} u_{ctrl} \quad (15)$$

where u_{ctrl} is the controller output, $u_{ctrl,corr}$ is the corrected control signal, U_{syst} is the supply voltage, and U_{ref} is a reference voltage. Given a desired value of wastegate position, a corresponding control signal can be calculated using the inverse of the actuator model. A compensation for supply voltage is then calculated using (15). This was proposed and tested on the LPT actuator in Criscuolo et al. (2011) and has been extended and to include the HPT and HPC actuator as well. The compensation was tested with a voltage disturbance and the results are shown in Figure 17, where open loop control with and without the voltage compensation has been subjected to the same disturbance. Despite the voltage disturbance, appropriately modifying the control signal with the aid of the developed model, the membrane position is kept almost constant, ensuring that the disturbance does not affect the boost pressure.

5.3 Vacuum tank and pump model

Another application of the developed system model is to use it to calculate the needed vacuum pressure, which in turn can be used to determine when it is necessary to run the vacuum pump. For example in the operating point in Figure 16, a vacuum pressure of 70 kPa would be enough for controlling the actuator. This can be related to the current conservative implementation that controls the pressure to always be below 35 kPa. Implementing a pump controller that tracks the needed pressure results in less usage of the pump and thereby energy savings.

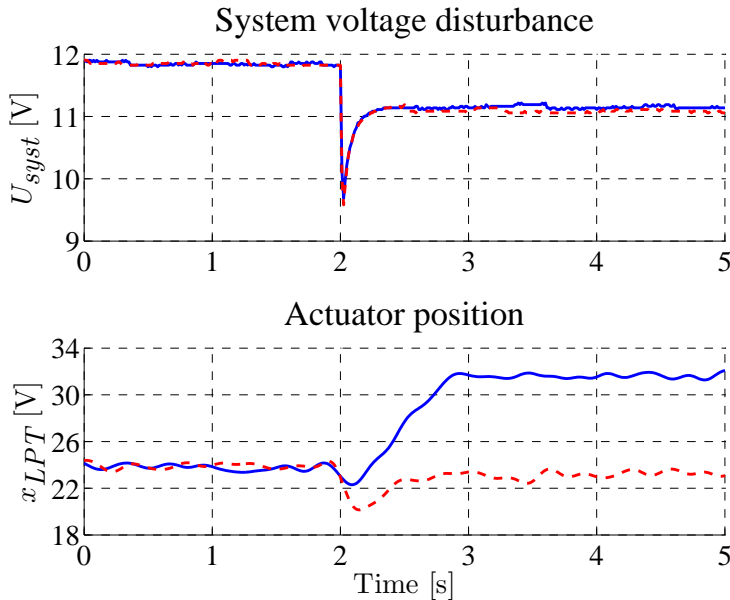


Figure 17: Compensator performance for the supply voltage disturbance. The lower plot shows the wastegate position without compensator (solid) and with compensator (dashed). The compensated wastegate position is almost unaffected by the supply voltage disturbance.

It is also of interest to detect excess air leakage that could result from a broken pressure hose, increased valve or actuator leakages, or other malfunctions. Running under such conditions leads to excessive use of the vacuum pump, which increases fuel consumption. Combining the tank pressure sensor and the developed model gives analytical redundancy and provides means for developing a residual and diagnosis system for detecting abnormal air leakages.

5.4 Model based boost control

As the last example, the developed system model can be included in the feed-forward loop of a model based boost control structure. An effective wastegate area reference (and thus position) can be calculated, based on required engine torque, surrounding conditions, and engine operating point, see for example Müller (2008); Hilding (2011); Moulin and Chauvin (2011). Provided the position, the models developed here gives the possibility to calculate the actuator control signal. A benefit of this feedforward is that disturbances due to surrounding conditions, like e.g. supply voltage, is effectively rejected. Combining this with for example the gain scheduled feedback in Criscuolo et al. (2011), enables integration of the system model in a complete model based boost control structure.

6 Summary and conclusions

A general modeling methodology has been developed and applied for a full vacuum actuation system used in turbocharged engines. The modeling covers the solenoid valves, pneumatic actuators, vacuum tank, and vacuum pump. The methodology is shown to work for all three actuators in a series sequential actuation system. Tank and pump models, with mass flow leakage, are shown to give a good description of the measurement data. The model parametrization methodology relies on low cost sensors and simple experiments. Significant variations are seen between the actuators, highlighting the need for a systematic method for determining parameters. It is observed that the solenoid valve can be described to function as a mechanical controller, which enabled the development of a compact yet accurate model for it. The model has a physical base which enables an engineer to develop model based control laws that account for changing conditions. The environment affects system performance, and the system voltage dependency is highlighted as important for control applications. The developed actuator model is the foundation for a nonlinear compensator, and it is demonstrated to be capable of rejecting system voltage disturbances.

Acknowledgments

This research was supported by the VINNOVA Industry Excellence Center LINK-SIC.

References

- R. Amirante, A. Innone, and L.A. Catalano. Boosted PWM open loop control of hydraulic proportional valves. *Energy Conversion and Management*, 49(8): 2225–2236, 2008.
- Per Andersson. *Air Charge Estimation in Turbocharged Spark Ignition Engines*. PhD thesis, Linköpings Universitet, December 2005.
- Brian Armstrong-Hélouvry, Pierre Dupont, and Carlos Canudas de Wit. A survey of models, analysis tools and compensation methods for the control of machines with friction. *Automatica*, 30(7):1083–1138, 1994.
- Yurij G. Borila. A Sequential Turbocharging Method for Highly-Rated Truck Diesel Engines. In *SAE World Congr.*, Techn. Paper 860074, February 1986.
- A. Chasse, P. Moulin, A. Albrecht, L. Fontvielle, A. Guinois, and L. Doléac. Double Stage Turbocharger Control Strategies Development. *SAE Int. J. of Engines*, 1(1):636–646, 2008.
- Ivan Crisculo, Oskar Leufvén, Andreas Thomasson, and Lars Eriksson. Model-based boost pressure control with system voltage disturbance rejection. In *Proc. of the IFAC World Congr.*, pages 5058–5063, August 2011.

- P. Dahl. A solid friction model. Technical report, The Aerospace Corporation, 1968. TOR-0158H3107-18I-1.
- K.-D. Emmenthal, G. Hagermann, and W.-H. Hucho. Turbocharging small displacement spark ignited engines for improved fuel economy. In *SAE World Congr.*, Techn. Paper 790311, February 1979.
- Lars Eriksson. Modeling and Control of Turbocharged SI and DI Engines. *Oil & Gas Science and Technology - Rev. IFP*, 62(4):523–538, 2007.
- Lars Eriksson and Lars Nielsen. Non-linear Model-Based Throttle Control. *Electronic Engine Controls*, SP-1500:47–51, March 2000.
- Lars Eriksson, Simon Frei, Christopher Onder, and Lino Guzzella. Control and Optimization of Turbo Charged Spark Ignited Engines. In *Proc. of the IFAC World Congr.*, Barcelona, Spain, July 2002a.
- Lars Eriksson, Lars Nielsen, Jan Brugård, Johan Bergström, Fredrik Pettersson, and Per Andersson. Modeling of a turbocharged SI engine. *Annual Reviews in Control*, 26(1):129–137, October 2002b.
- J. Galindo, H. Climent, C. Guardiola, and J. Domenech. Strategies for improving the mode transition in a sequential parallel turbocharged automotive diesel engine. *Int. J. of Automotive Technology*, 10(2):141–149, 2009a.
- J. Galindo, H. Climent, C. Guardiola, and J. Doménech. Modeling the Vacuum Circuit of a Pneumatic Valve System. *J. of Dynamic Systems, Measurement and Control*, 131(3), May 2009b.
- L. Guzzella, U. Wenger, and R. Martin. IC-Engine Downsizing and Pressure-Wave Supercharging for Fuel Economy. *SAE World Congr.*, March 2000.
- Elbert Hendricks. The Analysis of Mean Value Engine Models. In *SAE World Congr.*, Techn. Paper 890563, February 1989.
- Emil Hilding. Enthalpy Based Boost Pressure Control. Master’s thesis, Linköping University, SE-581 83 Linköping, 2011.
- A. Mehmood, S. Laghrouche, and M. El Bagdouri. Nonlinear Modeling of the VNT Pneumatic Actuator with Aero-dynamic Force. In *Proc. of the IFAC Symposium on Advances in Automotive Control*, July 2010.
- A. Mehmood, S. Laghrouche, and M. El Bagdouri. Modeling identification and simulation of pneumatic actuator for VGT system. *Sensors and Actuators A: Physical*, 165(2):367–378, 2011.
- Philippe Moulin and Jonathan Chauvin. Modeling and control of the air system of a turbocharged gasoline engine. *Control Engineering Practice*, 19(3):287–297, 2011.
- Martin Müller. Estimation and Control of Turbocharged Engines. In *SAE World Congr.*, Techn. Paper 2008-01-1013, April 2008.

- Peiman Naseradinmousavi and C. Nataraj. Nonlinear mathematical modeling of butterfly valves driven by solenoid actuators. *Applied Mathematical Modelling*, 35(5):2324–2335, 2011.
- J. Nitta, A. Minato, and N. Shimazaki. Performance Evaluation of Three-Stage Turbocharging System for Heavy-Duty Diesel Engine. In *SAE World Congr.*, Techn. Paper 2011-01-0374, April 2011.
- H. Olsson, K.J. Åström, C. Canudas de Wit, M. Gäfvert, and P. Lischinsky. Friction Models and Friction Compensation. *European J. of Control*, 4(3): 176–195, 1998.
- Dominique Petitjean, Luciano Bernardini, Chris Middlemass, S. M. Shahed, and Ronald G. Hurley. Advanced Gasoline Engine Turbocharging Technology for Fuel Economy Improvements. In *SAE World Congr.*, Techn. Paper 2004-01-0988, March 2004.
- R. Singh and C. Kunt. A linear time varying model for on-off valve controlled pneumatic actuators. In *Trans. of the ASME*, 1990.
- M. Taghizadeh, A. Ghaffari, and F. Najafi. Modeling and identification of a solenoid valve for PWM control applications. *Comptes Rendus Mecanique*, 337:131–140, 2009.
- Elif Erzan Topçu, İbrahim Yüksel, and Zeliha Kamaş. Development of electro-pneumatic fast switching valve and investigation of its characteristics. *Mechatronics*, 16(6):365–378, 2006.
- Jihong Wang, Junscheng Pu, and Philip Moore. A practical control strategy for servo-pneumatic actuator systems. *Control Engineering Practice*, 12(12): 1483–1488, 1999.
- Xue-Song Wang, Yu-Hu Cheng, and Guang-Zheng Peng. Modeling and self-tuning pressure regulator design for pneumatic-pressure-load systems. *Control Engineering Practice*, 15(9):1161–1168, 2007.
- Zhe Zhang, Kangyao Deng, Zhenbiao Wang, and Xiangguo Zhu. Experimental Study on the Three-phase Sequential Turbocharging System with Two Unequal Size Turbochargers. *SAE Int. J. of Fuels and Lubricants*, 1(4):1181–1186, 2009.

A Nomenclature

A description variables and subscripts used in the paper. Note that subscripts may be combined, for example p_{LPT} refers to the pressure in the low pressure turbine actuator.

Variable	Description	Subscript	Description
a	Model parameter	act	Actuator
b	Friction coefficient	aero	Aerodynamic
F	Force	amb	Ambient
k	Model parameter	C	Compressor
m	Mass	corr	Corrected
N	Rotational speed	ctrl	Control
p	Pressure	dyn	Dynamic
Π	Pressure ratio	fr	Friction
R	Gas constant	HP	High pressure
T	Temperature	LP	Low pressure
U	Voltage	lim	Limit
u	Control signal	ref	Reference
V	Volume	sp	Spring
x	Position	stat	Static
		T	Turbine
		tc	Turbocharger
		vac	Vacuum

Modeling and Control of Co-Surge in Bi-Turbo Engines[†]

Andreas Thomasson and Lars Eriksson

*Vehicular Systems, Department of Electrical Engineering,
Linköping University, SE-581 83 Linköping, Sweden.*

4

[†]This is a formatted version of “Modeling and Control of Co-Surge in Bi-Turbo Engines” by Andreas Thomasson and Lars Eriksson, IFAC World Congress 2011, Milano, Italy. ©IFAC 2011. Reproduced with the permission of IFAC. The original version was published in *ifac-papersonline.net*, <http://ifac-papersonline.net>, and can be found using the Digital Object Identifier (DOI): 10.3182/20110828-6-IT-1002.02338. The formatting is restricted to changing the article into a single-column format, adjusting sizes of figures and tables, and adjusting the referencing style.

Abstract

Using a bi-turbocharged configuration makes for better utilization of the exhaust energy and a faster torque response in V-type engines. A special surge phenomenon that should be avoided in bi-turbocharged engines is co-surge, which is when the two interconnected compressors alternately go into flow reversals. If co-surge should occur, the control system must be able to quell the oscillations with as little disturbance in torque as possible. This paper presents a model of a bi-turbocharged engine based on a Mean Value Engine Model that includes a More-Greizer compressor model for surge. The model is validated against measured data showing that it captures the frequency and amplitude of the co-surge oscillation. The effect of momentum conservation in the pipes is investigated by adding this feature to the control volumes before and after the compressor. This gives a slightly better mass flow shape with the drawback of increased simulation time, due to more states and a higher frequency content in the model. A sensitivity analysis is performed to investigate which model parameters have most influence on the co-surge behavior. It is shown that the largest influence comes from the turbocharger inertia, the volumes after the compressor and the “zero mass flow pressure ratio” during flow reversal in the compressor. The model is used to investigate principles for control strategies to detect and quell co-surge. The detection algorithm is evaluated on measured data.

1 Introduction

More advanced turbocharging concepts are constantly being developed to increase power density, and to reduce fuel consumption and emissions of internal combustion engines. For V-type engines one option is to use two smaller parallel turbos and let the exhausts from the two cylinder banks feed separate turbines. In this way the turbines can be placed closer to the exhaust ports than with a single larger turbo. Heat losses are reduced which increases the available energy to the turbochargers. With fewer cylinders feeding each turbine it is also possible to make better use of the pulsating flow, increasing the energy extracted from the exhaust.

In a bi-turbocharged engine the two air paths are connected before the throttle. If a disturbance alters the mass flow balance between them, when operating close to the surge line on an otherwise stable operating point, one compressor can be pushed into the surge region and the mass flow reverses. When the compressor recovers it can push the other compressor into surge, starting an oscillation where the mass flow through the compressors alternately reverses. Compressor surge should be avoided and considered when developing the control system for a bi-turbocharged engine.

1.1 Contributions and outline

Compressor surge has been extensively studied during the 70's and 80's and a well known modeling result is the Moore-Greitzer model (Greitzer, 1981). The majority of the work has been on turbo machinery with gas turbines. A survey of surge modeling and control is given in Willems and de Jager (1998) and there is also a substantial treatment in Gravidahl (1998). For automotive turbochargers there are only a few studies on surge where most utilize the Moore-Greitzer model, see e.g. Ammann et al. (2001) or Leufvén and Eriksson (2008). The main contribution of this paper is the analysis of experimental data and modeling of co-surge. In addition a method for co-surge detection and a co-surge controller are proposed.

Experimental data on co-surge and an analysis of the phenomenon is presented in section 2. In sections 3 and 4 a model for the bi-turbocharged engine, based on a Mean Value Engine Model (MVEM) structure, and surge capable compressor model is presented. The model's capability to capture co-surge is verified in section 5 and a parameter sensitivity analysis is presented. Section 6 investigates the effects of extending the model with pipes that conserve momentum. An algorithm for detecting co-surge and a control strategy for restoring the mass flow balance is presented. The detection algorithm is validated against measured data and the control strategy is evaluated on the model in section 7, followed by conclusions in section 8.

2 Co-surge

An example of co-surge measured in a test vehicle is shown in figure 1. The three mass flow sensors are placed approximately 50 cm after the air filter, 80 cm

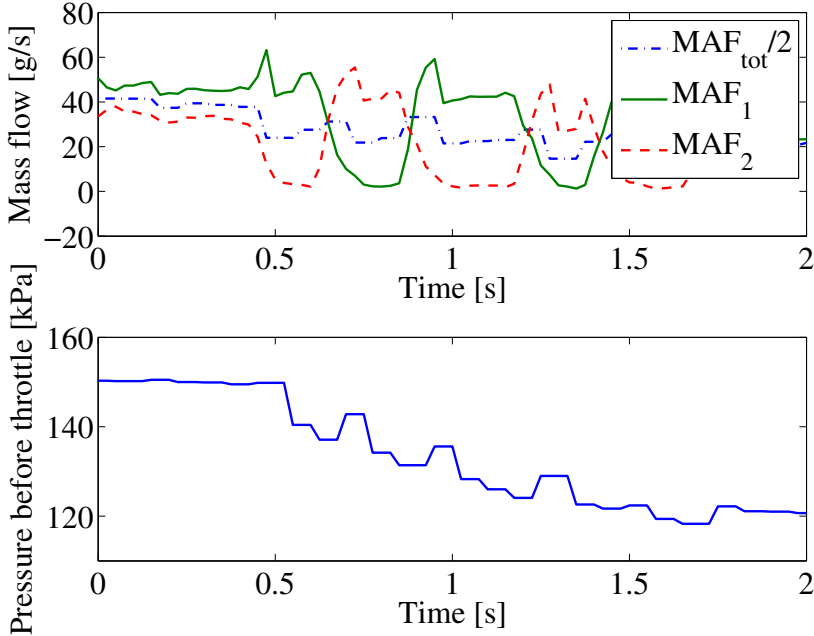


Figure 1: *Top*: An example of co-surge measured on a test vehicle. The green solid line and red dashed line are measured mass flows in the respective air path. The blue dash dotted line is half the total mass flow. The oscillation frequency is approximately 1.9 Hz. It should be mentioned that the mass flow sensors can not measure negative mass flow, and saturate at 0 g/s. *Bottom*: Corresponding boost pressure. The pressure is dropping with peaks of 7 kPa shortly after the mass flows switch.

before the compressors, one directly before and two directly after the air path is divided. The mass flow sensors are of hot film type, MAF_1 and MAF_2 are sampled at 40 Hz while MAF_{tot} is sampled at 12.5 Hz. The mass flow balance between the two air paths is slightly unbalanced. After a small decrease in mass flow, one compressor flow reverses, starting an oscillation between the compressors. Surge occurs when the pressure ratio is too high so that the mass flow can not be maintained. When the compressor enters this region the mass flow will start to reverse. The flow is not recovered until the pressure ratio has decreased sufficiently. Co-surge is a condition in the bi-turbo configuration, where the mass flow through the compressors alternately reverses. When one compressor enters surge more air will flow through the other compressor due to the pressure ratio decrease. As the first compressor recovers the second compressor is pushed into surge. Compared to normal surge, co-surge has a much lower frequency, roughly one order of magnitude. This indicates that co-surge is more than standard compressor surge with alternating flow reversals.

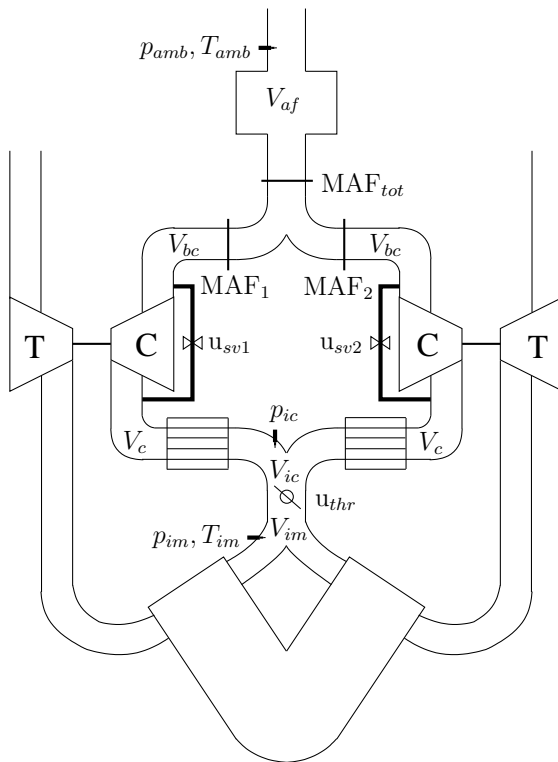


Figure 2: A sketch of the bi-turbocharged engine configuration studied in this paper. A mass flow sensor is positioned after the common air filter and two more directly after the two air paths split up. The actuators used in the control section are the two surge valves, u_{sv1} , u_{sv2} , and the throttle, u_{thr} .

3 Engine model

To investigate the effect of different engine components on co-surge, a physical model of the system is of use. Depending on the accuracy of the model it can give quantitative or qualitative results on the effect of different configurations and parameters. The model can also be used to test and evaluate different control strategies before trying them in the real environment.

The modeling approach taken is the component based Mean Value Engine Model (MVEM) outlined in Eriksson et al. (2002); Eriksson (2007). This uses control volumes, that contain states for pressure and temperature, and restrictions that govern the mass flow. A complete turbocharged spark ignited engine with these components is implemented and evaluated in Andersson (2005). For this investigation the MVEM components have been arranged in a bi-turbo structure to resemble the engine in figure 2. Two banks contain all doubled components, compressor, one cylinder bank, turbine and exhaust system. In the middle are the common parts for the two air paths, air filter, throttle and intake manifold.

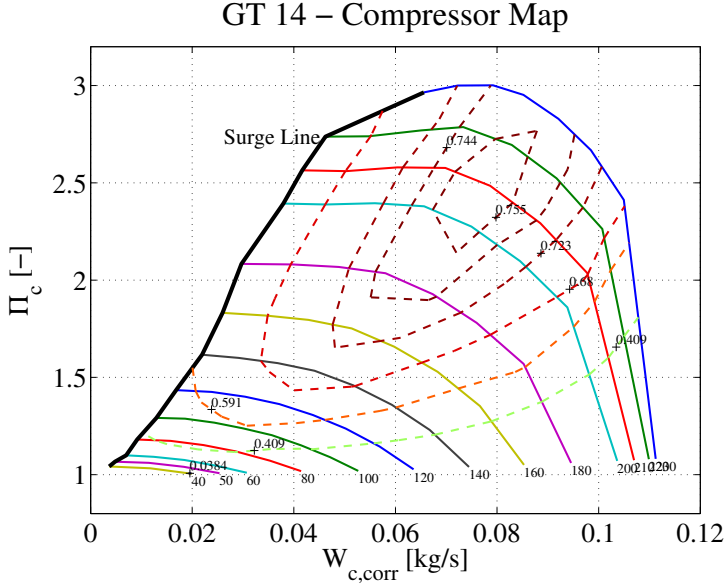


Figure 3: Example of a compressor map for car engine applications. Pressure ratio is plotted against corrected mass flow for different speed lines (given in thousands of rpm).

The two turbo shafts are modeled by Newtons second law of motion, utilizing the power balance between compressor and turbine and a viscous friction term:

$$J_{tc} \frac{\omega_{tc}}{dt} = \frac{P_t}{\omega_{tc}} - \frac{P_c}{\omega_{tc}} - k_{fric} \omega_{tc} \quad (1)$$

The compressor power consumption is derived from the first law of thermodynamics and given by the equation:

$$P_c = W_c c_p (T_{out} - T_{in}) \quad (2)$$

The expression for the turbine is similar, see Eriksson (2007) for the turbine model. Next section presents the surge capable compressor.

4 Compressor model

To model surge the compressor model must handle the reverse mass flow. This is achieved by the well known and well tested Moore-Greitzer model (Greitzer, 1981), that incorporates an additional state for the mass flow. An example of a compressor map is shown in figure 3. The surge line is the points on each speed line with lowest flow. These endpoints were determined by the gas stand operator as the smallest mass flow that had a stable reading on the gas stand mass flow meter. In the model it is necessary to have a description of the speed lines. Here a simple parametrization is used. The compressor map is parametrized using

the compressible dimensionless quantities for flow Φ and energy Ψ . They are defined as (Dixon, 1998)

$$\Phi = \frac{W_c}{ND^3} \frac{RT_{bc}}{p_{bc}} \quad (3)$$

$$\Psi = \frac{c_p T_{bc} (\Pi_c^{(\gamma-1)/\gamma} - 1)}{N^2 D^2} \quad (4)$$

where D is the compressor diameter, N is the rotational speed and R is the specific gas constant for air. When transformed into the $\Phi - \Psi$ domain, the speed lines in the compressor map gathers into almost a single curve (Eriksson, 2007). The model uses the relation between Φ and Ψ to span the compressor map and it is represented by the combination of a third and a second order polynomial (5).

$$\Psi(\Phi) = \begin{cases} a_3 \Phi^3 + a_2 \Phi^2 + a_1 \Phi + a_0 & \text{if } \Phi \leq \Phi_{\Psi_{max}}, \\ b_2 \Phi^2 + b_1 \Phi + b_0 & \text{if } \Phi > \Phi_{\Psi_{max}} \end{cases} \quad (5)$$

The separation into two regions increases the flexibility when studying the effect of the compressor map on co-surge. The shape of the speed lines in the surge region can be varied without altering the nominal region in the map and vice versa. The parameters a_i and b_i in $\Psi(\Phi)$ are determined from the parameters Ψ_{max} , $\Delta\Psi$, $\Phi_{\Psi_{max}}$ and Φ_0 together with the constraints $\Psi'(0) = 0$ and $\Psi'(\Phi_{\Psi_{max}}) = 0$, see figure 4. The most interesting part of the compressor map for this investigation is the region closest to the surge line and pressure ratios around $\Pi = 1.5$. For the test vehicle this is a high load operating point where measurements on co-surge have been made, and thus the model parameters are tuned to give best accuracy in that region. Compressor maps do not normally cover the surge region. The $\Delta\Psi$ parameter, that determines the dip of the speed line in the surge region, has been matched to recent work on surge capable compressor models by Leufvén and Eriksson (2011). The pressure build up, \hat{p}_c , is calculated from the current mass flow and speed by using equations (3) and (5) to find Ψ and solving (4) for the pressure after the compressor, giving

$$\hat{p}_c = \left(\frac{\Psi N^2 D^2}{c_p T_{bc}} + 1 \right)^{\frac{\gamma}{\gamma-1}} p_{bc} \quad (6)$$

The difference between pressure build up, \hat{p}_c and pressure after the compressor, p_c , results in a force that accelerates a flow plug that govern the mass flow.

$$\frac{dW_c}{dt} = \frac{\pi D^2}{4L} (\hat{p}_c - p_c) \quad (7)$$

4.1 Compressor efficiency

The temperature out of the compressor is determined by the compressor efficiency defined as

$$\eta_c = \frac{(\Pi_c)^{\frac{\gamma-1}{\gamma}} - 1}{\frac{T_{out}}{T_{in}} - 1} \quad (8)$$

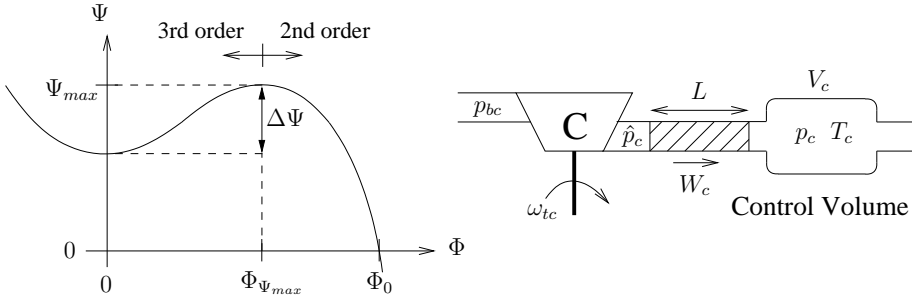


Figure 4: *Left:* Parameterization of the $\Phi - \Psi$ function. *Right:* The Moore-Greitzer compressor model, the pressure difference $\hat{p}_c - p_c$ results in an acceleration of the flow that governs the mass flow.

Here it is important to note that during a surge cycle, the flow reverses and the compressor works as a turbine. The efficiency definition differs between compressor and turbine operation by the change of denominator and numerator in 8, and inversion of the pressure ratio. For the surge capable compressor the temperature of the flow are therefore determined by

$$T_{out} = T_{in} \left(1 - \frac{1}{\eta_c^{sgn(W_c)}} \left(1 - (\Pi_c^{sgn(W_c)})^{\frac{\gamma-1}{\gamma}} \right) \right) \quad (9)$$

The compressor efficiency η_c is modeled from the compressor map as a product of η_{max} , the maximum efficiency, η_Φ and η_N , suggested as one alternative in Eriksson (2007). The later two describe the efficiency decrease when Φ and N diverge from their value at the maximum efficiency point.

5 Analysis of surge properties

The integrated engine and compressor models presented in sections 3 and 4 were used in simulation to re-create the measured co-surge cycles. A simulation is shown in figure 5. With parameters that correspond to the engine used in the measurements, the frequency in the co-surge oscillations is only slightly higher. The shape of the mass flow differs more. In the measured data the switch is simultaneous in the sense that one mass flow drops at the same time as one mass flow increases. In the simulation with this model one mass flow first recovers, then there is a period of time before the other mass flow drops. The switch between forward and backward flow is also faster in the simulation, but this can partly be explained by the absence of sensor dynamics in the model. The amplitude of the pressure oscillation is 10 kPa in the simulation, 3 kPa larger than the measurements. This variation could be the result of a slightly too large $\Delta\Psi$ parameter, which has a very large effect on the pressure amplitude.

To investigate the sensitivity to different parameter variations a simulation series was performed. The results are presented in table 1. The parameters that have the largest influence on the frequency are the dip in the Ψ - Φ function,

Table 1: Properties of the co-surge cycles for simulations with different parameter variations. Largest influence comes from $\Delta\Psi$, the compressor inertia and the volumes after the compressor. The phase deviation from 180° is small enough to be numerical errors.

Simulation	Frequency [Hz]		Δp [kPa]		Phase [deg]	
	Value	%	Value	%	Value	%
Standard	2.05	+0%	10.2	+0%	179	+0.0°
$V_{af} \times 2$	2.15	+5%	10.1	-1%	181	+1.3°
$V_{af} \times 0.5$	2.05	+0%	10.6	+4%	181	+1.2°
$V_c \times 2$	1.56	-24%	9.2	-10%	177	-2.5°
$V_c \times 0.5$	2.64	+29%	10.8	+7%	181	+1.3°
$V_{ic} \times 2$	1.66	-19%	9.6	-5%	177	-2.2°
$V_{ic} \times 0.5$	2.34	+14%	10.3	+2%	179	-0.7°
$L_x \times 2$	2.05	+0%	10.4	+2%	179	-0.0°
$L_x \times 0.5$	2.15	+5%	10.1	-0%	181	+1.8°
$J_{tc} \times 2$	1.76	-14%	11.8	+16%	178	-1.2°
$J_{tc} \times 0.5$	2.64	+29%	8.4	-17%	180	+0.5°
$\Delta\Psi \times 1.5$	1.46	-29%	14.8	+45%	179	-0.1°
$\Delta\Psi \times 0.75$	2.44	+19%	7.7	-24%	182	+2.3°

$\Delta\Psi$, the turbocharger inertia, J_{tc} and the volumes after the compressor, V_c and V_{ic} . The pressure dip is mostly affected by $\Delta\Psi$. The phase is almost 180° in all simulations, the small spread can be explained by the oscillation being not completely stationary and inaccuracy in the computation. The frequencies in the simulations range between 1.5 – 2.5 Hz which covers the frequency in the measurements. There are differences between the simulations and measurements and there will be variations in the model parameters through the use of lumped parameter models and uncertainty in the engine parameters, when tuning the model against data. This shows that the differences can be captured with small parameter variations, keeping the physical interpretation of the model.

6 Pipe dynamics investigation

Although the frequency and pressure oscillations of co-surge is captured by the MVEM and Moore-Greitzer compressor model, the shape of the mass flow does not fully resemble the measured data. The Moore-Greitzer model only includes momentum of a single flow plug after the compressor to model surge. Since the flow direction around the compressors switch back and forth during surge, the momentum of the gas in the pipes, both before and after the compressor, could have a large influence on the behavior. Therefore the effect of including a more detailed model of gas momentum in the pipes is investigated, by splitting the control volumes into several sections. Each section uses the equations for an ordinary control volume, but the mass flow across the boundary of each section is governed by a flow plug. The flow plug is considered to have a mass equal to half the mass of the sections upstream and downstream of the plug, see figure 6

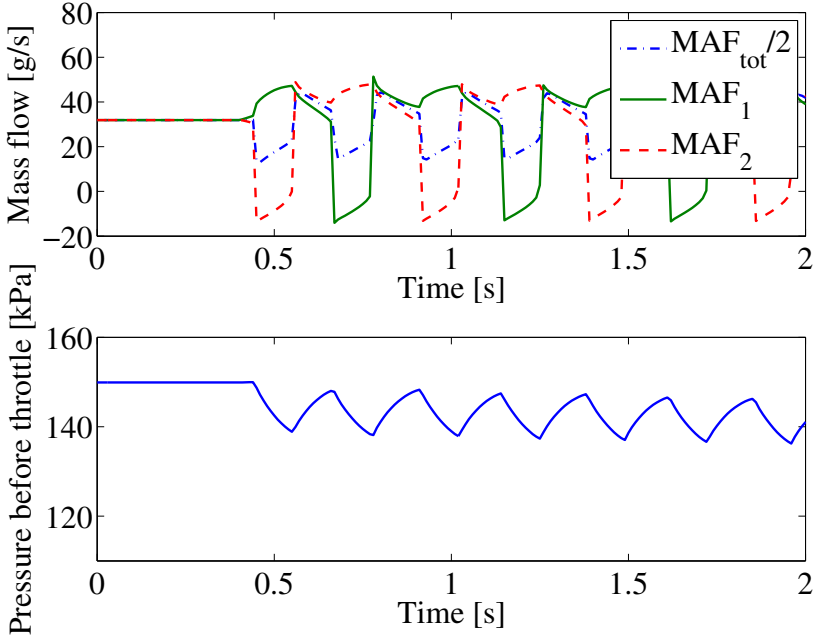


Figure 5: Co-Surge simulation with the standard MVEM and Moore-Greizer compressor model. The oscillation has almost the same frequency as the measured data. The amplitude of the pressure oscillation is 10 kPa which is slightly higher than in the measurements.

for an illustration. The acceleration of the plug is then determined by Newton's law of motion

$$\frac{dU_i}{dt} = \frac{2A(p_i - p_{i+1})}{m_i - m_{i+1}} - U_i k_{fric} \quad (10)$$

where U_i is the velocity of plug i , and p_i and m_i are the pressure and mass in control volume i . The damping term k_i represents friction in the pipes. This model which is used in Öberg and Eriksson (2007); Öberg (2009) is a simplified model of Andersen et al. (2006). Exchanging the standard control volume before and after the compressor, the effect of momentum conservation in the control volumes has been investigated.

6.1 Simulations with pipe dynamics

One simulation with pipe dynamics added to the model is shown in figure 7. In this simulation the pipes with dynamics have ten sections each. The co-surge oscillation frequency decreases by roughly 25% compared to the model without pipe dynamics with the same parameters. The mass flow becomes more oscillatory and the spike in mass flow after the switch in the measured data can now be seen in the simulation. However, the switching between reverse and forward flow for the compressors is still not simultaneous. The sensitivity to

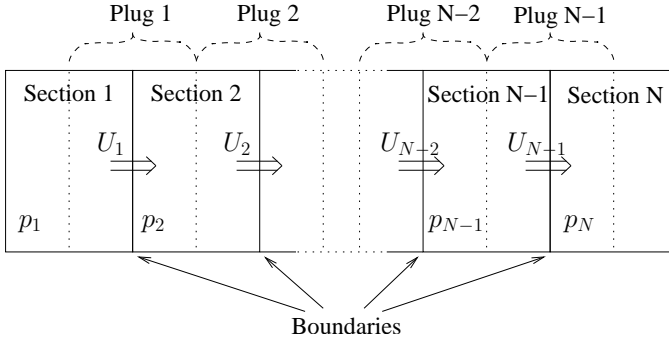


Figure 6: Model of pipe with momentum conservation. The control volume is split into several sections with a flow plug that governs the mass flow across the boundaries.

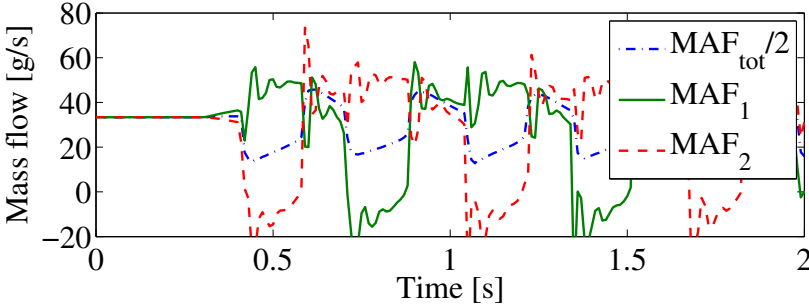


Figure 7: Co-Surge in the simulation model with pipe dynamics before and after the compressor. The spike in mass flow after the switch from backward to forward seen in the measured data flow is now visible in the simulation, but the switch is still not simultaneous.

parameter changes is similar to the model without pipe dynamics, but with the addition of pipe dynamics the influence of the control volume parameters is relatively larger. The main disadvantage of including pipe dynamics is that the model becomes more complex and stiff which increases simulation time. Since the qualitative properties are the same, the simpler model is considered to be enough for control purposes and is therefore used in the next section.

7 Control

To have the largest margin to the surge line for both compressors in a given operating point, the control system should strive for balance between the two mass flows. If co-surge occurs, the control system should take measures to stabilize the flows i.e. to minimize $\Delta W = |W_1 - W_2|$. This section presents a control strategy for quelling the mass flow oscillations that utilizes the two mass flow sensors, MAF_1 and MAF_2 , and use additive commands in the two surge

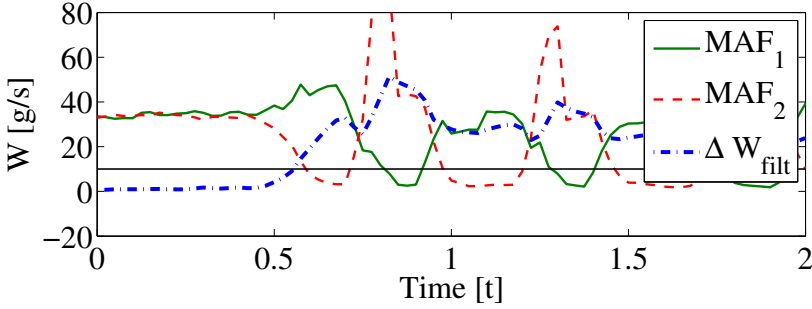


Figure 8: The detection procedure evaluated on a co-surge measurement. The green solid and the red dashed lines are the two mass flows, and the blue dash-dotted line is the filtered mass flow difference. For a threshold of 10 g/s, detection of co-surge would occur 0.13 s after the mass flows diverge.

valves and throttle, u_{sv1} , u_{sv2} and u_{thr} , see figure 2. The control strategy is evaluated on the developed engine model together with a detection algorithm that is the topic of the next subsection.

7.1 Detection

The detection algorithm is based on the difference in mass flow. The absolute value of this signal is filtered through a first order low pass filter with high cut-off frequency, removing disturbances while keeping a fast reaction time to unbalances. If the filtered signal is larger than the threshold value ΔW_{level} , co-surge is detected, see equation 11. The filter coefficient, k , and the threshold, ΔW_{level} , together determine the detection time and sensitivity to disturbances. Figure 8 shows how this works on one of the co-surge measurements. In this test case, a filter coefficient corresponding to 0.1 s rise time for the low-pass filter and a threshold of 10 g/s, would give detection 0.13 s after the mass flows diverge.

$$\frac{1-k}{1-kz^{-1}}|W_1 - W_2| \geq \Delta W_{level} \implies CS_{detect} = 1 \quad (11)$$

7.2 Co-surge quelling

When co-surge occurs due to a disturbance between the two mass flows, pushing one compressor into reverse flow, the original operating point with balanced mass flow is stable. The objective is therefore to quell the oscillation and return to this operating point as fast as possible and with as little torque disturbance as possible. The fast actuators that quickly can change the compressor operating point are the throttle and the surge valves. Opening the throttle moves the surge line to the left in the compressor map. Opening the surge valve reduces the pressure ratio and increases the mass flow felt by the compressor by recirculating a part of the compressed air.

Opening the surge valve too much or for too long will cause a large drop in boost pressure and thus reduced torque, which is undesirable. On the other hand, opening the throttle might not be enough if the opening angle already is large, and if the mass flow recovers it will be in an operating point with higher mass flow producing excess torque. Combining the two gives fast recovery and small torque disturbance.

When co-surge is detected the throttle is opened up and a small surge valve opening is commanded. When the flows equilibrate the surge valve is immediately closed and the throttle valve ramped down to its previous value, according to:

$$u_{sv}^+ = k_{sv} CS_{detect} \quad (12a)$$

$$u_{thr}^+ = \begin{cases} k_{thr} & \text{if } CS_{detect} = 1 \\ u_{thr}^+(k-1) - k_{thr} \frac{\tau_s}{\tau_{thr}} & \text{if } CS_{detect} = 0 \end{cases} \quad (12b)$$

Where u_{sv}^+ and u_{thr}^+ are additive to the surge valve and throttle command, $u_{thr}^+(k-1)$ indicates the previous sample, τ_s is the sample time and τ_{thr} is a tuning parameter that determines how fast the throttle is ramped down. The other tuning parameters are k_{sv} and k_{thr} that determine the size of the additive commands. They need to be large enough to quickly get out of surge but as small as possible to reduce torque disturbance. Future work is to develop a systematic method for the parameter tuning.

In figure 9 the control action is shown where the complete MVEM is used. A disturbance in the mass flow balance has been induced at time zero, pushing one flow into reverse. When one mass flow reverses the pressure and torque drops. As co-surge is detected at 0.05 s, the throttle and surge valve opens up and the reverse mass flow quickly recovers. When the co-surge indication drops, the surge valve is closed and the throttle is ramped down. Within 0.5 s the mass flows are balanced and the torque has reached the level before the disturbance.

8 Conclusions

Co-Surge in bi-turbocharged engines is analyzed. Measurements are presented where co-surge frequency is an order of magnitude lower than standard compressor surge, indicating that co-surge is more than standard compressor surge with alternating flow reversals. A model of a bi-turbocharged engine that can capture the frequency and amplitude of the co-surge phenomenon has been developed. In a validation against measured data it is shown that a mean value engine model together with a Moore-Greizer compressor model can capture the co-surge frequency but not fully recreate the shape of the mass flow oscillation. With the addition of momentum conservation in the pipes the agreement with measurement can be slightly improved, at the price of increased simulation time. A detection algorithm and a control strategy to quell co-surge is presented. The detection algorithm is shown to quickly detect co-surge in the measured data. Simulations on the model show that when the control is switched on, mass flow balance and torque level are recovered in 0.5 s.

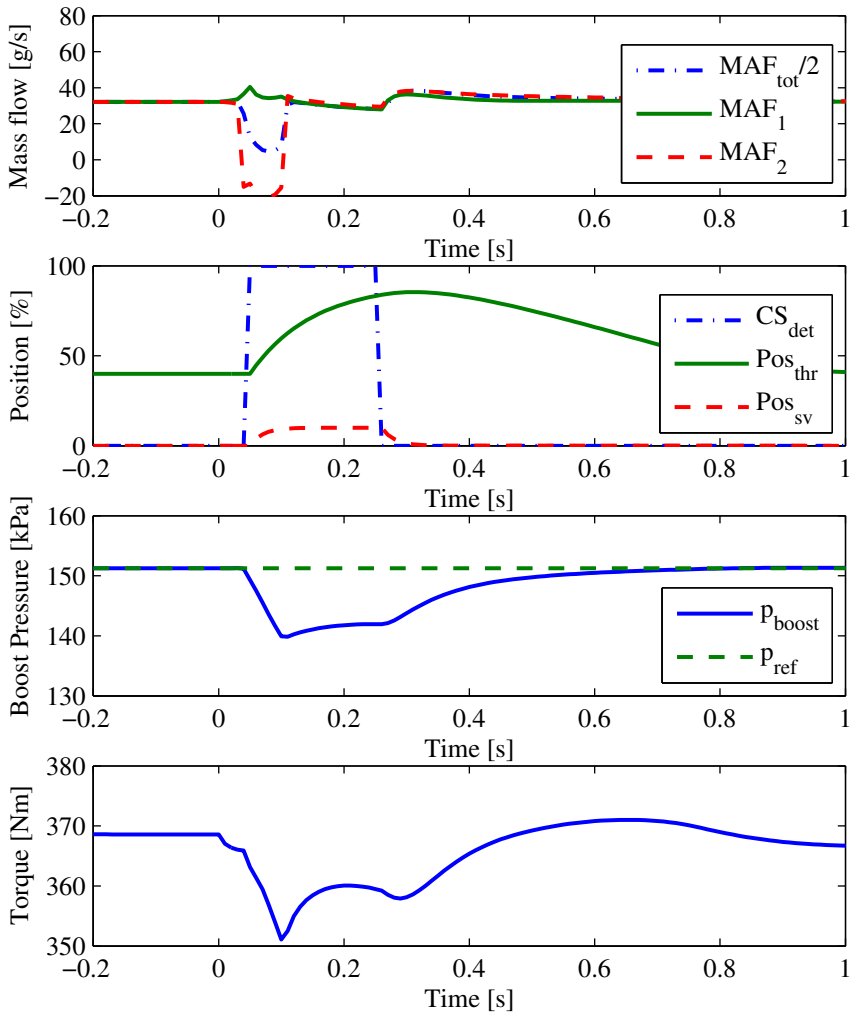


Figure 9: The described stabilization method evaluated on the model. The engine is operating in a stable operating point close to the surge line. At time zero a disturbance alters the mass flow balance, pushing one flow into reverse. When this is detected, the throttle is opened up together with a small and short opening of the surge valves. A stable operation is recovered and the torque is back to level within 0.5 s

References

- M. Ammann, N. P. Fekete, A. Amstutz, and L. Guzzella. Control-Oriented Modeling of a Turbocharged Common-Rail Diesel Engine. In *Proc. of the Int. Conference on Control and Diagnostics in Automotive Applications*, 2001.
- Stig Kildegård Andersen, Henrik Carlsen, and Per Grove Thomsen. Control volume based modelling in one space dimension of oscillating, compressible flow in reciprocating machines. *Simulation Modelling Practice and Theory*, 14 (8):1073–1086, October 2006.
- Per Andersson. *Air Charge Estimation in Turbocharged Spark Ignition Engines*. PhD thesis, Linköpings Universitet, December 2005.
- S.L. Dixon. *Fluid Mechanics and Thermodynamics of Turbomachinery*. Butterworth-Heinemann, 4th edition, 1998.
- Lars Eriksson. Modeling and Control of Turbocharged SI and DI Engines. *Oil & Gas Science and Technology - Rev. IFP*, 62(4):523–538, 2007.
- Lars Eriksson, Lars Nielsen, Jan Brugård, Johan Bergström, Fredrik Pettersson, and Per Andersson. Modeling of a turbocharged SI engine. *Annual Reviews in Control*, 26(1):129–137, October 2002.
- Jan Tommy Gravdahl. *Modeling and Control of Surge and Rotating Stall in Compressors*. PhD thesis, Norwegian University of Science and Technology, 1998.
- E.M. Greitzer. The Stability of Pumping Systems. *J. of Fluids Engineering*, 103 (1):193–242, June 1981.
- Oskar Leufvén and Lars Eriksson. Time to surge concept and surge control for acceleration performance. In *Proc. of the IFAC World Congr.*, pages 2063–2068, Seoul, Korea, July 2008.
- Oskar Leufvén and Lars Eriksson. Surge and Choke Capable Compressor Model. In *Proc. of the IFAC World Congr.*, pages 10653–10658, August 2011.
- Per Öberg. *A DAE Formulation for Multi-Zone Thermodynamic Models and its Application to CVCP Engines*. PhD thesis, Linköping University, 2009.
- Per Öberg and Lars Eriksson. Control Oriented Gas Exchange Models for CVCP Engines and their Transient Sensitivity. *Oil & Gas Science and Technology - Rev. IFP*, 62(4):573–584, 2007.
- Frank Willems and Bram de Jager. Modeling and Control of Rotating Stall and Surge: An Overview. In *Int. Conference on Control Applications*, pages 331–335, September 1998.

A Nomenclature

Symbol	Description	Subscript	Description
c_p	Specific heat	af	Air filter
γ	c_p/c_v	bc	Before compressor
η	Efficiency	c	Compressor
J	Inertia	$fric$	Friction
L	flow plug length	ic	Intercooler
MAF	Mass flow sensor	im	Intake manifold
N	Rotation speed	t	Turbine
Π	Pressure ratio	tc	Turbocharger
P	Power	thr	Throttle
p	Pressure	sv	Surge valve
R	Gas constant		
T	Temperature		
u	Control signal		
V	Volume		
W	Mass flow		
ω	Angular velocity		

Co-Surge in Bi-Turbo Engines - Measurements, Analysis and Control[†]

Andreas Thomasson and Lars Eriksson

*Vehicular Systems, Department of Electrical Engineering,
Linköping University, SE-581 83 Linköping, Sweden.*

[†]This is a formatted version of “Co-Surge in Bi-Turbo Engines - Measurements, Analysis and Control” by Andreas Thomasson and Lars Eriksson, submitted to Control Engineering Practice. The formatting is restricted to changing the article into a single-column format, adjusting sizes of figures and tables, and adjusting the referencing style.

Abstract

In parallel turbocharged V-engines, with two separate air paths connected before the throttle, an oscillation in the flow can occur. If the compressor operates close to the surge line, typically during low speed and high load, and a disturbance alters the mass flow balance, the compressors can begin to alternately go into surge. This phenomenon is called co-surge and is unwanted due to high noise and risk for turbocharger destruction. Co-surge is measured on a test vehicle in a chassis dynamometer and the system analyzed and modeled using a mean value engine model. The investigation shows that the alternating compressor speeds have an important role in the prolonged oscillation. A reconstruction of the negative flow from measurements is made and compared to simulation results, showing similar amplitudes, and supports the model validation. A new co-surge detection algorithm is presented, suitable for a pair of sensors measuring either mass flow, boost pressure or turbo speed in the two air paths. Furthermore, a new controller is proposed that uses a model based feedforward for the throttle, together with wastegate actuation to force the compressor speeds together and improve balance at the recovery point. This has shown to be sufficient with moderate to high pressure ratios over the throttle, only for zero or very low pressure drop the use of bypass valves are necessary. The advantage of not opening the bypass valves is a smaller drop in boost pressure which also reduces the torque disturbance. The performance of the controller is evaluated both in simulation and in the test vehicle.

1 Introduction

The automotive industry constantly strives to reduce fuel consumption and emissions of the internal combustion engine. One strategy that has proved to be successful over the years is to replace naturally aspirated engines with smaller turbocharged engines, Emmenthal et al. (1979); Watson and Janota (1982). Turbocharging increases air density in the intake which increase power density and thus allows the turbocharged engine to produce the same maximum power as a comparatively larger naturally aspirated engine. This is beneficial in low- to mid-load operating points where the engine usually operates, since pumping and friction losses is reduced, Guzzella et al. (2000). More advanced turbocharging concepts are being developed to further increase power density, Petitjean et al. (2004). A configuration that has increased in popularity is the use of two parallel identical turbochargers for V-type engines, one powered by each bank of cylinders. This allows the turbines to be mounted closer to the exhaust ports than if a single turbocharger where to be used, which reduces heat losses and makes better use of the pulsating flow from the exhaust, allowing more energy to be extracted trough the turbine.

In the most common parallel turbocharged configuration, the two air paths are connected before the throttle and a single throttle and intake manifold is used. This introduces an interesting balancing problem, since the same total mass flow can be realized with different flows from each air path. For balanced operation these should always be equal, but if the flow from one air path should drop for some reason, the other will start to take over, producing more flow. This interaction between the compressors is remarkable when operating close to the surge line, if the balance between the compressors are disturbed and one compressor enters surge. That mass flow will then drop to zero or below, while the other compressor will produce twice the flow. When the surging compressor recovers it will have a higher speed than the first compressor and risks pushing that compressor into surge instead, starting an oscillation between the air paths called co-surge. Failing to quell this oscillation will result in unwanted sound, drop in torque and in worst case, compressor damage.

This phenomena is not new, it was mentioned already in Watson and Janota (1982), but has received very little attention in the literature. Compressor surge is otherwise a well studied phenomena, and a well known and utilized result is the Moore-Greitzer model, see Greitzer (1981). A rich treatment of surge modeling and control can also be found in for example Willems and de Jager (1998) or Gravdahl (1998). Most work has been done on turbo machinery with gas turbines. There are few studies focusing on automotive size turbochargers, where most utilizes the Moore-Greitzer, see e.g. Ammann et al. (2001) or Leufvén and Eriksson (2008).

1.1 Contributions and outline

One main contribution in this paper is an analysis of the co-surge oscillation, using both measurements from a test vehicle in chassis dynamometer and simulations. The analysis results in a new controller that tries to force the turbo speeds together during co-surge. The controller takes ideas from Thomasson and Eriksson (2013), but uses a model based feedforward for the throttle, and wastegate actuation to increase stability and enable faster recovery from co-surge. The controller is evaluated both in simulation and test vehicle. The simulations are based on a Mean Value Engine Model (MVEM) developed in Thomasson and Eriksson (2011), which is briefly summarized in the paper for completeness. Measurements of co-surge is also presented with an attempt to reconstruct the negative flow that can not be measured by the mass flow sensors, which is then compared to simulation results. In addition, a new co-surge detection algorithm is presented that uses a pair of sensors, measuring either mass flow, boost pressure or turbo speed in the two air paths.

Section 2 describes the test vehicle and the experimental setup used for the measurements and experiments in the paper. In Section 3 measurements of co-surge is presented, and the phenomena is described and compared to normal surge in a single compressor. Section 4 outlines a control oriented Mean Value Engine Model (MVEM) able to capture the quantitative behavior of co-surge. The model is used both in the analysis and as part of the controller validation in the following sections. This is followed by an analysis of the co-surge oscillation in Section 5. Detection and control of co-surge are the subject of Section 6 and 7 respectively, which includes validation both in simulation and test vehicle, followed by conclusions in Section 8.

2 Test setup

The test vehicle is equipped with a gasoline V6-engine with two parallel turbochargers, each powered from one bank of cylinders. A sketch of the engine is shown in Fig. 1, that also defines the nomenclature which is also available in A. The engine is equipped with three hot film mass flow sensors. The total flow is measured 10 cm after the air filter, 30 cm before the air path is divided. The two other, that measure the flow in each path, are placed 10 cm after the division of the air path, approximately 80 cm before the compressors. Pressures are measured before and after each compressor, before the throttle and in the intake manifold. The turbochargers are equipped with speed sensors. The measurement and control system is a dSpace MicroAutoBox and a RapidPro system, connected to a computer running ControlDesk. The actuators used by the control algorithm are the throttle, the bypass valves and the wastegates. The throttle and wastegate are continuously actuated while the bypass valves are of ON/OFF type. For the tests the vehicle is mounted in a vehicle dynamometer with one electric motor connected to each wheel on the rear axle. Although the test vehicle is equipped with lots of sensors for modeling, the detection algorithm only uses either pair of p_{ac} , MAF or N_{tc} sensors. The proposed controller uses p_{ic} and p_{im} , and in the controller with balancing also the two turbo speed sensors are utilized.

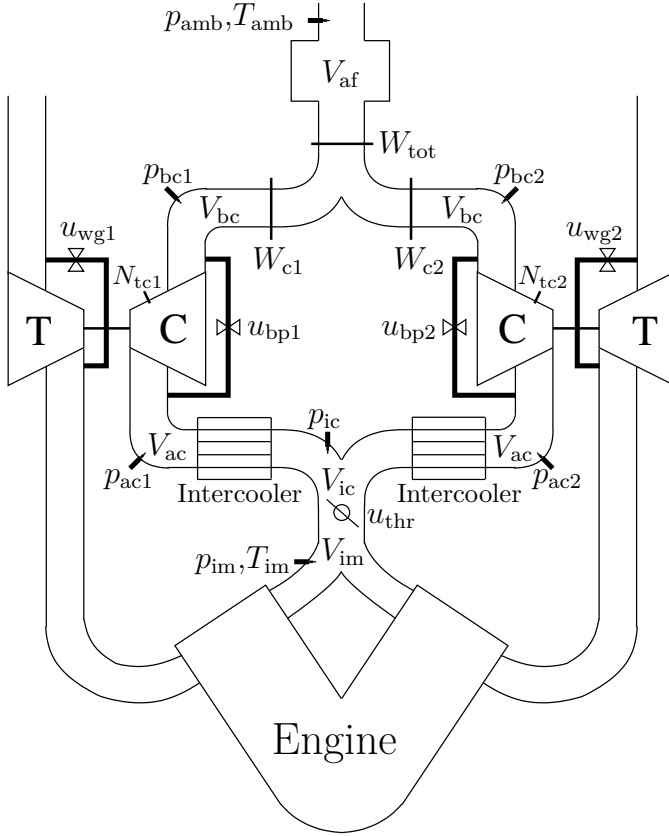


Figure 1: A sketch of the bi-turbocharged engine configuration. A mass flow sensor, W_{tot} , is positioned after the air filter and two more, W_{c1} and W_{c2} , directly after the air path split up. The actuators used in the control section are the throttle, u_{thr} , the bypass valves, u_{bp1} , u_{bp2} , and the wastegates, u_{wg1} , u_{wg2} . Pressures are measured before and after each compressor, before the throttle and in the intake manifold.

3 Surge and co-surge

Compressor surge is well known system instability phenomena. When the compressor mass flow gets too low, at high pressure ratio, the mass flow can stall, start to fluctuate and even reverse through the compressor. Surge can be categorized in at least four different types, Mild surge, Classical surge, Modified surge and Deep surge, de Jager (1995). Among these four only deep surge has reversed flow, and is thus the one most closely related to co-surge which has reversed flow during large part of the surge cycle, as will be shown shortly.

The left plot of Fig. 2 shows an example of surge measured in the test vehicle. A small throttle closing is made at $t = 0$ s which pushes both compressors into surge. The mass flow oscillation is around 10 Hz and dies out after a few cycles. An example of co-surge is shown in the right plot. The situation is similar, a throttle disturbance is made at $t = 0$ s, but instead of going into surge

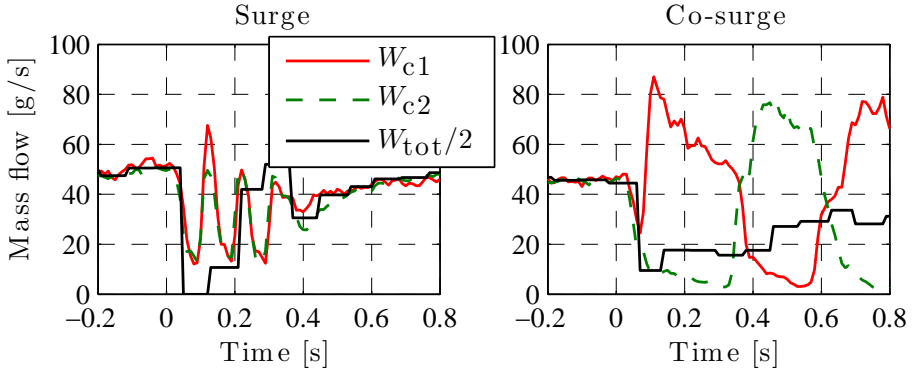


Figure 2: A comparison between surge (left plot) and co-surge (right plot), measured on the test vehicle. In the first case both compressors go into surge simultaneously, similar to surge in a single compressor system. In the second case, the first compressor takes over all mass flow when the second compressor surges. Upon recovery the first compressor is pushed into surge, starting an oscillation with alternating flow reversals. Note that the mass flow sensors can not measure negative flow.

simultaneously, when one compressor goes into surge the other produces more mass flow instead. When the surging compressor recovers it pushes the other into surge and vice versa, resulting in an oscillation which doesn't die out unless some measure is taken. Compared to normal surge, the frequency of co-surge is much lower and the magnitude of the mass flow and turbo speed oscillation is larger.

The mass flow sensors can not measure negative flow, but by comparing the total mass flow to the sum of the two separate flows, it is clear that the sum of the two flows is larger than the total flow. An estimation of the flow reversal can be computed by assuming that the total flow is not reversed, and that the total flow and the larger measured flow is correct, giving:

$$\widehat{W}_{c1} = \begin{cases} W_{tot} - W_{c2} & \text{if } W_{c1} < W_{c2} \text{ \& } W_{tot} - W_{c2} < 0 \\ W_{c1} & \text{otherwise} \end{cases}$$

$$\widehat{W}_{c2} = \begin{cases} W_{tot} - W_{c1} & \text{if } W_{c2} < W_{c1} \text{ \& } W_{tot} - W_{c1} < 0 \\ W_{c2} & \text{otherwise} \end{cases}$$

The resulting plot for the same measurement as the right plot of Fig. 2 (and Fig. 4) is shown in Fig. 3. This estimation of the reversed flow is of course very rough but the magnitude is large enough to conclude that reversed flow does occur during a large part of the surge cycle.

Fig. 4 gives a more detailed picture of the phenomenon. At $t = 0$ s the throttle closes by 10% for 0.3 s and is then returned to its original position. At first both mass flows drop but shortly afterward one compressor rapidly recovers to produce all mass flow while the other goes into surge. When the second compressor recovers it has a higher turbo speed than the first compressor,

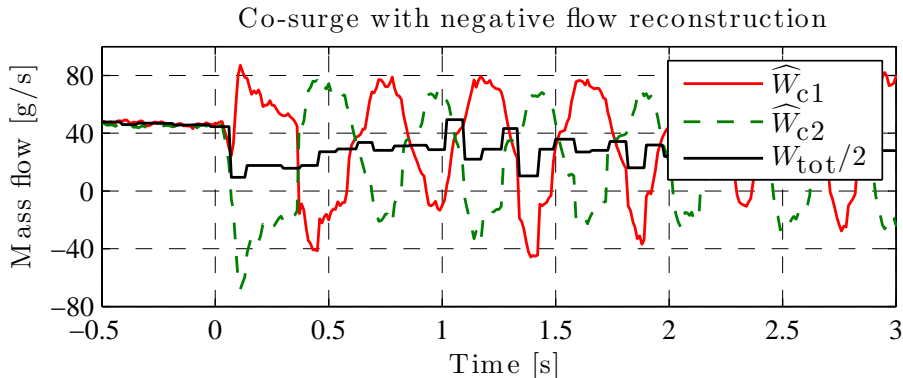


Figure 3: An estimation of the reversed mass flow based on the total mass flow sensor. The estimates show that reversed flow with significant magnitude occurs during a large part of the surge cycle.

and as a result will produce more mass flow. The reason for this is that the compressor that surges doesn't consume any torque, while the compressor which produces higher mass flow consumes more torque. If the operating point is too close to the surge line, the first compressor is then pushed into surge which results in a sustained oscillation with alternating flow reversals in each air path. Despite that the non surging compressor is producing more flow, it does not fully counteract the loss of the other compressor mass flow, and the total mass flow drops during the oscillation, resulting in a drop in torque. The turbo speed will also oscillate with a phase lag of 90° compared to the mass flow.

4 Control oriented engine model

To be able to perform fast simulations of a complete engine model on a standard desktop computer, zero dimensional mean value engine models are very attractive. A mean value model of an SI engine is presented in for example Hendricks and Sorenson (1990). A component based turbo charged MVEM was outlined in Eriksson et al. (2002); Eriksson (2007), which is the base for the model used in this paper. The model was first presented in Thomasson and Eriksson (2011) but is briefly summarized here for completeness and readability of the paper. The methodology is to divide the model into components, flow restrictions and control volumes. The restriction components determine the mass flow through them depending on surrounding conditions, and the control volumes contain states for pressure and temperature. The components are then arranged in series, where a control volume always follow a restriction and vice versa.

For this application these components can be arranged in a structure representing the parallel turbocharged engine in Fig. 1. An overview of the simulink model is shown in Fig. 5. The blue blocks are control volumes, the magenta colored blocks are restrictions and the two yellow blocks are a collection of other blocks, that contain all doubled components in the air path such as compressor, turbine, intercooler, on side of the V-engine etc.

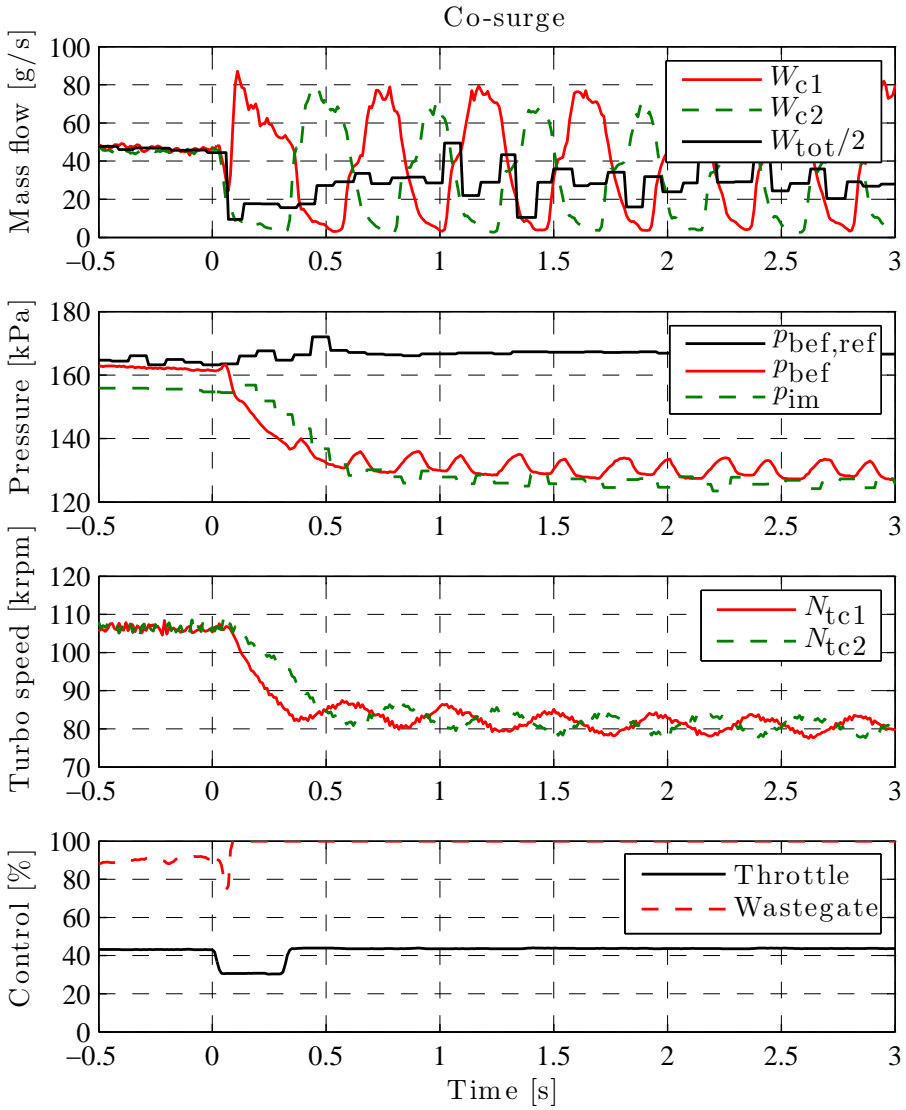


Figure 4: Co-surge measured on the test vehicle. A throttle disturbance is made at $t = 0$ s and initially both mass flows drop. Shortly afterward the mass flow through the first compressor rapidly increase to produce all mass flow as the other goes onto flow reversal.

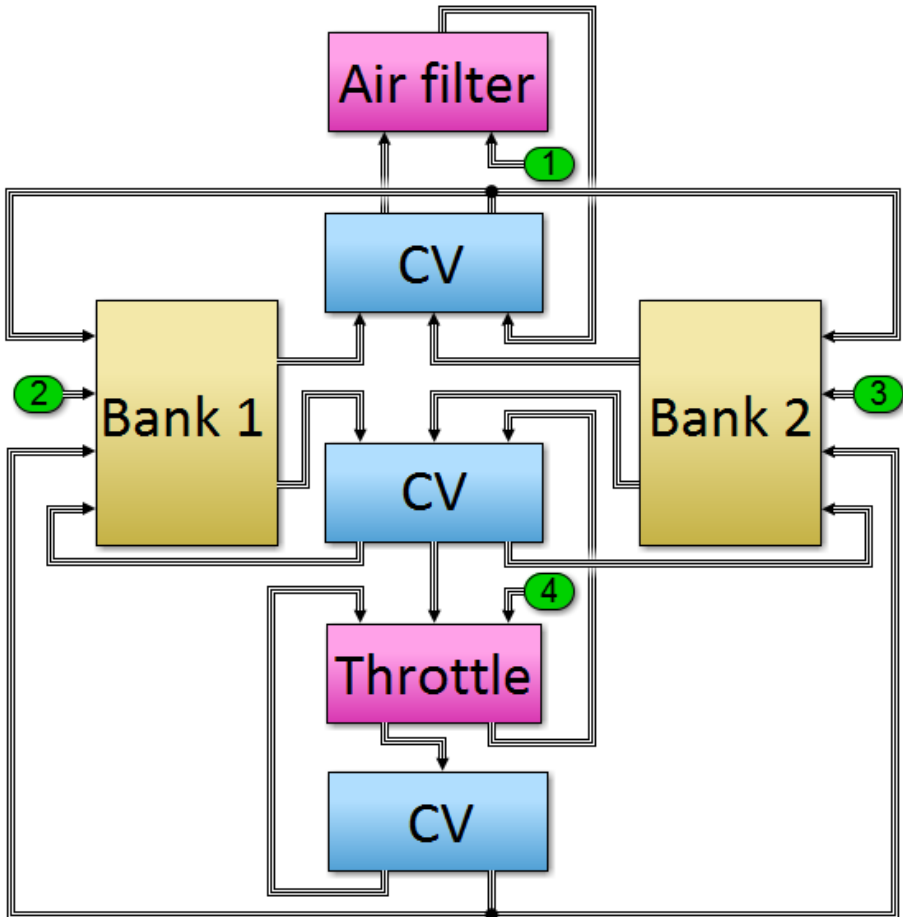


Figure 5: Overview of the simulink model for the parallel turbocharged engine. Magenta colored blocks are restrictions (Air filter, Throttle), blue are control volumes (CV) and yellow blocks are collections of other blocks (Bank 1,2), in this case all doubled blocks such as compressor, turbine etc.

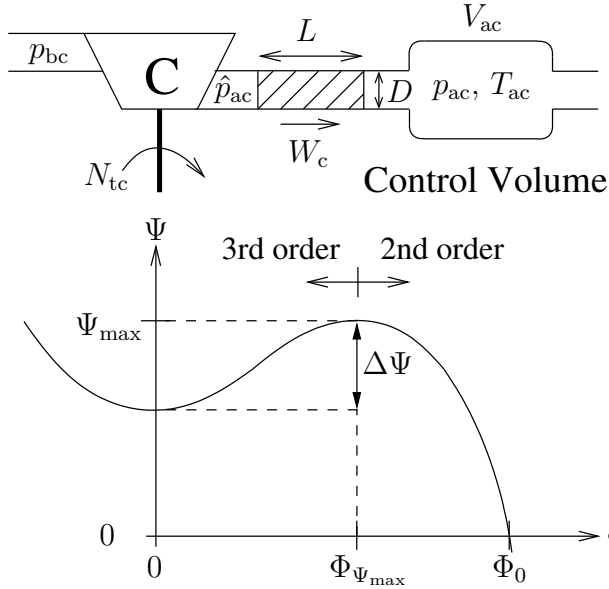


Figure 6: *Top*: The Moore-Greitzer compressor model. The pressure difference $\hat{p}_{ac} - p_{ac}$ results in an acceleration of the flow plug that governs the mass flow. *Bottom*: Parameterization of the $\Phi - \Psi$ function.

4.1 Compressor model

From the measurements in section 3 it is clear that in order to capture the co-surge phenomena, the engine model needs to handle reverse flow through the compressors. One way to achieve this is to use the well known and well tested Moore-Greitzer model, Greitzer (1976, 1981). The model was first developed for axial flow compressors, but has been shown to work also for centrifugal compressors in Hansen et al. (1981). The model includes an additional state for the mass flow which is calculated from the state equation:

$$\frac{dW_c}{dt} = \frac{\pi D^2}{4L} (\hat{p}_{ac} - p_{ac}) \quad (1)$$

The idea behind the model is that the difference between the pressure built by the compressor, \hat{p}_{ac} , and the actual pressure after the compressor, p_{ac} , results in a force on a flow plug after the compressor, with length L and diameter D , see the top of Fig. 6.

The model requires a description of the pressure build up as a function of compressor speed and mass flow, which is given by the compressor map. To reduce the model size a simple parameterization of the map is used in this investigation. The parameterization is based on the dimensionless numbers for flow, Φ , and energy, Ψ , defined as in Dixon (1998)

$$\Phi = \frac{W_c}{ND^3} \frac{RT_{bc}}{p_{bc}} \quad (2)$$

$$\Psi = \frac{c_p T_{bc} (\Pi_c^{(\gamma-1)/\gamma} - 1)}{N^2 D^2} \quad (3)$$

and depends on the compressor diameter, D , the temperature before the compressor, T_{bc} , the specific gas constant, R , and $\Pi_c = \hat{p}_{ac}/p_{bc}$. In the $\Phi - \Psi$ domain, the compressor speed lines are gathered into almost a single line (Eriksson, 2007), and the relation between Φ and Ψ can be used to model the pressure build up in the compressor as a function of mass flow and compressor speed.

4.2 Model validation

The model's ability to capture the measured co-surge phenomena is evaluated by comparing simulations with the measured co-surge cycles. Fig. 7 shows a simulation under the same operating conditions as the measurement in Fig. 4, at time $t = 0$ s a throttle disturbance is made and the system enters co-surge. The model is clearly able to capture the main behavior in the measurements such as the frequency and amplitude of the mass flow, pressure and turbo speed oscillations. The turbo speed oscillation lags the mass flow by 90° which is in agreement with the measurement. The main difference is the initial drop in turbo speed that is not captured by the model. There is also a more rapid transition between negative and positive flow in simulations, this is partly due to sensor dynamics and partly due to inertia of the gas in the pipes which is not included in the model. This is further investigated in the next subsection.

The simulation should also be compared to the estimation of the reversed flow in Section 3, Fig. 3. The magnitude is similar except for the spikes down to -40 g/s, which is not seen in simulation. The duration of the spikes might however be overestimated due to low sampling rate of the W_{tot} signal, which is received from the CAN bus at 12.5 Hz.

4.3 Control volumes with inertia

In the Moore-Greitzer compressor model the inertia of air directly after the compressor is used to model the surge behavior. However, during co-surge the flow of air switches direction in a large part of the parallel air paths. The momentum of air in these pipes could therefore have a large influence on the co-surge behavior, which makes this interesting to study. Without going to a full 1D simulation, this can be investigated by adding momentum conservation to the pipes in a similar manner as in the Moore-Greitzer model. Each pipe is divided into several sections and the mass flow between the sections is governed by a flow plug, illustrated in Fig. 8. The acceleration of the flow plug is calculated by Newton's law of motion:

$$\frac{dW_i}{dt} = \frac{2A(p_i - p_{i+1})}{m_i - m_{i+1}} - W_i k_{fric} \quad (4)$$

where U_i is the velocity, p_i is the pressure and m_i the mass in control volume i and k_{fric} is viscous friction. This model has been used in Öberg and Eriksson (2007); Öberg (2009) and is based on a more advanced model in Andersen et al. (2006).

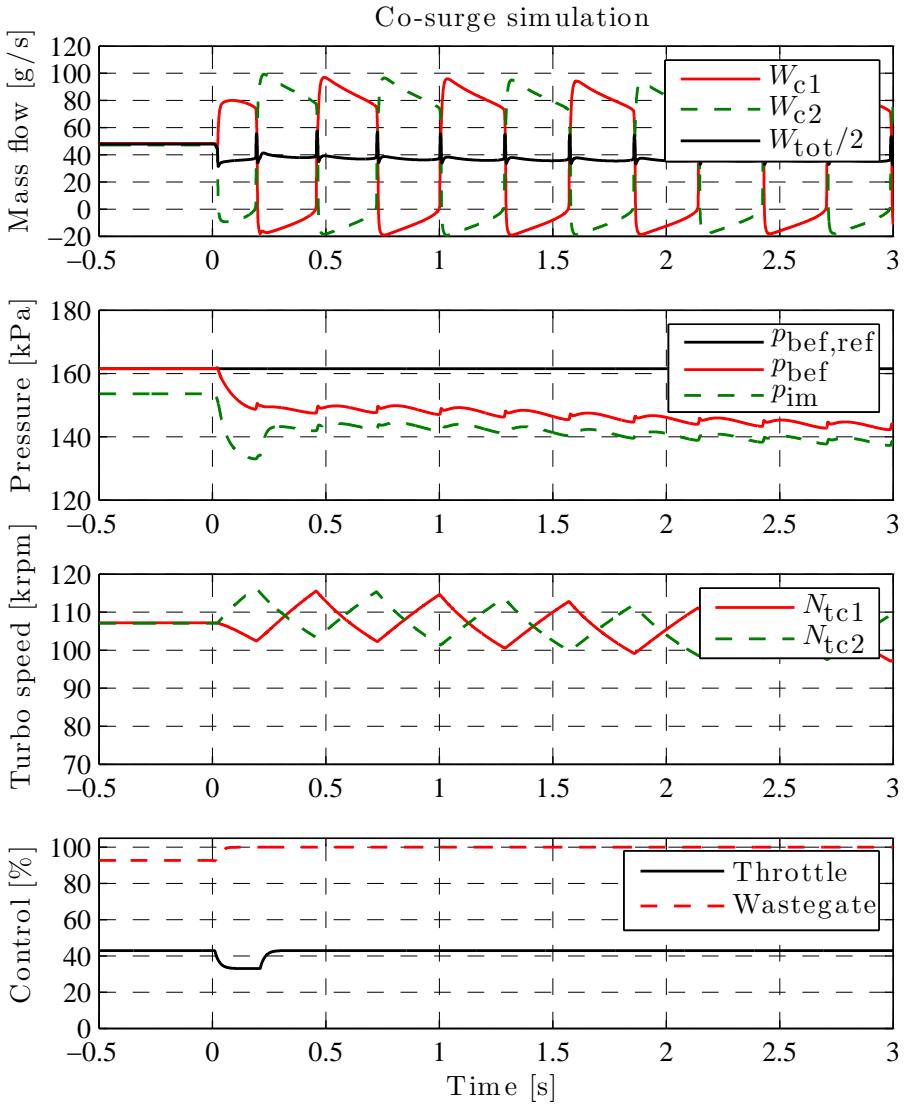


Figure 7: Co-surge resulting from simulations under similar operating conditions as the measurements in Fig. 4. The main behavior is captured by the model, both frequency and amplitude of the mass flow, pressure and turbo speed oscillations.

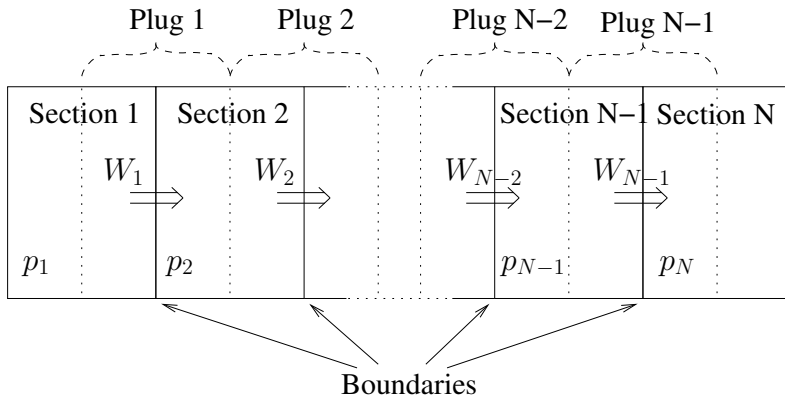


Figure 8: Model of pipe with momentum conservation. The control volume is split into several sections with a flow plug that governs the mass flow across the boundaries.

A first investigation with momentum conservation in pipes for co-surge was made in Thomasson and Eriksson (2011), where this extension was shown to give qualitative improvements to the mass flow shape during surge, but similar quantitative results. Since then the model and the parameterization has gradually been improved which is why this approach is revisited. A co-surge simulation with this extension of the model is shown in figure 9. The frequency of oscillation is slightly lower due to the increased air inertia. There are also high frequency oscillations in the mass flows following the transient but apart from these details the model behaves very similar to the model without pipe dynamics. The added model complexity and simulation time does not contribute with sufficient differences to motivate their use in the following sections. The MVEM is sufficiently accurate for the analysis.

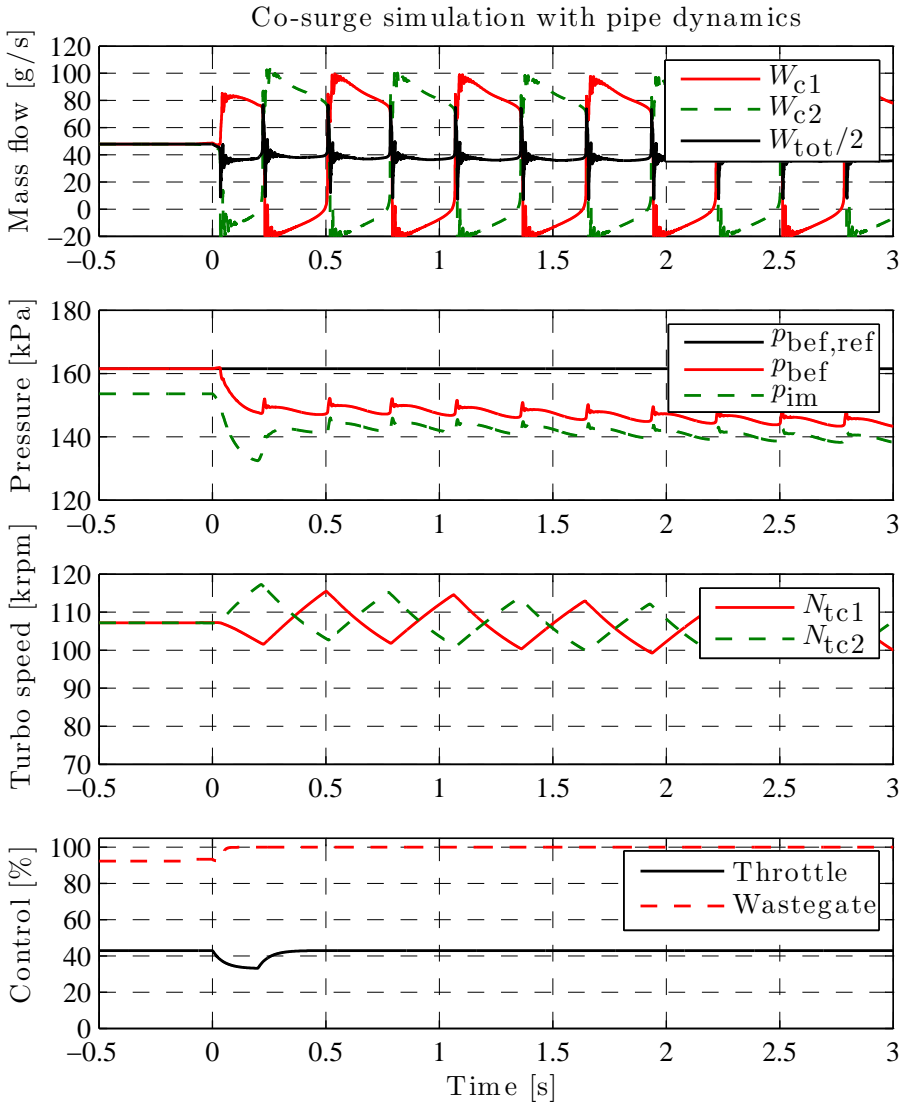


Figure 9: Co-surge simulation with inertia in the pipes around the compressor. The overall behavior is similar to the model without air inertia, but there is rapid oscillations during the transitions between positive and negative flow.

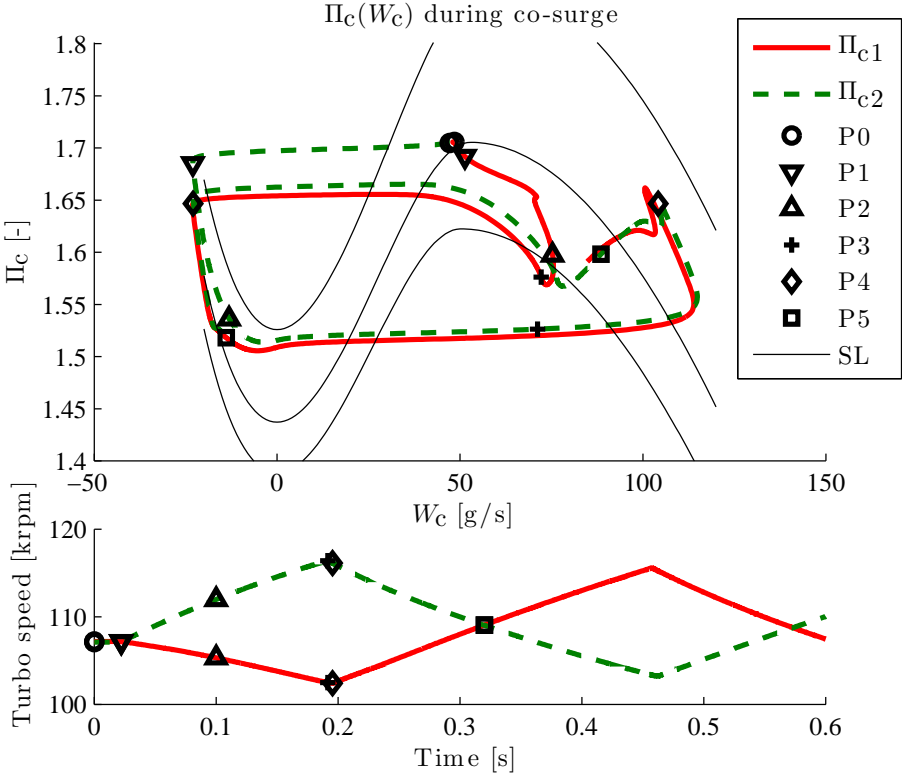


Figure 10: *Top*: Pressure ratio versus mass flow for the compressors during the beginning of co-surge. In the background are the compressor speed lines (SL) for the initial turbo speed as well as the maximum and minimum speed during the cycle. *Bottom*: The corresponding compressor speeds.

5 Co-surge analysis

When the system enters co-surge the speed of the two turbochargers start to diverge. When the surging compressor recovers it will therefore be at a higher speed than the other compressor, producing more flow at a lower pressure ratio. The compressor with the lower flow will therefore be pushed up to the left in the compressor map after the recovery, possibly past the surge line. The top subfigure of Fig. 10 shows the pressure ratio over the compressors plotted against the compressor mass flows during the onset of co-surge, below the compressor speeds versus time is shown (this is the first 0.6 s of the simulation in Fig. 7). At the starting point (P0) the flows are slightly unbalanced when a disturbance in throttle is made. The mass flows rapidly diverge, at the point (P1), 0.2 s after the disturbance, the mass flow has reversed, and the pressure ratio starts to drop. The point (P2) is in the middle of the first surge cycle, the pressure now drops slower as compressor one produces more flow due to the lower pressure ratio. When the surging compressor recovers and the mass flows have become

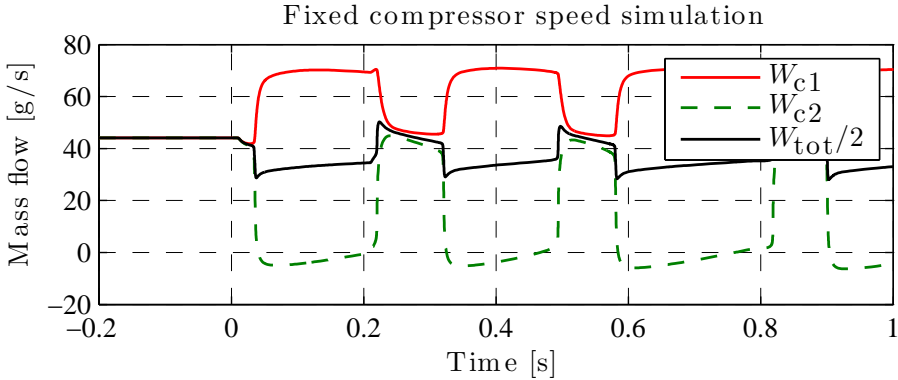


Figure 11: Simulation with fixed compressor speed close to the surge line. At $t = 0$ the speed for compressor two is lowered by 1% and that compressor enters surge. Instead of alternating flow reversals only the compressor with lower speed continues to surge.

equal (P3), the turbo speed of that compressor is higher. The pressure ratio is also lower since during surge the direction of the mass flow is from the side with positive flow to the surging side. This higher speed and lower pressure ratio will make the mass flow rapidly increase, pushing the other compressor up to the left in the map. At the point when equal pressure is reached (P4) the other compressor has already entered surge, and the mass flow reversed. The surging compressor will now start to accelerate and the other decelerate, the turbo speeds will be equal approximately during the middle of the next surge cycle (P5) and then diverge again, and the oscillation continues.

The key here is the different compressor speeds when the compressor flow recovers, which causes the mass flow to increase very rapidly upon recovery, pushing away the other compressor. That this is the main cause of the continuing oscillation co-surge can be strengthened by simulations with fixed compressor speed. In Fig. 11 such a simulation is shown. At first the compressors are balanced, but at $t = 0$ a change in the speed for compressor two is made. Instead of an alternating flow reversals the compressor with the lowest speed will now be the only compressor that surges. For fixed compressor speeds it could also be the case that the compressor with lower speed goes into reverse flow and never recovers. This depends on if the other compressor is able to produce all the mass flow without the pressure dropping below the pressure ratio at zero flow for the surging compressor.

5.1 Implications for control

The conclusion is that, assuming identical compressors, it is the compressor speeds that needs to be balanced to recover from co-surge with as much margin as possible. When the system has not entered co-surge, balanced compressor speeds is achieved by balancing the mass flows. When the system enters co-surge

however, the compressor with highest flow will not have the highest compressor speed. A controller that tries to balance the mass flows by increasing the compressor speed for the compressor with lower flow, by closing the corresponding wastegate, would therefore worsen the situation. If the system relies on parallel mass flow sensors to balance the compressor operation, the system consequently needs to detect if co-surge occurs and turn off the balancing. Additionally the total mass flow drops when the system enters co-surge. To reduce torque disturbance the controller should therefore try to increase the mass flow when entering co-surge. This will also increase the margin to the surge line at the recovery point. The next section treats detection of co-surge followed by co-surge control in Section 7.

6 Detection

The possibility to detect co-surge, as well as the accuracy and speed of the detection will depend on which sensors are available. This section investigates the performance of the detection with different available sensors. In this sections investigates detection using a pair of sensors, one in each air path, measuring either mass flow, pressure or turbo speed.

6.1 Mass flow sensors

When the system enters co-surge the mass flows will rapidly diverge. If the mass flow in each air-path is measured, the most straightforward is to use the difference in mass flow. In Thomasson and Eriksson (2011, 2013), a low-pass filtered difference and hysteresis was used for detection. In this paper another method is suggested, suitable for different sensor types.

By studying measurements it is clear that the difference in mass flow will be low for all operating points except when entering co-surge and for very short disturbances. Thus if the mass flow difference exceed a threshold for only a few samples it can be concluded that the system has entered co-surge. In the opposite direction, since the transition between positive and negative flow during co-surge is relatively fast, if the difference is below a threshold for a period of time that is longer than the transition time, the system is no longer in co-surge. This can be written as in Algorithm 1, where CS is a boolean variable that indicate co-surge. The other variables are time, t , the mass flow difference, ΔW , the set and reset mass flow thresholds, $\Delta W_{\text{set,lim}}$ and $\Delta W_{\text{reset,lim}}$, and the set and reset time windows, $\Delta t_{\text{set,lim}}$ and $\Delta t_{\text{reset,lim}}$.

An evaluation of the detection algorithm is shown in Fig. 12. The thick solid line in the bottom subfigure shows that detection is made about 0.1 s after the disturbance when using mass flow sensors.

6.2 Pressure sensors

A cheaper option than mass flow sensors would be to use pressure sensors after each air path. When the mass flow in the first compressor reverses, there will be a flow from the high pressure side of the other compressor, trough the junction

Algorithm 1 Co-surge detection with mass flow sensors.

```

if  $\Delta W > \Delta W_{\text{set,lim}} \forall t \in [t - \Delta t_{\text{set,lim}}, t]$  then
  CS(t) = 1
else if  $\Delta W < \Delta W_{\text{reset,lim}} \forall t \in [t - \Delta t_{\text{reset,lim}}, t]$  then
  CS(t) = 0
else
  CS(t) = CS(t - ts)
end if

```

of the two air paths and back to the surging compressor. This is caused by a pressure difference which can be used for detected in a similar manner as the mass flow difference in Algorithm 1, by changing ΔW to Δp . Looking at Δp in the middle subfigure of Fig. 12 it can be seen that it reacts faster than the other sensors, but is only large during the transients between positive and negative flow. This means that it is required that the pressure difference is small during longer period of time before it can be concluded that co-surge has ended, which means that $\Delta t_{\text{reset,lim}}$ have to be increased.

The dashed line in the bottom subfigure of Fig. 12 shows that detection with pressure difference is indeed faster than using mass flow sensors, detection is made already 0.04s after the disturbance. Another reason that these sensors react faster is that they are located closer to the turbochargers compared to the mass flow sensors, which are placed directly after the air paths split, see figure 1. A downside with using pressure instead of mass flow sensors is that for unbalanced but positive flow the pressure difference is very small, making it unsuitable for balancing.

6.3 Turbo speed sensors

It was concluded in section 5 that it is important to keep the turbo speeds balanced, and the inclusion of turbo speed sensors could therefore be beneficial for balancing and control of co-surge. As pointed out earlier, when the system enters co-surge the turbo speeds will start to differ, and if turbo speed sensors are available these could be used for co-surge detection as well as control. The detection is not expected to be as fast using pressure sensors, because the speeds does not start to differ until the system enters co-surge, which can be seen in the middle subfigure of Fig. 12. On the other hand, compared to using pressure sensors it very easy to distinguish between surge and co-surge, since the turbo speeds diverge a lot more during co-surge compared simultaneous surge in both compressors. The detection algorithm itself can be done very similar to Algorithm 1, but using turbo speed difference, ΔN , instead of ΔW , and different Δt limits. Turbo speed sensors could also be used as an alternative to parallel mass flow sensors for balancing during normal operation.

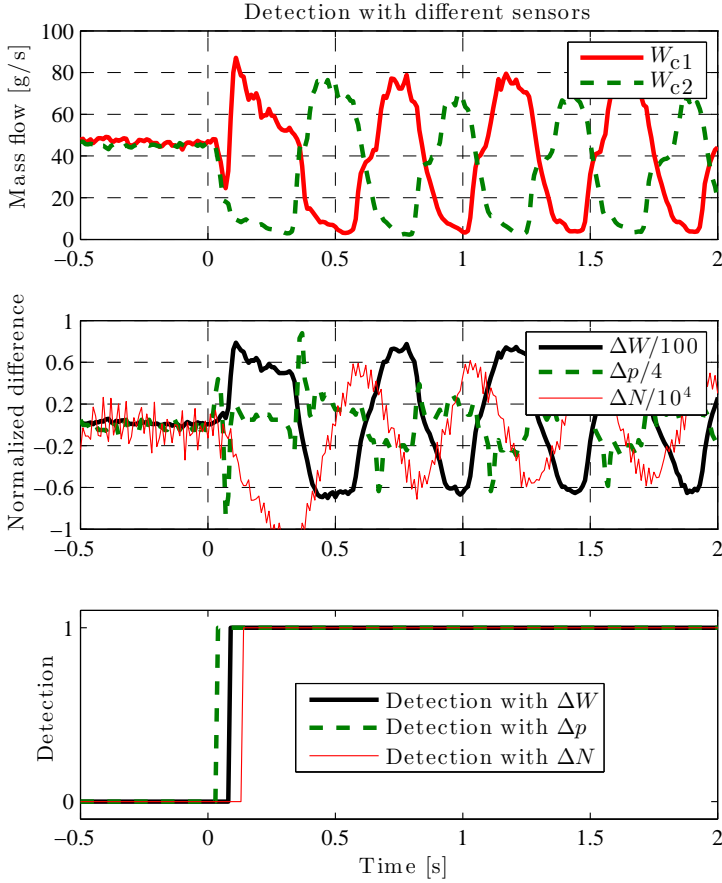


Figure 12: Evaluation of co-surge detection using different sensors. *Top*: Mass flows in the two air paths. *Middle*: Normalized mass flow, pressure and turbo speed difference. *Bottom*: Detection using mass flows (thick solid blue line), pressures (dashed green line) and turbo speeds (thin solid red line).

6.4 Sensor combinations

Pressure sensors are the fastest to detect when co-surge is about to begin, however they are also slowest to determine when co-surge has ended, which is fastest with turbo speed sensors. Combining these two would give the fastest detection of both the beginning and end of co-surge. However the difference in detection time is small, and if the control system requires mass flow measurement, adding a second sensor and putting them in the separate air paths might be best option, since it allows direct measurement of the two separate flows.

7 Co-surge control

In the literature several methods for surge control in single compressors have been proposed, de Jager (1995). The most basic is surge avoidance, where the compressor is controlled with a safety margin to the surge line, Gravdahl (1998). Active surge control works by stabilizing the compressor in the otherwise unstable operating region to the left of the surge line, using a close-coupled valve after the compressor, see for example Willems and de Jager (1998); Gravdahl and Egeland (1999). Surge detection and avoidance strategies tries to avoid the drawbacks of operating with a safety margin by detecting the onset of surge and then act to move the operating point away from the unstable region, de Jager (1995).

Controlling co-surge is partly a different problem. When co-surge occurs due to a disturbance between the two mass flows, at a constant operating point, the corresponding point with balanced mass flows is stable. The objective of the control system is then to return this point with balanced flow and as little torque disturbance as possible. Failing to do that will result in unwanted sound, drop in torque and in worst case, compressor damage.

The actuators available for the controller are the throttle, the two bypass valves, and the two wastegates. Of these only the throttle and bypass yield a very rapid change in the compressor operating point, therefore at least one of these is needed for fast controller response if the system would enter co-surge. By opening the throttle, boost pressure is reduced for a given mass flow and the operating point moves to the right in the compressor map, away from the surge region. The mass flow will also increase, partly counteracting the reduction in total mass flow that occurs during co-surge. By opening the bypass valves, the pressure ratio is reduced and the mass flow felt by the compressor is increased by recirculating part of the compressed air. This also moves the operating point of the compressor away from the surge region, but boost pressure and actual mass flow is reduced, leading to greater torque disturbance.

The throttle opening is calculated by a model based feedforward that utilizes a compressible restriction model for the throttle mass flow:

$$W_{\text{thr}} = \frac{p_{\text{bef}}}{\sqrt{T_{\text{ic}} R}} A_{\text{eff}}(u_{\text{thr}}) \Psi \left(\frac{p_{\text{im}}}{p_{\text{bef}}} \right) \quad (5)$$

The throttle reference position is calculated by exchanging p_{im} and W_{thr} for the reference values $p_{\text{im,ref}}$ and $W_{\text{thr,ref}}$. Solving for u_{thr} gives:

$$u_{\text{thr,ff}} = A_{\text{eff}}^{-1} \left(\frac{W_{\text{thr,ref}} \sqrt{T_{\text{ic}} R}}{p_{\text{bef}} \Psi \left(\frac{p_{\text{im,ref}}}{p_{\text{bef}}} \right)} \right) \quad (6)$$

The mass flow reference, $W_{\text{thr,ref}}$, is calculated using the volumetric efficiency of the engine

$$W_{\text{thr,ref}} = \eta_{\text{vol}} \frac{2 p_{\text{im,ref}} N V_{\text{D}}}{R_{\text{air}} T_{\text{im}}} \quad (7)$$

Boost pressure drops when co-surge begins and the reference remains constant, the feedforward will immediately open the throttle as long as it would not make

the intake pressure above the reference with the current boost pressure. To avoid that the throttle closing after recovery pushes the system into surge again, the throttle closing after co-surge is rate limited

$$u_{\text{thr,ff}}^* = \max(u_{\text{thr,ff}}, u_{\text{thr,ff}}(t - t_s) - k/t_s) \quad (8)$$

where t_s is the sample time and k is the maximum retard rate. In addition to this, if the pressure drop over the throttle is very low when co-surge begins, only opening the throttle is not enough to quell the oscillation, see Thomasson and Eriksson (2013). In that case actuating the bypass valves is necessary. The bypass control is implemented as

$$u_{\text{bp}} = \begin{cases} 1, & \text{if CS} = 1 \text{ and } \Delta p_{\text{thr}}(t_{\text{CS}}) < \Delta p_{\text{lim}} \\ 1, & \text{if CS} = 1 \text{ and } p_{\text{im}} \geq p_{\text{im,ref}} \\ 0, & \text{otherwise} \end{cases} \quad (9)$$

where $\Delta p_{\text{thr}}(t_{\text{CS}})$ is pressure drop over the throttle when co-surge is detected and Δp_{lim} is a threshold for opening the bypass valves.

7.1 Controller evaluation

The co-surge control strategy described by (6)-(9) has been evaluated both in simulation and test vehicle. An example from the simulations are shown in Fig. 13. The engine runs at a constant operating point close to the surge line. A small throttle disturbance is introduced at $t = 0$ and the mass flows rapidly diverge. The system detects co-surge and as a result of the dropping boost pressure the throttle is opened. The mass flow from compressor two recovers and overshoots the other mass flow but does not push the other into surge, and after 0.5 s the flows are balanced. After about 1 s the boost pressure has returned to the same level as before the disturbance.

The controller is also implemented in the test vehicle. The vehicle is mounted on a chassis dynamometer and driven with the engine in a similar operating point as the simulation. A throttle disturbance is introduced at $t = 0$, resulting in co-surge, see Fig. 14. After the disturbance the mass flows rapidly diverge, which is detected by the control system. The pressure drop over the throttle is larger than Δp_{lim} , and therefore only the throttle is opened. The mass flow rapidly recovers and the system has returned to the previous operating point in about 0.5 s.

Comparing measurement and simulation the qualitative behavior is similar. The mass flow for the surging side drops rapidly, and when it recovers overshoots the other mass flow. The pressure drop in both simulation and measurement is about 10 kPa and the turbo speeds diverge, although a little bit less in the measurement. The throttle closing is slightly faster in the measurement. This is a result of the boost pressure rising back to the reference faster than in the simulation, where there is a small undershoot in boost pressure.

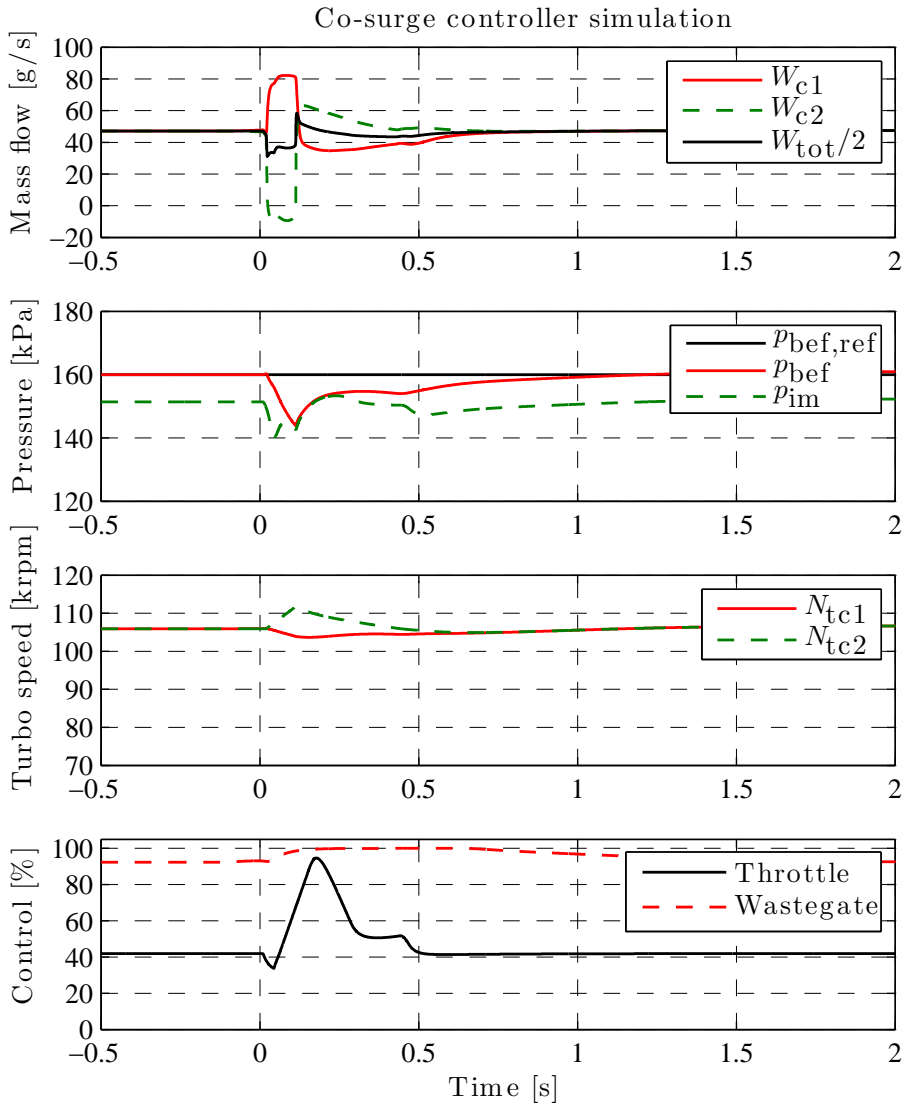


Figure 13: Simulation with the co-surge controller. At $t = 0$ s a disturbance in throttle is made and the mass flows start to diverge. The detection and control algorithm detects the problem and opens the throttle. After less than 0.5 s the oscillation has been quelled and the mass flow difference limited, and after about 1 s the same stationary point as before the disturbance is reached.

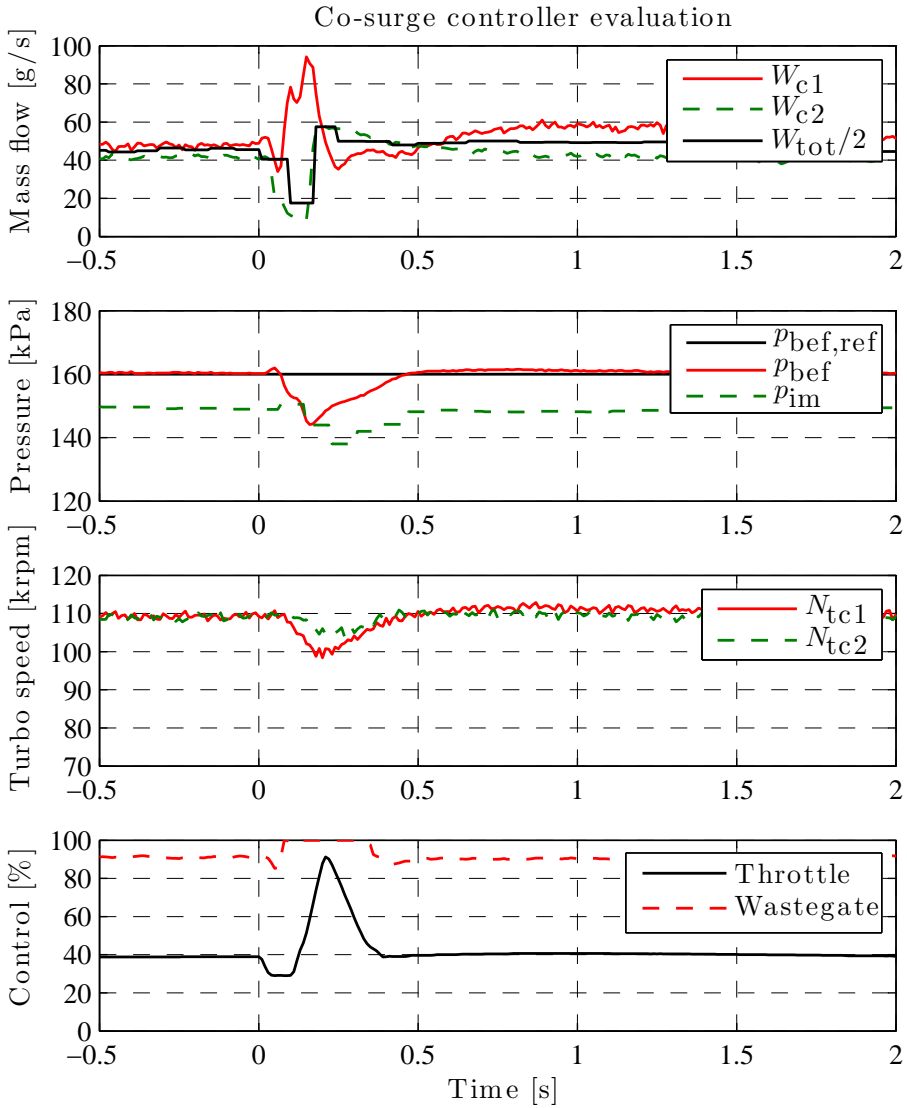


Figure 14: Evaluation of the controller (6)-(9) in the test vehicle. The overall behavior is similar to the measurement, the amplitude in mass flow and pressure drop, the surging mass flow overshooting the other at recovery, and the recovery time. The initial opening of the throttle differs due to the implementation, the disturbance is added to the throttle opening also after co-surge is detected until 0.3s

7.2 Turbo speed balancing during co-surge

When the system enters co-surge the two turbo speeds start to diverge. The compressor which does not produce any flow accelerates while the other decelerates, and upon recovery the difference in turbo speed will determine how unbalanced the operating point is and if the system will continue in co-surge. This was strengthened by the fixed speed simulation in Section 5, where only the compressor with lowest speed enters surge repeatedly. This suggests that if the system enters co-surge, the controller should try to control the compressor speeds as close together as possible. This makes the recovery point more balanced, hopefully avoiding that the other compressor is pushed into surge.

In this paper a PD-controller that tries to force the turbo speeds together during co-surge is proposed. An I-part would be too slow to contribute during surge, but could of course be used to keep the system balanced during normal operation. The controller acts on the wastegates, adding u_{wg}^+ to the control signal for the turbo with lower speed and deducting u_{wg}^- from the control signal for the turbo with higher speed.

$$\begin{aligned} u_{wg}^+ &= K_{wg}^+ (1 + \tau_{wg} s) e_{Ntc} \\ u_{wg}^- &= K_{wg}^- (1 + \tau_{wg} s) e_{Ntc} \end{aligned} \quad (10)$$

where s denotes the Laplace variable and τ_{wg} is chosen as the time constant for the wastegate actuator. The controller error, e_{Ntc} , is the absolute difference in turbo speed, with a small dead zone, N_{dz} .

$$e_{Ntc} = \max(|N_{tc1} - N_{tc2}| - N_{dz}, 0) \quad (11)$$

This balancing controller works in parallel with the control strategy for the throttle and bypass valves proposed in the previous section, described by (6)-(9).

The stabilizing effect of trying to balance the turbo speeds during co-surge is first demonstrated by the simulation in Fig. 15. The engine is operated in the same operating point as before, with a disturbance introduced at $t = 0$ s. The system enters co-surge and the throttle opens. Additionally the wastegate of turbo one closes while the other opens, as a result of the diverging turbo speeds. Compared to the case without balancing in Fig. 13, the initial period with reverse flow is slightly longer. However, upon recovery the flows are more balanced and the time until the flows converge are shorter. The time until the system reaches the same operating point as before the disturbance is also smaller, about 0.7 s compared to 1 s without the balancing controller.

Corresponding results from the test vehicle is shown in Fig. 16. Compared to the controller without balancing, the overshoot of the recovering mass flow is a lot smaller, smaller than predicted by the simulations. The flows after recovery is almost equal, and on the same level as before the disturbance. The effect of the differentiated wastegate action on the turbo speeds is that the difference is reduced faster, resulting in the more balanced recovery point. The boost pressure response is very similar to both simulations and the previous controller. In conclusion the test vehicle experiments confirm simulation results, that forcing the turbo speeds together results in more balanced recovery point, reducing the risk of a continuing oscillation.

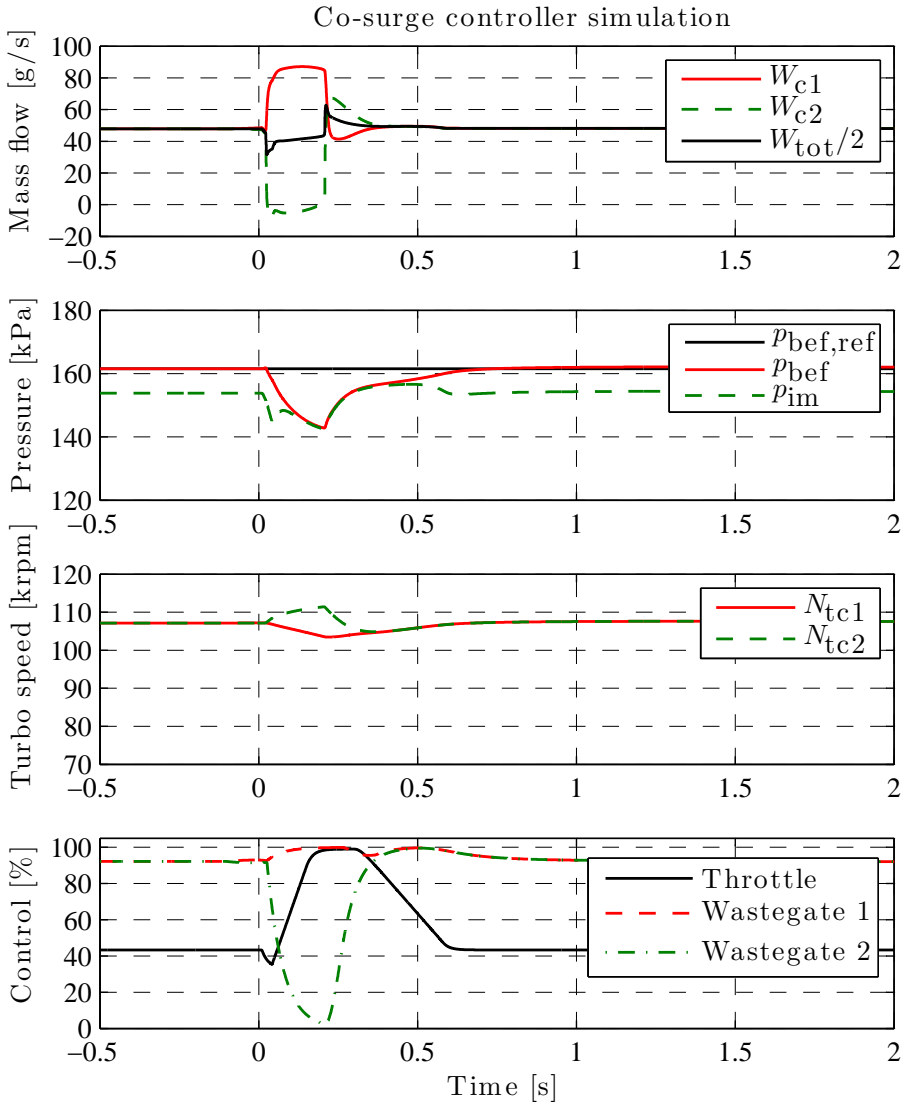


Figure 15: Simulation of the co-surge control strategy (6)-(9) together with the turbo speed balancing (10). Compared to the controller without balancing, the time with reversed flow is slightly longer, but the point of recovery is more balanced, with less mass flow overshoot for the recovering compressor.

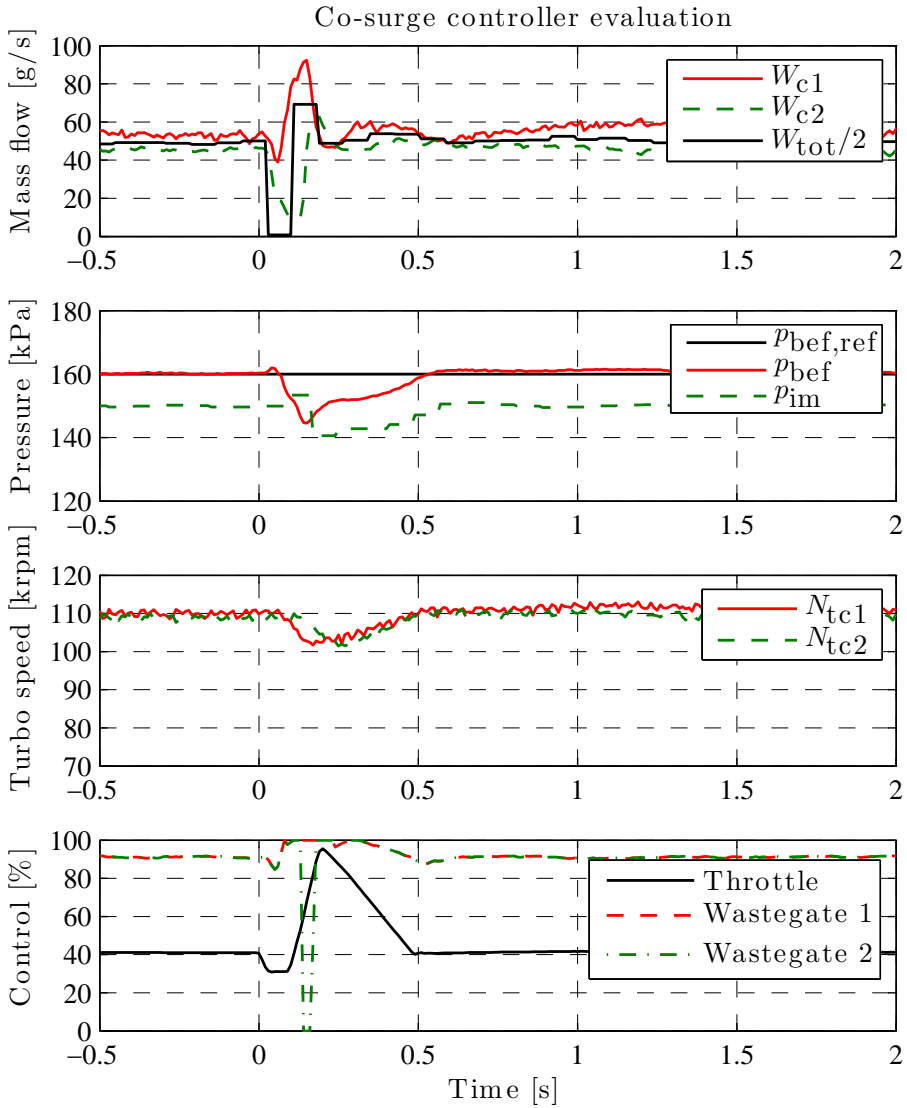


Figure 16: Evaluation in test vehicle of the co-surge control strategy (6)-(9) together with the turbo speed balancing (10). When comparing to the controller without turbo speed balancing the trend is the same as for the simulation. The recovery point is more balanced for both mass flow and turbo speed, and the boost pressure behavior is similar.

8 Conclusions

The paper presents data on co-surge and gives an analysis of the phenomena based on the movement in the compressor map. The analysis highlights the importance of the varying compressor speeds for the co-surge oscillation. During the surge cycle the turbo speeds diverge and if the difference at the recovery point is too high, the other compressor is pushed into surge and the oscillation continues. Co-surge detection with different sensors is investigated, and a general algorithm is proposed that can use any pair of the following sensors, either parallel pressure, mass flow or turbo speed. The fastest detection is with pressure sensors mounted close to the compressors, however, unlike mass flow or turbo speed sensors these are not suitable for balancing. A controller that aims to quell the co-surge oscillation and return to the previous operating point has also been presented and validated both in simulation and in a test vehicle. The controller is able to quell the oscillation and return to stable operation within less than 1 s. Additionally turbo speed balancing is added to this controller, which reduces the imbalance in both mass flow and turbo speed at the point of recovery. This reduces the risk of a prolonged oscillation and has been evaluated both in simulation and test vehicle. The evaluations confirms that the mass flows are more balanced after recovery, shortening the time to regain balanced flow.

Acknowledgments

This research was supported by the VINNOVA Industry Excellence Center LINK-SIC.

References

- M. Ammann, N. P. Fekete, A. Amstutz, and L. Guzzella. Control-Oriented Modeling of a Turbocharged Common-Rail Diesel Engine. In *Proc. of the Int. Conference on Control and Diagnostics in Automotive Applications*, 2001.
- Stig Kildegård Andersen, Henrik Carlsen, and Per Grove Thomsen. Control volume based modelling in one space dimension of oscillating, compressible flow in reciprocating machines. *Simulation Modelling Practice and Theory*, 14 (8):1073–1086, October 2006.
- Bram de Jager. Rotating stall and surge control: A survey. In *Proc. of the IEEE Conference on Decision and Control*, volume 2, pages 1857–1862, December 1995.
- S.L. Dixon. *Fluid Mechanics and Thermodynamics of Turbomachinery*. Butterworth-Heinemann, 4th edition, 1998.
- K.-D. Emmenthal, G. Hagermann, and W.-H. Hucho. Turbocharging small displacement spark ignited engines for improved fuel economy. In *SAE World Congr.*, Techn. Paper 790311, February 1979.

- Lars Eriksson. Modeling and Control of Turbocharged SI and DI Engines. *Oil & Gas Science and Technology - Rev. IFP*, 62(4):523–538, 2007.
- Lars Eriksson, Lars Nielsen, Jan Brugård, Johan Bergström, Fredrik Pettersson, and Per Andersson. Modeling of a turbocharged SI engine. *Annual Reviews in Control*, 26(1):129–137, October 2002.
- Jan Tommy Gravdahl. *Modeling and Control of Surge and Rotating Stall in Compressors*. PhD thesis, Norwegian University of Science and Technology, 1998.
- Jan Tommy Gravdahl and Olav Egeland. Centrifugal Compressor Surge and Speed Control. *IEEE Trans. on Control Systems Technology*, 7(5):567–579, September 1999.
- E.M. Greitzer. Surge and rotating stall in axial flow compressors-Part I: Theoretical compression system model. *J. of Engineering for Power*, 98(2):190–198, April 1976.
- E.M. Greitzer. The Stability of Pumping Systems. *J. of Fluids Engineering*, 103(1):193–242, June 1981.
- L. Guzzella, U. Wenger, and R. Martin. IC-Engine Downsizing and Pressure-Wave Supercharging for Fuel Economy. *SAE World Congr.*, March 2000.
- K.E. Hansen, P. Jørgensen, and P.S. Larsen. Experimental and Theoretical Study of Surge in a Small Centrifugal Compressor. *J. of Fluids Engineering*, 103(3):391–395, 1981.
- Elbert Hendricks and Spencer C. Sorenson. Mean value modelling of spark ignition engines. *SAE Trans. J. of Engines*, 99(3):1359–1373, 1990.
- Oskar Leufvén and Lars Eriksson. Time to surge concept and surge control for acceleration performance. In *Proc. of the IFAC World Congr.*, pages 2063–2068, Seoul, Korea, July 2008.
- Per Öberg. *A DAE Formulation for Multi-Zone Thermodynamic Models and its Application to CVCP Engines*. PhD thesis, Linköping University, 2009.
- Per Öberg and Lars Eriksson. Control Oriented Gas Exchange Models for CVCP Engines and their Transient Sensitivity. *Oil & Gas Science and Technology - Rev. IFP*, 62(4):573–584, 2007.
- Dominique Petitjean, Luciano Bernardini, Chris Middlemass, S. M. Shahed, and Ronald G. Hurley. Advanced Gasoline Engine Turbocharging Technology for Fuel Economy Improvements. In *SAE World Congr.*, Techn. Paper 2004-01-0988, March 2004.
- Andreas Thomasson and Lars Eriksson. Modeling and Control of Co-Surge in Bi-Turbo Engines. In *Proc. of the IFAC World Congr.*, Milano, Italy, 2011.

Andreas Thomasson and Lars Eriksson. Co-Surge Detection and Control for Bi-Turbo Engines with Experimental Evaluation. In *Proc. of the IFAC Symposium on Advances in Automotive Control*, Tokyo, Japan, 2013.

N. Watson and M.S. Janota. *Turbocharging the Internal Combustion Engine*. The Macmillan Press Ltd, 1982. ISBN 0-333-24290-4.

Frank Willems and Bram de Jager. Modeling and Control of Rotating Stall and Surge: An Overview. In *Int. Conference on Control Applications*, pages 331–335, September 1998.

A Nomenclature

Symbol	Description	Subscript	Description
A	Area	af	Air filter
CS	Co-surge detected	ac	After compressor
c_p	Specific heat	bc	Before compressor
D	Diameter	bp	Bypass
ΔX	Difference in X	CS	Co-surge
e	Error	c	Compressor
γ	c_p/c_v	fric	Friction
L	Flow plug length	ic	Intercooler
N	Rotation speed	im	Intake manifold
p	Pressure	lim	Limit
Π	Pressure ratio	ref	Reference
R	Gas constant	tc	Turbocharger
SL	Speed line	thr	Throttle
T	Temperature	tot	Total
t	Time	wg	Wastegate
t_s	Sample time		
τ	Time constant		
u	Control signal		
V	Volume		
W	Mass flow		

Linköping studies in science and technology. Dissertations.
Division of Vehicular Systems
Department of Electrical Engineering
Linköping University

- No. 1 Magnus Pettersson *Driveline Modeling and Control*, 1997
- No. 2 Lars Eriksson *Spark Advance Modeling and Control*, 1999
- No. 3 Mattias Nyberg *Model Based Fault Diagnosis: Methods, Theory, and Automotive Engine Applications*, 1999
- No. 4 Erik Frisk *Residual Generation for Fault Diagnosis*, 2001
- No. 5 Per Andersson *Air Charge Estimation in Turbocharged Spark Ignition Engines*, 2005
- No. 6 Mattias Krysander *Design and Analysis of Diagnosis Systems Using Structural Methods*, 2006
- No. 7 Jonas Biteus *Fault Isolation in Distributed Embedded Systems*, 2007
- No. 8 Ylva Nilsson *Modelling for Fuel Optimal Control of a Variable Compression Engine*, 2007
- No. 9 Markus Klein *Single-Zone Cylinder Pressure Modeling and Estimation for Heat Release Analysis of SI Engines*, 2007
- No. 10 Anders Fröberg *Efficient Simulation and Optimal Control for Vehicle Propulsion*, 2008
- No. 11 Per Öberg *A DAE Formulation for Multi-Zone Thermodynamic Models and its Application to CVCP Engines*, 2009
- No. 12 Johan Wahlström *Control of EGR and VGT for Emission Control and Pumping Work Minimization in Diesel Engines*, 2009
- No. 13 Anna Pernestål *Probabilistic Fault Diagnosis with Automotive Applications*, 2009
- No. 14 Erik Hellström *Look-ahead Control of Heavy Vehicles*, 2010
- No. 15 Erik Höckerdal *Model Error Compensation in ODE and DAE Estimators with Automotive Engine Applications*, 2011
- No. 16 Carl Svärd, *Methods for Automated Design of Fault Detection and Isolation Systems with Automotive Applications*, 2012.
- No. 17 Oskar Leufvén, *Modeling for control of centrifugal compressors*, 2013.
- No. 18 Christofer Sundström, *Model Based Vehicle Level Diagnosis for Hybrid Electric Vehicles*, 2014.